MANGANESE(III) SCHIFF BASE COMPLEXES WITH PSEUDOHALIDE LIGANDS - MONOMERS, DIMERS, CHAINS AND NETWORKS

A Thesis

Submitted for the Degree of

Doctor of Philosophy

By

Govindu Gari Bhargavi

School of Chemistry

University of Hyderabad

Hyderabad – 500046

India

FEBRUARY 2009

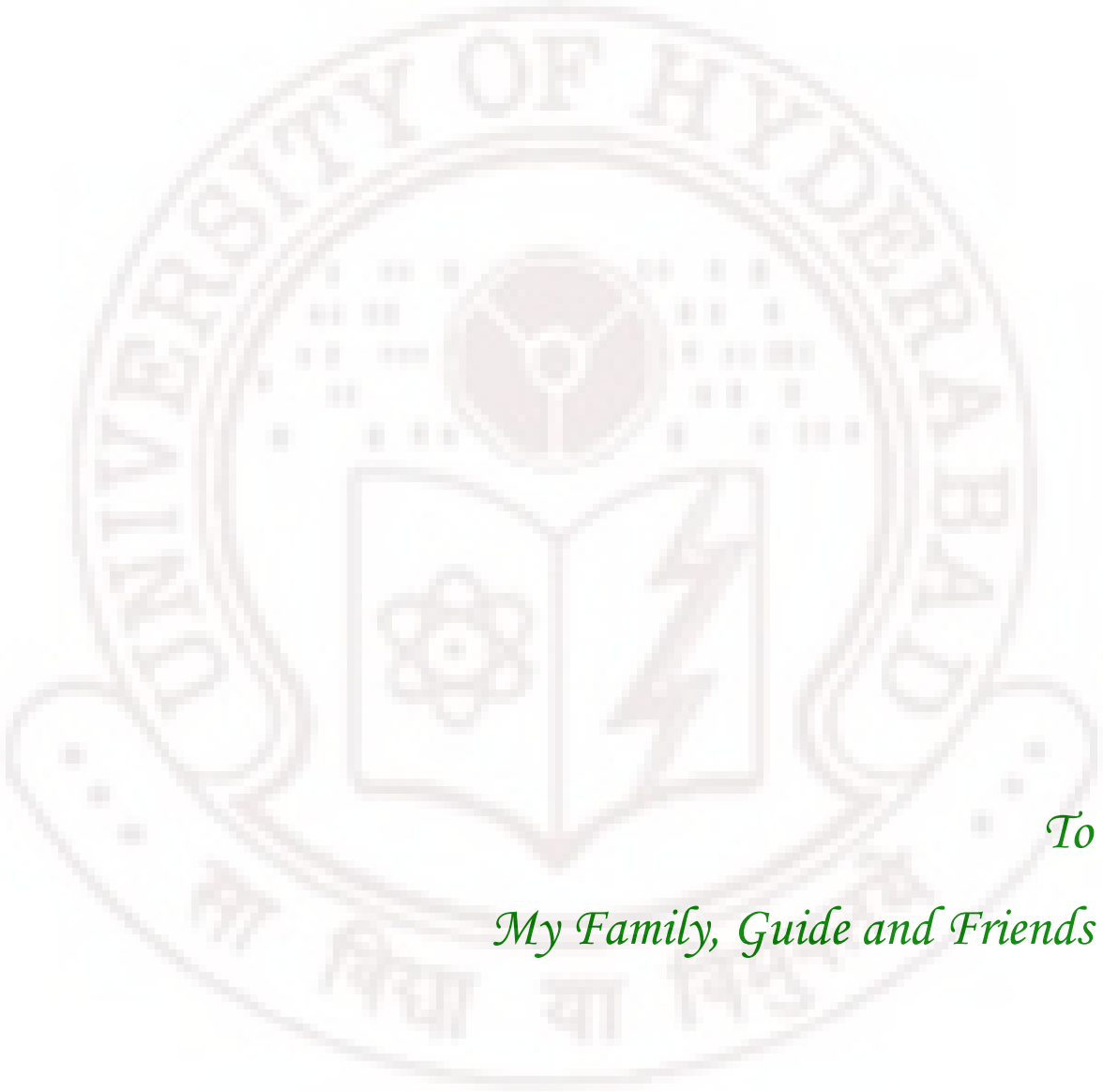

To

My Family, Guide and Friends

గురు మధ్యే స్థితంవిశ్వం విశ్వమధ్యే
స్థితో గురు:
గురుర్విశ్వం నచాన్యోస్థి తస్మై శ్రీ
గురవేనమ:

CONTENTS

CHAPTER II

Synthesis, Crystal Structure and Magnetic Properties of Dimeric Mn^{III} Schiff Base Complexes Including Pseudohalide Ligands. Ferromagnetic Interactions through Phenoxo Bridges and Single Molecule Magnetism

CHAPTER III

Antiferromagnetic interactions through phenoxo bridges and lattice water. Synthesis, Structure and Magnetic properties of $[Mn(acphen)NCS]_2$ and $[Mn(acphpn)(H_2O)NCS].2H_2O$

CHAPTER IV

Antiferromagnetic interactions in a zig-zag End-on polymer bridged by a *trans*-μ-(1,1)-azide. Synthesis, structure and magnetic properties of $[Mn(5\text{-}Clsalpn)N_3]_n$, and phenoxo bridged $[Mn(5\text{-}Clsalpn)N_3]_2$.

CHAPTER V

Synthesis, Crystal Structure and Electronic spectra of $[Mn(salmen)NCO]_2$, $[Mn(salmen)NCS]_2$, $[Mn(5\text{-}Clsalen)NCO]_2$, $[Mn(4\text{-}MeOsalen)(H_2O)N_3]$, $[Mn(4\text{-}MeOsalen)N_3]_n$ and $[Mn(4\text{-}MeOsalen)(H_2O)NCS]$

STATEMENT

I hereby declare that the matter embodied in this thesis is the result of investigations carried out by me in the School of Chemistry, University of Hyderabad, India under the supervision of Prof. M. V. Rajasekharan.

In keeping with the general practices of reporting scientific observations, due to acknowledgment has been made wherever the work described is based on the findings of other investigators.

Govindu Gari Bhargavi

CERTIFICATE

Certificate that the work embodied in this thesis entitled "***MANGANESE(III) SCHIFF BASE COMPLEXES WITH PSEUDOHALIDE LIGANDS – MONOMERS, DIMERS, CHAINS AND NETWORKS***" has been carried out by **Ms. Govindu Gari Bhargavi** under my supervision and the same has not been submitted elsewhere for any degree.

Hyderabad — M. V. RAJASEKHARAN

February 2009 — (Thesis Supervisor)

DEAN

School of Chemistry

ACKNOWLEDGEMENTS

I express my deepest respect and the most sincere gratitude to my supervisor Prof. M. V. Rajasekharan, for his invaluable guidance and encouragement at all stages of my work. I have been fortunate enough to work with him and learnt a lot. I am greatly indebted to his assistance and understanding in the matters of non academic concern which have helped me endure some difficult times during my research work.

I am thankful to Prof. E. D. Jemmis, Prof. M. Peiasamy, and Prof. D. Basavaiah, Deans, School of Chemistry for providing the necessary facilities to carry out research work. I thank all the faculty members of the School of Chemistry for their help and suggestions on various occasions.

I thank all the technical and non-teaching staff of the School of Chemistry and CIL for their help and cooperation. My special thanks to Dr. Raghavaiah for his help during X-ray data collection.

I express my sincere thanks to Prof. J.-P. Tuchagues and Prof. J.-P. Costes at Laboratoire de Chimie du CNRS, Toulouse, France, for the collaboration work on magnetic studies of Mn(SB)X.

I extend my sincere thanks to CSIR and DRDO for the financial assistance through out my research.

I would like to thank all my teachers, particularly Mr.Krishna Reddy, Mr.Srinivasulu and Mrs. Radha Lakshmi, whose impressive lectures motivated me to take up my career into realm of *Chemistry*. I thank my present and former labmates for their help and teamwork.

It is a great pleasure to remember my childhood and M.Sc friends for their affection and help. I thank all of my friends in HCU who made my stay peaceful, enjoyable and memorable in the campus.

I must express a very special appreciation to Dr. P.M.Sreekanth for his love and constant encouragement through out my ups and downs.

Finally, I thank all my family members for their love and constant support. Their support has been unconditional and I am grateful to them.

I thank GOD who is giving me the strength through out my life.

G. Bhargavi

ABBREVIATIONS AND DEFINITIONS

AF	antiferromagnetic interaction
D	zero field splitting
F	ferromagnetic interaction
acphpn	*N,N′*-bis(2-hydroxyacetophenone)-1,3-diaminopropane
acphen	*N,N′*-bis(2-hydroxyacetophenone)-1,2-diaminoethane
5-Clsalpn	*N,N′*-bis(5-chlorosalicylidene)-1,3-diaminopropane
5-Clsalen	*N,N′*-bis(5-chlorosalicylidene)-1,2-diaminoethane
4-MeOsalen	*N,N′*-bis(4-methoxysalicylidene)-1,2-diaminoethane
(1*R*, 2*R*)-salcy	(*R*, *R*)-*N,N'*-bis(salicylidene)-1,2-diaminocyclohexane
SB	Schiff base
salen	*N,N′*-bis(salicylidene)-1,2-diaminoethane
salpn	*N,N′*-bis(salicylidene)-1,3-diaminopropane
salmen	*N,N′*-bis(salicylidene)-1,2-diaminopropane
SMM	single molecule magnetism

$R1$ = $\Sigma||F_o| - |F_c|| / \Sigma|F_o|$.

$wR2$ = $[\Sigma w(F_o^2 - F_c^2)^2 / \Sigma(wF_o^4)]^{1/2}$

w^{-1} = $[\sigma^2(F_o)^2 + (AP)^2 + BP]$, $P = [2F_c^2 + \text{Max}(F_o^2, 0)]/3$

S = $[\Sigma\{w(F_o^2 - F_c^2)^2\}/(n\text{-}p)]^{1/2}$

U_{eq} = $1/3(U_{11}a^2a^{*2} + U_{22}b^2b^{*2} + U_{33}c^2c^{*2} + U_{23}b^*c^*bc\cos\alpha + U_{12}a^*b^*ab\cos\gamma + U_{13}a^*c^*ac\cos\beta)$

$$\chi_m = \frac{g^2\,\mu_B^2\,N}{3KT}\,\frac{\sum_i S^i\left(S^i+1\right)n^i\,e^{-Ei/kT}}{\sum_i n^i\,e^{-Ei/kT}}$$

(*Dimer equation*)

$$\chi_m = \frac{N g^2 \mu_B^2\, S(S+1)}{3k(T-\theta)}\,\frac{[1-u(y)]}{[1+u(y)]}$$

(*Antiferromagnetic chain equation*)

PREFACE

Schiff base complexes of manganese(III) are well known for the variety of the structures formed and associated magnetic properties as well as catalytic applications. Of particular interest is the role of Mn(III) as well as other oxidation states of manganese in biological electron transfer. The five coordinate complexes of the general formula Mn(SB)X where SB is a tetradentate Schiff base and X is an anionic ligand often become six-coordinated through coordination with solvent, formation of 1D-chain polymers via bridging through X, or dimerisation via bridging through the phenoxo-oxygen. Additional non-covalent interactions may lead to formation of networks in the solid state. Dimerisation and polymerisation are of more widespread occurrence when X is a pseudohalide like azide or thiocyanate. The present thesis extends the earlier work done in the research group on the pseudohalide complexes.

As part of the present study, several phenoxo-bridged dinuclear complexes as well as 1D-chain complexes have been prepared using conventional synthetic procedures, crystallized and characterized using X-ray crystallography. In some cases polymorphs have been identified which includes the first Mn(III) 1,1-azide bridged chain. In many cases detailed magnetic studies have also been made. The study of molecular magnetism has undergone rapid developments during the past three decades starting with magneto-structural correlations made by measuring exchange coupling parameters for a variety of transition metal complexes and culminating in the characterization of high spin ground states and single molecule

magnetism(SMM). Along with bio-inorganic model building, realization of high spin ground states with high nuclearity manganese complexes has provided some of the motivation for research in manganese coordination chemistry. In recent times, SMM has been observed for some phenoxo-bridged Mn(III) dimers as well. In the present study also a few such ferromagnetic dinuclear complexes exhibiting slow relaxation of magnetization at low temperatures (<10 K) have been obtained. There are also cases in which weak interactions in the crystal lattice provided significant pathways for magnetic exchange.

Part of the work being reported in this thesis have been communicated for publication:

1. Synthesis, Crystal Structure and Magnetic Properties of Dimeric Mn^{III} Schiff BaseComplexes Including Pseudohalide Ligands. Ferromagnetic Interactions through Phenoxo Bridges and Single Molecule Magnetism. G. Bhargavi, M. V. Rajasekharan, J.-P. Costes and J.-P. Tuchagues. (in press *Polyhedron*)
2. Antiferromagnetic interactions through phenoxo bridges and lattice water. Synthesis, structure, and magnetic properties of new Mn(III) Schiff base complexes in combination with thiocyanate ligand. G. Bhargavi, M. V. Rajasekharan, and J.-P. Tuchagues. (Communicated to *Inorg. Chem. Acta*)

CHAPTER I

Mn(III) tetradentate Schiff base complexes with pseudohalides: A brief introduction

1.1. Introduction

Tetradentate Schiff base (SB) ligands form Mn(III) complexes of the type Mn(SB)X. The simplest SB ligand of this type is salen formed by condensing 1,2-diaminoethane with salicylaldehyde. Often the sixth coordination position is occupied by a solvent molecule (S), usually water. Numerous complexes of the type Mn(SB)Cl[1-15] and Mn(SB)(S)Cl[16-25] have been reported. The former include the widely used Jacobson catalyst, where SB is a chiral ligand leading to asymmetric epoxidation[26,27] and aziridination[28,29] of olefins. Besides the chloro complexes, analogous complexes where X is a pseudohalide ion are also known: N_3^-,[30-43] NCS^-,[15,32,44-51] NCO^-,[30,52-54] CN^-.[55] Since the present thesis deals with pseudohalide complexes, a brief statement about the coordination modes of the pseudohalide ions is given in the next section.

1.2. Coordination modes of pseudohalide ions:[56,57] Different observed coordination modes are depicted below. References are given only for Mn(III) complexes.

1.2.1. Coordination modes of azide (N_3^-): The azide ion in ionic salts is linear and symmetric, having equal N-N distances (1.167 Å). But the covalently bonded azide has unequal bond distances (In *M*-N_1-N_2-N_3, N_1-N_2 distance is more than N_2-N_3). In

coordination complexes the azide ion has different kinds of binding modes like N-bonded terminal, μ-(1,3), μ-(1,3/1,1), μ-(1,1), μ-(1,1,1), μ-(1,1,3) as shown in Scheme 1.1. Depending upon the coordination mode of the azide ion, the IR spectra of the compounds are different.

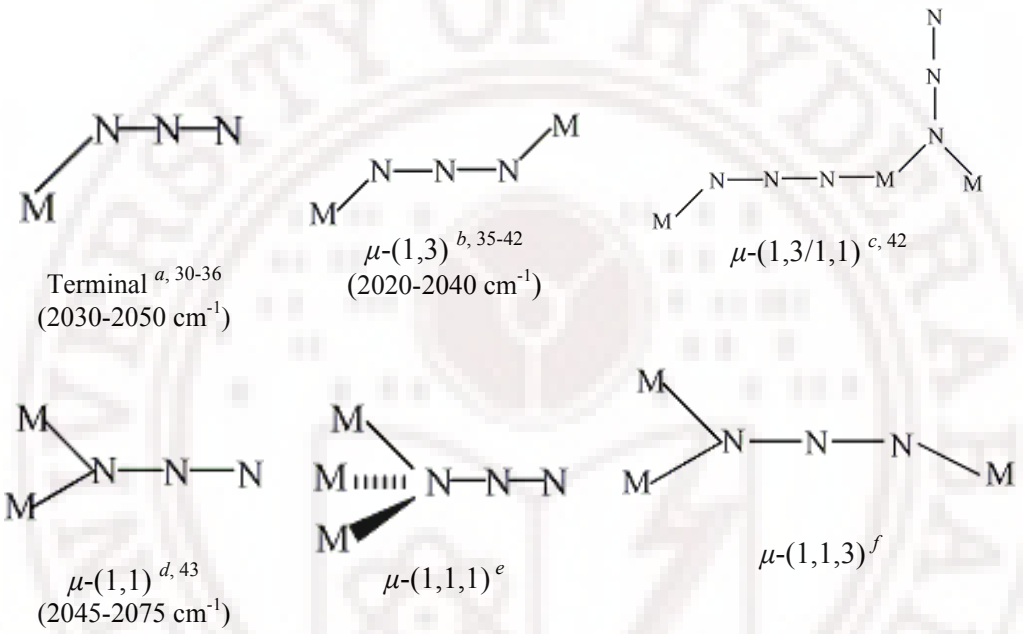

Scheme 1.1. Different coordination modes of azide ion. References and IR frequencies ($\nu_a N_3^-$) are given for Mn(III)-azide complexes. CSD search results: [a]1455 for all transition metals, 15 Mn^{3+}. [b]415 for all transition metals, 9 Mn^{3+}. [c]35 for all transition metals, 1 Mn^{3+}. [d]525 for all transition metals, 1 Mn^{3+}. [e]26 for all transition metals. [f]18 for all transition metals.

1.2.2. Coordination modes of thiocyanate (NCS^-): Being an ambidentate ligand thiocyanate may coordinate the metal center through the nitrogen (M-NCS) or the sulfur (M-SCN) or both (M-NCS-M). The N-C and C-S bond distances of the thiocyanate ion are 1.149 Å and 1.689 Å, respectively. The coordination bond distance of N-bonded thiocyanate is less than S-bonded thiocyanate ion. The CN

stretching frequency of the N-bonded compound is nearly 2050 cm^{-1}, lower than that of S-bonded complex (nearly 2100 cm^{-1}). The bridging ion has frequencies in between the above values. The CS stretching vibrations are at 780-860 cm^{-1} for N-bonded and 690-720 cm^{-1} for S-bonded coordination complexes. The N-bonded complexes exhibit single sharp bending vibration at about 480 cm^{-1}, whereas the S-bonded complexes show several bands of low intensity near 420 cm^{-1}. Some important coordination modes of the thiocyanate ion are shown in Scheme 1.2.

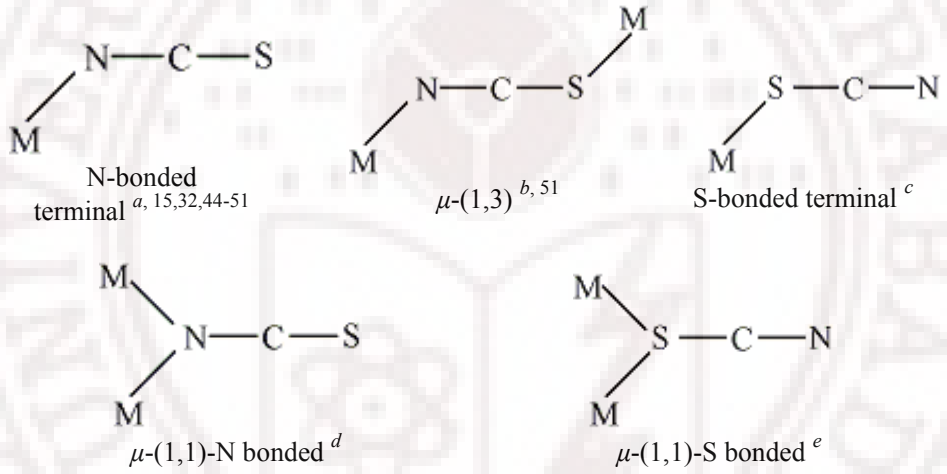

Scheme 1.2. Different coordination modes of thiocyanate ion. References are given for Mn(III)-thiocyanate complexes. [a]2801 for all transition metals, 28 Mn^{3+}. [b]191 for all transition metals, 1 Mn^{3+}. [c]2 for all transition metals. [d]42 for all transition metals. [e]21 for all transition metals.

1.2.3. Coordination modes of cyanate (NCO^-): The linear cyanate ligand may coordinate the metal center through the nitrogen (M-NCO) or the oxygen (M-OCN) or both (M-NCO-M). The N-C and C-O bond distances of the cyanate ion are 1.17 Å and 1.23 Å, respectively. Majority of the reported complexes are N-bonded. The observed ranges for asymmetric stretching, symmetric stretching and bending

vibrations of the cyanate are 2050-2250, 1200-1400 and 420-480 cm^{-1}, respectively. Expected coordination modes of the cyanate ion are shown in Scheme 1.3.

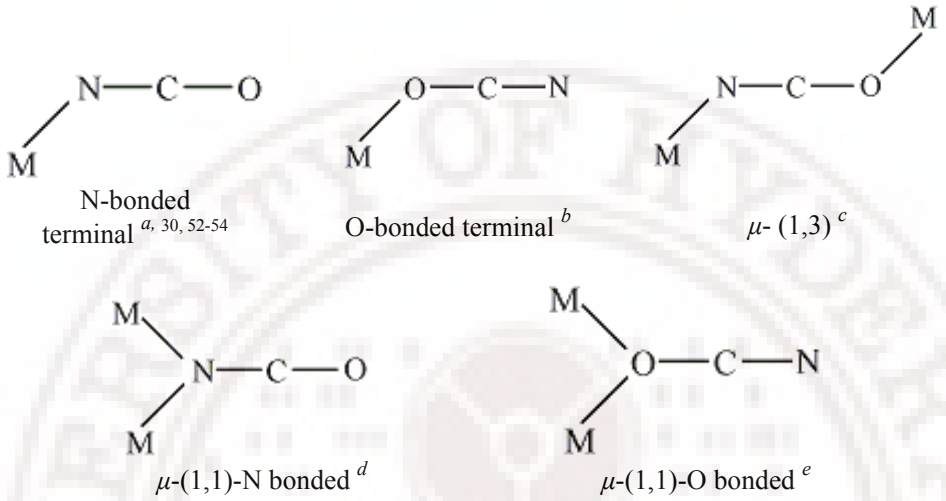

Scheme 1.3. Different coordination modes of cyanate ion. Reference is given for Mn(III)-cyanate complex. [a]260 for all transition metals, 4 Mn^{3+}. [b]16 for all transition metals. [c]12 for all transition metals. [d]51 for all transition metals. [e]1 for all transition metals.

1.3. Classification of the Mn(SB)X complexes:

1.3.1. Mononuclear complexes: these are divided into two types. (i) Five coordinated complexes[1-15,44-47] in which the manganese ion has square pyramidal geometry. The tetradentate Schiff base ligand coordinates the Mn(III) atom in equatorial mode and the axial position is occupied by an anionic ligand. (ii) Six coordinated complexes[16-25,32-35,42,48-51] have distorted octahedral geometry and the tetradentate ligand binds the Mn(III) atom in the equatorial mode and axial positions are occupied by anionic ligand and solvent molecule.

1.3.2. Dinuclear complexes: In these complexes the tetradentate Schiff base ligand can coordinate in two different modes. (i) Equatorial mode: In all phenoxo-bridged dimeric complexes[30], the tetradentate SB coordinates in the equatorial mode. (ii) *Cis*-octahedral mode: This mode, seen for example in $[Fe(salpn)N_3]_{2,}$[38] wherein the azide ion acts as a bridging ligand is not known for Mn(III) complexes.

1.3.3. Polymers: Depending upon the crystallization conditions, the Mn(SB)X complexes may sometimes build *trans*-μ-(1,3)-bridged 1D-polymeric chains along the Jahn-Teller axis.[35-42,51] In these complexes the tetradentate Schiff ligand coordinates in the equatorial mode, and the axial positions are occupied by X. A mixed *trans*-μ-(1,3/1,1)-azide bridged complex[42] as well as a *trans*-μ-(1,1)-azide bridged polymer with an additional carboxylate ligand[43] has been reported. With the bidentate ligand acac, *trans*-μ-(1,3)-azide bridged polymeric chain is obtained in $Mn(acac)_2N_3$.[41]

1.3.4. Weak interactions: Aggregation of mononuclear complexes into dimers and networks via H-bonding involving coordinated or lattice solvent molecules have been reported.[32]

1.4. Magnetic Properties:[58]

1.4.1. Mononuclear complexes: The low temperature magnetic moment in magnetically dilute Mn(III) compounds is influenced by zero field splitting. The splitting arises from a dipolar interaction of the form S.***D***.S which lifts the 5-fold degeneracy in zero field as shown below.

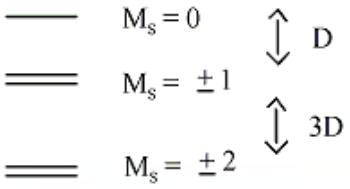

The above scheme assumes axial symmetry so that the interaction can be written has $D\{S_z^2 - \frac{1}{3}S(S+1)\}$, where $D = \frac{3}{2}D_{\parallel}$ and $D_{\perp} = -\frac{1}{2}D_{\parallel}$.

Further, the above ordering of levels assume a negative value of *D*, which is usually the case for octahedral Mn(III) complexes[59a-c] wherein the axial component of the ligand is weaker than the equatorial component. The *D* parameter is generally small (0-2 cm^{-1}) so that significant increase in magnetic moment is felt only below about 8K.

Often mononuclear complexes are not magnetically dilute in the solid state. This is due to presence of weak intermolecular interactions such as H-bonding and π-stacking. In such situations one or more exchange terms are superimposed on the zero field term in the spin Hamiltonian. It is not normally practical to include each exchange coupling individually since such an approach may lead to over parametrization. Instead, it may be possible to model the intermolecular interaction using the molecular field approximation,[59d] which simply adds a single average term to the molecular susceptibility.

1.4.2. Dinuclear complexes: The spin Hamiltonian can be written as $\beta S_1 \cdot \boldsymbol{g_1} \cdot H + \beta S_2 \cdot \boldsymbol{g_2} \cdot H - 2J S1 \cdot S2 + S_1 \cdot \boldsymbol{D_1} \cdot S_1 + S_2 \cdot \boldsymbol{D_2} \cdot S_2 + S_1 \cdot \boldsymbol{D_{12}} \cdot S_2 + d_{12}$ S1 x S2 (positive *J* implies ferromagnetic coupling such that for $S_1 = S_2 = 1/2$, the singlet-triplet gap = 2*J*). Often simplifying assumptions are made in using this Hamiltonian.[58b] If the exchange

parameter *J* is sufficiently large compared to zero field splitting it may be possible to use the dimer equation[60] to fit magnetic susceptibility data. However if *J* is not large enough zero field splitting can not be neglected and the susceptibility has to be calculated by including the population of energy levels at each temperature, the energy level being derived by diagonalisation of the full Hamiltonian matrix.[61] In both approaches interdimer interactions may be included within the molecular field approximation.

Several phenoxo-bridged complexes have been characterized (Table 1.1). The exchange parameters are within the range –3.4 to 12.6 cm^{-1}. Some of the phenoxo-bridged complexes are ferromagnetic and have been investigated for their single molecule magnetism (SMM).[30,64,69] SMM implies the following: (i) High spin ground state for the molecule and (ii) molecular compound after being magnetized by an applied field retains its magnetism even when the field is removed. This implies slow relaxation within a zero dimensional system (molecule). Usually this is observed only at very low temperature (≤ 10K). Relaxation is then studied by frequency dependent measurements in an AC susceptibility apparatus. In AC susceptibility measurements, magnetic susceptibility is measured at small (~1 Oe) oscillating magnetic field. A plot of both in-plane (χ') and out-of-plane (χ'') component of the susceptibility is plotted against temperature. An SMM compound shows a maximum in both plots. The maxima shift to higher temperature as the frequency is increased. The inverse of the frequency gives an estimate of the relaxation time (τ) at the temperature corresponding to the maximum in the χ'' verses T plot. A plot of log ι verses 1/T is generally straight line as a result of the Arrhenius law.

$$\tau = \tau_0 e^{\frac{T_0}{T}}$$

This measurement yields τ_0 and T_0. These quantities can also be determined in presence of a static field. It should be mentioned that if there are more than one relaxation mechanisms, the Arrhenius plot may correspond to more than one straight line. In Mn(III) phenoxo-bridged dimers the negative *D* value of the dimer is believed to favor slow relaxation and the emergence of the SMM property.

Table 1.1. Selected bond distances (Å) and bond angles (º) and magnetic parameter of few phenoxo-bridged Mn(III) dimers. (F = ferro, AF = antiferromagnetic interaction, NI = non interaction and ND = no data in the literature)

	Mn-O	Mn-O*	O-Mn-O*	Mn-O-Mn*	Mn-Mn*	F/AF	Magnetic Properties				
							g	J/cm^{-1}	D/cm^{-1}	zJ/cm^{-1}	Ref.
1	1.916(1)	2.513(1)	79.43	100.58(4)	3.428	F	2.022	0.42(2)	0.0006	0.002	This thesis
2	1.902(2)	2.588(2)	81.46	98.55	3.433	F	2.000	0.58(1)	-2.32	–0.06	
3	1.912(1)	2.493(1)	78.76	101.23	3.425	AF	1.997	–0.20(2)	-0.009	–0.05	
4	1.907(2)	2.411(2)	77.88	102.1(1)	3.374	AF	2.017	–0.7(1)	–0.6(1)	–0.02	
5	1.922(2)	2.492(2)	78.53	101.5(5)	3.437	F	2.01	0.88	-0.025	0.026	
a	1.901(5)	2.412(6)	79.42(2)	100.6(2)	3.334(3)	F	2.0000	6.30	–1.70		62
b	1.894(3)	2.411(3)		100.4	3.325	F	2.0150	3.70		0.41	63
c	1.911(2)	2.341(2)	80.42(7)	99.58(7)	3.258(5)	F	1.96	1.8	–4.5		64
d	1.909(2)	2.434(2)	78.42(1)	101.6(1)	3.381(1)	F	1.93	1.79	–2.53	–0.79	15
e	1.896(3)	2.662(3)	79.4(1)	100.6(1)	3.541(1)	F	1.96	1.20	–0.38		
f	1.872(2)	3.441(2)	83.76(8)	96.24(8)	4.092(8)	F	1.99	0.55	–1.25		
g	1.877(2)	3.758	83.43(1)	96.57	4.388(9)	F	2.03	0.12	–1.00		
h	1.892(5)	3.505(5)	85.8(2)	94.2(2)	4.102(2)	F	2.04	0.38	–1.87		
i	1.891(1)	2.813(5)	99.57(5)		3.641(5)	F	1.98	1.35	–1.9		30
j	1.863(4)	3.190(2)	98.4(2)		3.922(2)	F	1.98	0.6	–1.0		
k	1.898(1)	2.793(0)	97.82(0)		3.584	F	2.03	0.73	–0.3		
l	1.918(7)	2.728(2)	100.0(1)		3.597(3)	F	2.00	0.55	–4.1		
m	1.908	2.395(3)	99.85(1)		3.307(4)	AF	1.96	–0.45	–1.0		
n	1.93(6)	2.120(3)		99.93(7)	3.539(6)	F	2.01	0.42	0		36
o	1.88(1)	2.87(1)	83.22	96.76	3.611	F	1.99	1.32			31
p	1.912(4)	2.375(5)	78.2(2)	101.83	3.341(2)	AF	2.00	–0.55			

q	1.912(3)	2.305(2)	76.6(1)	103.4(1)	3.318(1)	AF		–1.68			65
r	1.906(6)	2.419(7)			3.350	AF					66
s	1.891(3)	2.490(3)	80.7(1)	99.3(1)	3.361	AF					67
t	1.880(6)	2.750(6)	81.3(2)	98.7(2)	3.558(3)	AF					68
u	1.923(3)	2.539		100.00	3.441(1)	NI					51
v	1.902(3)	2.557(3)	80.14(1)	99.86	3.438	-	-	-	-	-	46b

1. $[Mn(salpn)NCO]_2$. 2. $[Mn(salmen)N_3]_2$. 3. $[Mn(acphpn)N_3]_2$. 4. $[Mn(acphen)NCS]_2$. 5. $[Mn(5\text{-}Clsalpn)N_3]_2$. [a]$[Mn(salen)(H_2O)]_2(ClO4)_2$. [b]$[Mn(L)(H_2O]_2(ClO_4)_2$[L=*N,N'*-bis(2-hydroxyacetophenylidene)-1,2-diaminopropane]. [c]$[Mn(salpn)H_2O]_2$. [d]$[Mn(saltmen)(H_2O)]ClO_4$. [e]$[Mn(naphtmen)(H_2O)]ClO_4$. [f][Mn(saltmen)(NCS)]. [g][Mn(naphtmen)(NCS)]. [h][Mn(naphtmen)(Cl)]. [i]$[Mn(saltmen)(O_2CCH_3)]_2.2CH_3CO_2H$. [j]$[Mn(saltmen)(N_3)]_2$. [k]$[Mn(salen)(NCO]_2$. [l][Mn(3,5-Brsalen)(3,5-Brsalicylaldehyde)]$_2$. [m]$[Mn(5\text{-}Brsalen)(CH_3OH)]_2.(ClO_4)_2$. [n]$[Mn(5\text{-}Clsalen)N_3]_2$. [o]$[Mn_2(L2^{2-})_2(N_3)_2]$, [L2 = bis-(*o*-hydroxyacetophenone)-ethylenediimine]. [p]$[Mn_2(L1^{2-})_2(N_3)_2]$, [L1 = *N, N'*-(1,1-dimethylethylene)-bis-(salicylaldiimine)]. [q]$[Mn(L)(H_2O)]_2.(ClO_4)_2$ [L = *N*-(acetylacetonylidene)-N'-(α-methylsalicylidene)-ehtylenediamine]. [r]$[Mn_2(bsalen)_2(H_2O)_2](ClO_4)_2$ [bsalen = *N,N'*-ethylenebis(5-bromosalicylideneiminato) dianion]. [s]$[Mn(salen)(H_2O)]_2(ClO_4)_2.H_2O$. [t][Mn((salen)(NCS)]. [u]$[Mn(salpn)NCS]_2$. [v][Mn((salen)(Him)]$_2(ClO_4)_2$.2MeOH. [w][Mn(saltmen)(H_2O)](TCNQ). [x]$[Mn_2(5\text{-}Clsalltmen)_2(H_2O)]_2(ClO_4)_2$. [y]$[Mn_2(5\text{-}Clsalltmen)_2(5\text{-}Clsal)]_2(ClO_4)_2$. [z]$[Mn(L^2)(TCEA)][L^2$=*N,N'*-(1,1,2,2-tetramethylethylene)bis(3-hydroxy-4-napthylideneiminate] (TCEA = tricyanoethenolate). [v]$[Mn(salen)NCS]_2$.

1.4.3. Extended systems: Magnetic characterization of linear chain compounds have been reported for azide and thiocyanate complexes.[35-39,41a,43,51] These chains are built from 1,3-pseudohalide bridges. The interaction is antiferromagnetic with *J* in the range, –3.0 to –6.5 cm^{-1}. Spin canting leading to weak ferromagnetism has been observed.[35,36,51] While mononuclear as well as dinuclear complexes often assemble into higher dimensional structures via intermolecular interactions, a systematic study of the effect of these interaction on magnetic property has not yet been made.

***1.5. Electronic spectra of Mn(III) compounds*:** For d^4 ion in octahedral symmetry, a single d-d band is expected. However low symmetry distortions lead to splitting of this band giving rise to 3 bands in the high energy end of visible region extending into UV. Charge transfer and intra ligand absorption bands are superimposed on the d-d bands. When chiral Schiff base ligands are used, it is possible to observe circular dichroism (CD) for the absorption bands.[70] This may help in the assignment, because circular dichroism arising from the chiral center in the ligand is expected to be more pronounced for intra ligand and charge transfer bands than d-d bands.

1.6. Scope of the present work:

(i) Preparation of several Mn(SB)X, where SB is tetradentate Schiff base ligand including chiral ligands and X is a pseudohalide ion. The ligand systems used are given in Scheme 1.4.

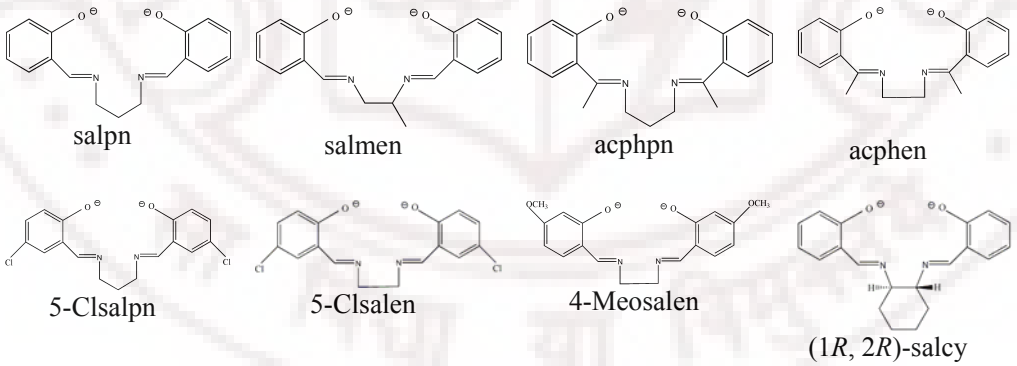

Scheme 1.4.

Nomenclature of the Schiff bases are given in the list of abbreviation.

(ii) Structural characterization of the above complexes and observation of polymorphs wherever possible. Polymorphs may arise due to different mode of aggregation of Mn(SB)X: dimerisation through phenoxo-bridge; 1,3-bridged chain; 1,1-bridged chain.

(iii) Characterization of intermolecular interaction which may have important bearing on magnetic properties.

(iv) Measurements of the magnetic data wherever possible with collaboration with other groups. Measurements include variable temperature magnetic susceptibility at static and oscillating fields in order to characterize SMM systems.

(v) Analysis and interpretation of magnetic data and attempts at magneto-structural correlation.

1.7. References

1. Hirotsu, M.; Nakajima, K.; Kojima, M.; Yoshikawa, Y. *Inorg. Chem.* **1995**, *34*, 6173.
2. Das, D.; Cheng, C. P. *J. Chem. Soc. Dalton Trans.* **2000**, 1081.
3. Egami, H.; Irie, R.; Sakai, K.; Katsuki, T. *Chem. Lett*. **2007**, *36*, 46.
4. Martinez, A.; Hemmert, C.; Gornitzka, H.; Meunier, B. *J. Organomet. Chem.* **2005**, *690*, 2163.
5. Lenoble, G.; Lacroix, P. G.; Daran, J. C. *Inorg. Chem.* **1998**, *37*, 2158.
6. Pecoraro, V. L.; Butler, W. M. *Acta Crystallogr.* **1986**, *C**42***, 1151.

7. Cho, S. -H.; Ma, B.; Nguyen, S. T.; Hupp, J. T.; Albrecht, T. E. -S. *Chem. Commun.* **2006**, 2563.

8. Jacobsen, E. N.; Zhang, W.; Muci, A. R.; Ecker, J. R.; Deng, L. *J. Am. Chem. Soc.* **1991**, *113*, 7063.

9. Pospisil, P. J.; Carsten, D. H.; Jacobsen. E. N. *Chem. -Eur. J.* **1996**, *2*, 974.

10. Rispens. M. T.; Metsma, A.; Feringa, B. L. *Recl. Trav. Chim. Pays-Bas.* **1994**, *113*, 413.

11. Yoon, J. W.; Yoon, T. -S.; Lee, S.W.; Shin. W. *Acta Crystallogr.* **1999**, *C55*, 1766.

12. Fronczek, F. R.; Bu, X. R. J. *CCDC No.* TOVNIB02, **2002**.

13. Starikova, Z. A.; Antipin, M. Y.; Danilova, T. I.; Permyakov, E.A.; Rozenberg, V. I. *Russ. J. Inorg. Chem.* **2002**, *47*, 1623.

14. Oki, A. R.; Hodgson. D. J. *Inorg. Chim. Acta.* **1990**, *170*, 65.

15. Miyasaka, H.; Clerac, R.; Ishii, T.; Chang, H.; Kitagawa, S.; Yamashita, M. *J. Chem. Soc., Dalton Trans*. **2002**, 1528.

16. Mitra, K.; Biswas, S.; Lucas, C. R.; Adhikary, B. *Inorg. Chim. Acta.* **2006**, *359*, 1997.

17. Panja, A.; Shaikh, N.; Ali, M.; Vojtisek, P.; Banerjee, P. *Polyhedron*, **2003**, *22*, 1191.

18. Bermejo, M. R.; Castineiras, A.; Garcia J. C. -M.; Rey, M.; Sousa, A.; Watkinson, M.; McAuliffe, C. A.; Pritchard, R. G.; Beddoes, R. L. *J. Chem. Soc. Dalton Trans.* **1996**, 2935.

19. Motevalli, M. M.; Watkinson, M. *Acta Crystallogr.* **2002**, *C58*, m258.

20. Dang, L. -L.; Huo, Y. -Q.; Wang, W.; Li. J. *Acta Crystallogr.* **2005**, ***E61***, m332.

21. Horwitz, C. P.; Dailey, G. C.; Tham, F. S. *Acta Crystallogr.* **1995**, *C**51***, 815.

22. Hwang, I. -C.; Ha, K.; *Z. Kristallogr. -New Cryst.Struct*. **2006**, *221*, 363.

23. Hwang, I. -C.; Ha, K.; *Z. Kristallogr. -New Cryst.Struct*. **2006**, *221*, 365.

24. Korendovych, I.V.; Rybak, E.V. -A. *Acta Crystallogr.* **2004**, *C**60***, m82.

25. Hwang, I. -C.; Ha, K. *Acta Crystallogr.* **2007**, *E63*, m2365.

26. Zhang, W.; Loebach, J.L.; Wilson, S.R.; Jacobsen, E. N. *J. Am. Chem. Soc*. **1990**, *112*, 2801.

27. Jacobsen, E.N. Ojima, I. (Ed.), *Catalytic Asymmetric Synthesis*, VCH, New York, **1993**, p. 159.

28. Noda, K.; Hosoya, N.; Irie, R.; Ito, Y.; Katsuki, T. *Synlett.* **1993**, 469.

29. Li, Z.; Conster, K.R.; Jacobsen, E.N. *J. Am. Chem. Soc.* **1993**, *115*, 5326.

30. Lu, Z.; Yuan, M.; Pan, F.; Gao, S.; Zhang, D.; Zhu, D. *Inorg. Chem*. **2006**, *45*, 3538 (and references therein).

31. Saha, S.; Mal, D.; Koner, S.; Bhattacherjee, A.; Gutlich, P.; Mondal, S.; Mukherjee, M.; Okamoto, K. -I. *Polyhedron*, **2004**, *23*, 1811.

32. Nastase, S.; Tuna, F.; Maxim, C.; Muryn, C. A.; Avarvari, N.; Winpenny, R. E. P.; Andruh, M. *Cryst. Growth Des*. **2007**, *7*, 1825.

33. Zhang, K. -L.; Xu, Y.; Song, Y.; Zhang, Y.; Wang, Z.; You, X. -Z. *J. Mol. Struct.* **2001**, *570*, 137.

34. Sen, S.; Mitra, S.; Luneau, D.; Fallah, M. S. E.; Ribas. J. *Polyhedron*, **2006**, *25*, 2737.

35. Yuan, M.; Zhao, F.; Zhang, W.; Wang, Z. -M. Gao, S. *Inorg. Chem.* **2007**, *46*, 11235.

36. Ko, H. H.; Lim, J. H.; Kim, H. C.; Hong, C. S. *Inorg. Chem*. **2006**, *45*, 8847.

37. Panja, A.; Shaikh, N.; Vojtisek, P.; Gao, S.; Banerjee. P. *New J. Chem*. **2002**, *26*, 1025.

38. Reddy, K. R.; Rajasekharan, M. V.; Tuchagues, J. -P. *Inorg. Chem*. **1999**, *37*, 5978.

39. Li, Hui.; Zhong, Z. J.; Duan, C. -Y.; You, X. -Z.; Mak, T. C. W.; Wu. B. *Inorg. Chim. Acta.* **1998**, *271*, 99.

40. Feng, Y. -L. *Chin. J. Struct. Chem.* **2002**, *21*, 352.

41. (a) LI, W.; Li, Z.; Li, L.; Liao, D.; Jiang, L. *J. Solid State Chem*. **2007**, *180*, 2973. (b) Stults, B. R.; Marianelli, R. S. Day, V. W. *Inorg. Chem*. **1975**, *14*, 722.

42. Darensbourg, D. J.; Frantz, E. B. *Inorg. Chem*. **2007**, *46*, 5967.

43. He, Z.; Wang, Z. -M.; Gao, S.; Ya**n,** C. -H. *Inorg. Chem*. **2006**, *45*, 6694.

44. Mikuriya, M.; Yamato, Y.; Tokii, T. *Bull. Chem. Soc. Jpn.* **1992**, *65*, 1466.

45. Biswas, S.; Mitra, k.; Schwalbe, C.H.; Lucas, C. R.; Chattopadhyay, S. K.; Adhikary. B. *Inorg. Chim. Acta*. **2005**, *358*, 2473.

46. Li, H.; Zhong, Z. J.; Duan, C. -Y.; You, X. -Z.; Mak, T. C. W.; Wu, B. *J. Coord. Chem.* **1997**, *41*, 183.

47. Yun-Long, F.; Shi-Xiong, L. *Chin. J. Struct. Chem.* **1996**, *15*, 47. *CAS No*: ZULEV.

48. Chakraborty, J.; Samanta, B.; Pilet, G.; Mitra, S. *Struct. Chem.* **2006**, *17*, 585.

49. (a) Feng, Y. -L.; Liu, S. -X. *J. Coord. Chem.* **1998**, *44*, 81. (b) Shou-Bin, W.; Kun, T.; Bao-Hua, Y.; Sheng, L. *Acta Crystallogr.* **2008**, *E64*, m543.

50. (a) Bertoncello, K.; Fallon, G. D.; Murray, K. S.; Tiekink, E. R. T. *Inorg. Chem.* **1991**, *30*, 3562. (b) Joseph, A. B.; Martin L. K.; Myoung, S. L.; Dimitri, P. K.; William, E. H.; Vincent L. P. *Inorg. Chem.* **1989**, *28*, 180. (c) Weiss, M. C.; Goedken, V. L. *Inorg. Chem.* **1979**, *18*, 274.

51. Sailaja, S.; Reddy, K. R.; Rajasekharan, M. V.; Hureau, C.; Riviere, E.; Cano, J.; Girerd, J. J. *Inorg. Chem.* **2003**, *42*, 180.

52. Mikuriya, M.; Yamato, Y.; Tokii, T. *Chem. Lett*. **1991**, 1429.

53. Mikuriya, M.; Yamato, Y.; Tokii, T. *Bull. Chem. Soc. Jpn.* **1992**, *65*, 2624.

54. Rae, A. D.; Mossin, S.; Sorensen, H.O. *Acta Crystallogr.* **2005**, *B**58***, 407.

55. Matsumoto, N.; Sunatsuki, Y.; Miyasaka, H.; Hashimoto, Y.; Luneau, D.; Tuchagues, J. -P. *Angew. Chem. Int. Ed.* **1999**, *38*, 171.

56. Vrieze, K.; van Koten, G. In *Comprehensive Coordination Chemistry*; Wilkinson, G., Gillard, R. D., McCleverty, J. A., Eds; PergamonPress: Oxford, England, **1987**; Vol. 2, p 225.

57. Nakamoto, K. *Infrared and Raman Spectra of Inorganic and coordination Compounds*; 3 ed.; John Wiley & Sons, Inc.: New York, **1997**, pp 270.

58. (a) Willett, R. D.; Gatteschi, D.; Kahn, O. *Magneto-Structural Correlations in Exchange Coupled Systems,* NATO-ASI Series C 140*,* Reidel, Dortrecht **1985**.

(b) Khan, O. *Molecular Magnetism*, VCH, New York, **1993**. (c) Gatteschi, D.; Sessoli, R.; Villain, J. *Molecular Nanomagnets*, Oxford University Press, New York, **2006**.

59. (a) Kennedy, B. J.; Murray, K. S. *Inorg. Chem*. **1985**, *24*, 1557. (b)Whittaker, J. W.; Whittaker, M. M. *J. Am. Chem. Soc*. **1991**, *113*, 5528. (c) Zhang, Z.-Y.; Brouca-Cabarrecq, C.; Hemmert, C.; Dahan, F.; Tuchagues, J.-P. *J. Chem. Soc. Dalton Trans*. **1995**, 1453. (d) Khan, O. *Molecular Magnetism*, VCH, New York, **1993,** p. 26, 131.
60. O'Connor, C. J. *Prog. Inorg. Chem.* **1982***, 29*, 203.
61. Garge, P.; Chikate, R.; Padhye, S.; Savariault, J.-M.; de Loth, P.; Tuchagues, J.-P. *Inorg. Chem*. **1990**, *29*, 3315.
62. Shyu, H.; Wei, H.; Wang, Y. *Inorg. Chim. Acta* **1999**, *290*, 8.
63. Karmakar, R.; Choudhury, C. R.; Bravic, G.; Sutter, J.-P.; Mitra, S. *Polyhedron* **2004**, *23*, 949.
64. Lecren, L.; Wernsdorfer, W.; Li, Y.-G.; Vindigi, A.; Miyasaka, H.; Clerac, R. *J. Am. Chem. Soc*. **2007**, *129*, 5045.
65. Matsumoto, N.; Zhong, Z.; Okawa, H.; Kida, S. *Inorg. Chim. Acta* **1989**, *160*, 153.
66. Bermejo, M. R.; Castineiras, A.; Garcia-Montergudo, J. C.; Rey, M.; Sousa, A.; Watkinson, M.; McAuliffe, C. A.; Pritchard, R. G.; Beddose. R. I. *J. Chem, Soc., Dalton Trans.* **1996**. 2935.

67. Garcia-Deibe, A.; Sousa, A.; Bermejo, M. R.; MacRory, P. P.; McAuliffe, C. A.; Pritchard, R. G.; Hellowell, M. *J. Chem. Soc., Chem. Commun*. **1991**, 728.

68. (*a*) Mikuriya, M.; Yamato, Y.; Tokii, T. *Bull. Chem. Soc. Jpn*. **1992**, *65*, 1466. (*b*) Kennedy, B. J.; Murray, K. *Inorg. Chem*. **1985**, *24*, 152.

69. Miyasaka, H.; Saitoh, A.; Abe, S. *Coord. Chem. Rev.* **2007**, *251*, 2622.

70. Wen, H. -R.; Wang, C. -F.; Li, Y. -Z.; Zuo, J. -L.; Song, Y.; You, X. -Z. *Inorg. Chem.* **2006**, *45*, 7032.

UNIVERSITY OF HYDERABAD

CHAPTER II

Synthesis, Crystal Structure and Magnetic Properties of Dimeric Mn^{III} Schiff Base Complexes Including Pseudohalide Ligands. Ferromagnetic Interactions through Phenoxo Bridges and Single Molecule Magnetism

2.1. Introduction

Schiff base complexes of Mn^{III}, though well known, continue to generate interest due to their potential applications in fields as diverse as homogeneous catalysis and magnetic materials.[1] Complexes of general formula Mn(SB)X, where SB is a tetra-dentate Schiff base and X is usually an anionic ligand, often crystallize as phenoxo-bridged dimers which may exhibit a range of magnetic interactions depending upon the bridge geometry.[2-19] Some of these complexes have been investigated in detail for their SMM (single molecule magnet) properties.[6,19] Magnetic properties of one dimensional chains formed by bridging ligands (for example, azide[20]) and more recently, coordination networks resulting from second coordination sphere interactions[21] have also been reported. In this chapter, three new phenoxo-bridged complexes, Mn(salpn)NCO (**1**), Mn(salmen)N_3 (**2**), and Mn(acphpn)N_3 (**3**) crystallographic structure determination, spectral and variable temperature magnetic studies discussed in detail. The Schiff bases involved are depicted in Scheme 1.4. Even though these new complexes do not greatly enlarge in the of bridging geometries already reported for this class of compounds, they do not

demonstrate the role of intermolecular interactions in causing dramatic differences between otherwise similar magnetically coupled systems. In particular, compound **1**, unlike any other previously reported phenoxo-bridged Mn(III,III) system remains ferromagnetic in the entire temperature rang 2 – 300 K with a high spin (S = 4) ground state.

2.2. Experimental Section

2.2.1. Synthesis

All chemicals used for synthesis were reagent grade. The Schiff bases were formed *in situ* in the presence of the appropriate metal salt. **Caution:** Azide compounds are potentially explosive and should be prepared only in small quantities and handled with care.

[Mn(salpn)NCO]$_2$ (1): In a beaker open to the atmosphere, salicylaldehyde (0.244 g, 1.00 mmol) and 1,3-diaminopropane (0.071 g, 1.0 mmol) were stirred in 40 mL of ethanol. $Mn(CH_3COO)_2.4H_2O$ (0.245 g, 1.00 mmol) was added, and stirring was continued for about 1 h. To the resulting solution, NaOCN (0.130 g, 2.00 mmol) dissolved in a minimum amount of water was added, stirring continued for 3 h, to complete the aerial oxidation of Mn^{II}. The filtered solution was kept in a refrigerator (5º C) for one week when dark green crystals deposited. Yield: 0.234 g (0.62 mmol, 62%). Anal. Calcd. for $C_{18}H_{16}N_3O_3Mn$: C, 57.1; H, 4.27; N, 11.14. Found: C, 57.20; H, 4.23; N, 11.23. Characteristic IR absorptions (cm^{-1}): ν_a(NCO) 2160, ν_s(NCO) 1313, δ(NCO) 615, $\nu_{schiff\ base}$(C=N) 1620.

$[Mn(salmen)N_3]_2$ (2): In a beaker open to the atmosphere, salicylaldehyde (0.244 g, 1.00 mmol) and 1,2-diaminopropane (0.074 g, 1.0 mmol) were stirred in 40 mL of methanol. $Mn(CH_3COO)_2.4H_2O$ (0.245 g, 1.00 mmol) was added, and stirring was continued for about 1 h. To the resulting solution, NaN_3 (0.130 g, 2.00 mmol) dissolved in a minimum amount of water was added and stirring continued for 3 h to complete the aerial oxidation of Mn^{II}. The resulting microcrystalline precipitate was filtered off and dried. Yield: 0.306 g (0.81 mmol, 81%). It was recrystallized by slow evaporation of an acetonitrile solution at room temperature yielding dark-brown X-ray quality crystals. Anal. Calcd. for $C_{18}H_{16}N_5O_2Mn$: C, 54.12; H, 4.27; N, 18.57. Found: C, 54.19; H, 4.32; N, 18.98. Characteristic IR absorptions (cm^{-1}): $\nu_a(N_3)$ 2035, $\nu_s(N_3)$ 1309, $\delta(N_3)$ 599, $\nu_{schiff\ base}(C=N)$ 1612.

$[Mn(acphpn)N_3]_2$ (3): In a beaker open to the atmosphere, $Mn(CH_3COO)_2.4H_2O$ (0.245 g, 1.00 mmol) and NaN_3 (0.130 g, 2.00 g) were dissolved in 30 mL methanol and filtered. 2-Hydroxyacetophenone (0.272 g, 2.00 mmol) and 1, 3-diaminopropane (0.071 g, 1.0 mmol) were dissolved in 30 mL methanol and filtered. The two solutions were mixed and stirred for 2h to complete the aerial oxidation of Mn^{II}. The filtered solution was kept at room temperature for three days to obtain dark green crystals. Yield: 0.254 g (0.63 mmol, 63%). Anal. Calcd. for $C_{19}H_{20}N_5O_2Mn$: C, 56.25; H, 4.98; N, 17.26. Found: C, 56.45; H, 4.98; N, 17.36. Characteristic IR absorptions (cm^{-1}): $\nu_a(N_3)$ 2038, $\nu_s(N_3)$ 1300, $\delta(N_3)$ 522, $\nu_{schiff\ base}(C=N)$ 1587.

2.2.2. Physical Measurements

IR spectra were obtained in KBr pellets using Shimadzu FT-IR 8000 spectrometer. Elemental analysis of the complexes was performed on a FLASH EA SERIES CHNS analyzer. Absorption spectra for **1-3** in methanol were measured on a Shimadzu UV-3100 PC spectrometer. The magnetic susceptibility was measured in the 1.98-300 K temperature range using a Quantum Design MPMS SQUID susceptometer. The samples were pressed into pellets to avoid orientation effects of the microcrystals during magnetic measurements. Diamagnetic corrections were applied using Pascal's constants.[22] The magnetic susceptibilities have been computed both with the program SUSCEP[23] based on the expression derived from the isotropic spin-exchange Hamiltonian $\hat{H} = -2J\hat{S}_1\hat{S}_2$ ($S_1 = S_2 = 2$) and van Vleck's equation,[24] and by exact calculations of the energy levels associated to the spin Hamiltonian through diagonalization of the full matrix with a general program for axial symmetry.[25] In the latter case, least-squares fittings were accomplished with an adapted version of the function-minimization program MINUIT.[26]

2.2.3. X-ray Crystallography

X-ray data were collected for compounds **1-3** on a Bruker SMART APEX CCD X-ray diffractometer, using graphite-monochromated Mo-Kα radiation (λ = 0.71073 Å). Data were reduced using SAINTPLUS,[27] and a multi-scan absorption correction using SADABS[28] was performed. The structures were solved using SHELXS-97 and full matrix least squares refinements against F^2 were carried out using SHELXL-97.[29] All ring hydrogen atoms were assigned on the basis of

Table 2.1 Crystallographic data and structure refinement for **1**, **2** and **3**

	1	**2**	**3**
Formula	$C_{36}H_{32}Mn_2N_6O_6$	$C_{34}H_{32}Mn_2N_{10}O_4$	$C_{38}H_{40}Mn_2N_{10}O_4$
Formula weight	754.56	754.58	810.68
Crystal system	monoclinic	monoclinic	monoclinic
a (Å)	8.6269(5)	8.6770(17)	8.4760(5)
b (Å)	13.6701(8)	13.731(3)	20.2098(12)
c (Å)	14.3355(8)	14.326(3)	10.3259(6)
α (º)	90	90	90
β (º)	105.1050(10)	104.316(3)	91.2810(10)
γ (º)	90	90	90
V (Å^3)	1632.18(16)	1653.8(6)	1768.37(18)
Space group	$P\,2_1/n$	$P\,2_1/n$	$P\,2_1/n$
Z	2	2	2
T (K)	100(2)	298(2)	298(2)
ρ_{calcd} (g cm^{-3})	1.535	1.515	1.522
μ (mm^{-1})	0.832	0.820	0.772
θ Range (º)	2.09 - 28.26	2.09 - 28.31	2.02 - 28.24
h/*k*/*l* indices	-11, 11/ -18,18/ -18, 19	–11, 11/ –17, 18/ –18, 18	–11,11/ –26, 26/ –13, 13
Reflections collected	18686	18714	20250
Unique reflection, R_{int}	4047, 0.0218	3969, 0.0536	4221, 0.0280
GooF	1.363	1.058	1.028
$R_1[I > 2\sigma(I)]$	0.0351	0.0616	0.0360
wR_2 [all data]	0.0986	0.1361	0.0916
$\Delta\rho_{max}$, $\Delta\rho_{min}$ (e.Å^{-3})	0.328, -0.223		
Weight. scheme (A, B)	0.0518, 0.46	0.0702, 0.58	0.0588, 0.29

geometrical considerations and were allowed to ride upon the respective carbon atoms. All hydrogen atoms were assigned fixed U_{iso} values, equal to $1.2U_{eq}$ of the parent atom for ring and $1.5U_{eq}$ for methyl hydrogens. Crystallographic data and structure refinement parameters are presented in Table 2.1.

2.3. Results and Discussion

2.3.1. Crystal Structures

All three complexes crystallize in the $P2_1/n$ space group. Complexes **1** and **2** have almost identical formula weights and nearly equal unit cell dimensions, even though their chemical compositions are different. The crystals of all three complexes contain dinuclear Mn^{III} entities (Figure 2.1), wherein the two centrosymmetrically related five-coordinate metal centers are held by two weak phenoxo bridges (Mn···O in the 2.49-2.59 Å range). Within each five-coordinate unit, the tetradentate Schiff base ligand chelates in the equatorial mode, while the axial position is occupied by a nitrogen atom from the pseudo-halide ion, azide or cyanate, coordinating in a bent mode. The equatorial donor atoms (O_2N_2) are very nearly coplanar even though the manganese atom deviates significantly from this plane (0.16 Å in **1**; 0.20 Å in **2**; 0.13 Å in **3**). The mean planes of the two halves of the Schiff base ligands (excluding the methylene groups) are inclined with respect to each other by 15º in the three crystals. There are only slight differences in the Mn–(N,O) distances in the three complexes: Mn–O(*eq*.)$_{av}$, Mn–N(*eq*.)$_{av}$, Mn–N(*ax*.) are respectively, 1.90, 2.01, 2.14 Å in **1**; 1.88, 1.99, 2.14 Å in **2**; 1.89, 2.01, 2.17 Å in **3**. The overall coordination geometry of each

Mn^{III} ion is thus distorted octahedral with the Jahn-Teller elongation along the NCO/NNN–Mn...O axis.

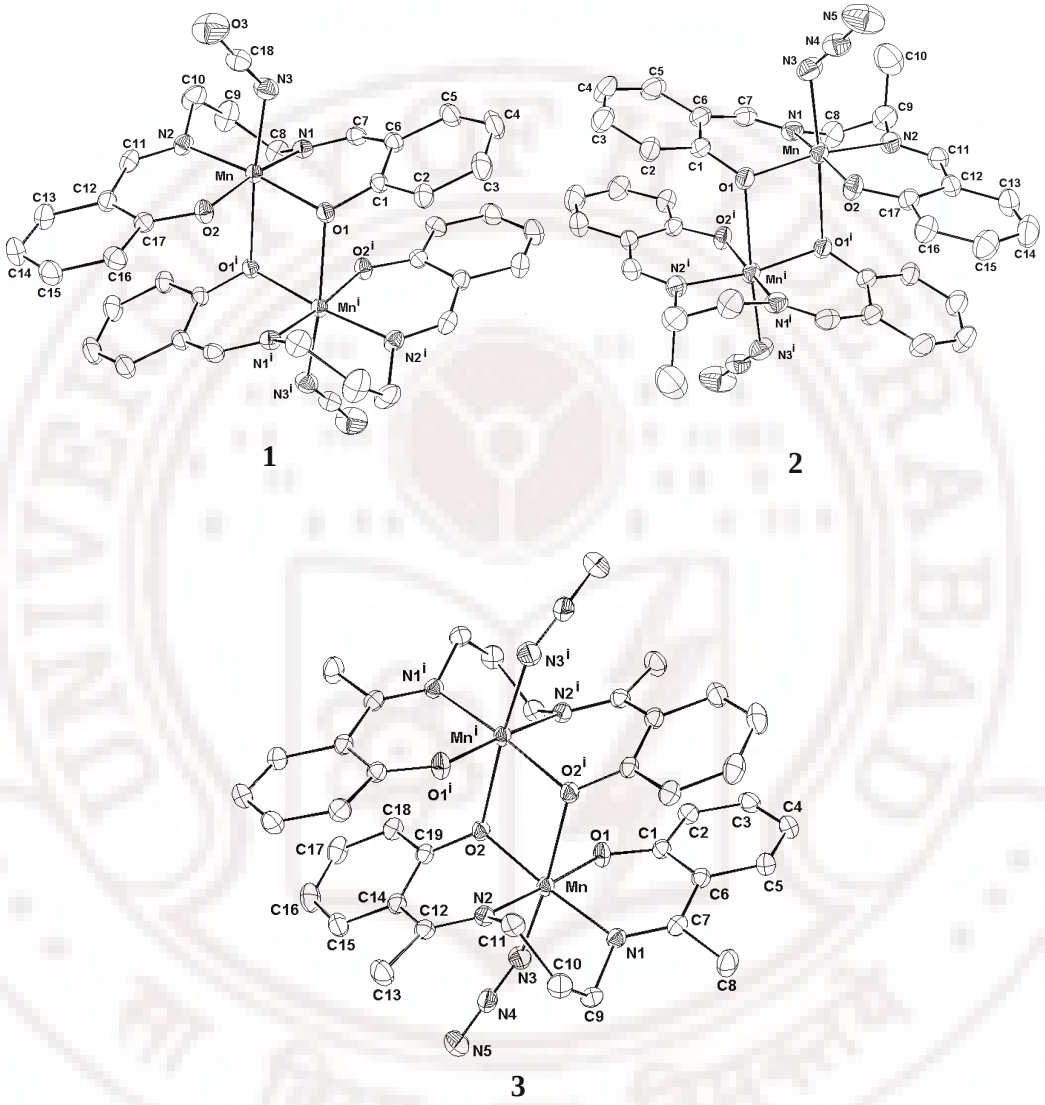

Figure 2.1 ORTEP view of the dimers in $[Mn(salpn)NCO]_2$ (**1**) $[Mn(salmen)N_3]_2$ (**2**) $[Mn(acphpn)N_3]_2$ (**3**). Hydrogen atoms are omitted, and the thermal ellipsoids are represented at the 30% probability level.
i = $–x$+1,$–y$+1,$–z$+1 for **1**; $–x$+1,$–y$+1,$–z$+1 for **2**; $–x$,$–y$+2,$–z$ for **3**.

Table 2.2 Selected bond lengths [Å] and angles [°] for $[Mn(salpn)NCO]_2$ (**1**)

Mn-O1	1.9162(11)	Mn-N1	2.0261(13)	Mn-N3	2.1394(15)
Mn-O2	1.8757(11)	Mn-N2	1.9920(13)	Mn-O1#1	2.5130(11)
N3-C18	1.169(2)	C18-O3	1.195(2)		
O1-Mn-N1	87.73(5)	O2-Mn-N1	169.90(5)	O1-Mn-O1#1	79.42(4)
O1-Mn-N2	170.78(5)	O2-Mn-N2	90.58(5)	O2-Mn-O1#1	86.42(4)
O1-Mn-N3	96.07(6)	O2-Mn-N3	95.82(6)	N1-Mn-O1#1	83.50(5)
N1-Mn-N3	94.29(6)	O2-Mn-O1	91.07(5)	N2-Mn-O1#1	91.63(5)
Mn-N3-C18	135.11(14)	N2-Mn-N1	89.06(6)	N3-Mn-O1#1	175.02(5)
N3-C18-O3	178.2(2)	Mn-O1-Mn#1	100.58(4)	#1 –*x*+1, –*y*+1, –*z*+1	

Table 2.3 Selected bond lengths [Å] and angles [°] for $[Mn(salmen)N_3]_2$ (**2**)

Mn-O1	1.903(2)	Mn-N1	1.988(3)	Mn-N3	2.137(3)
Mn-O2	1.860(2)	Mn-N2	1.984(3)	Mn-O1#1	2.589(2)
N3-N4	1.183(5)	N4-N5	1.153(5)		
O1-Mn-N1	88.85(11)	O2-Mn-N1	169.18(11)	O1-Mn-O1#1	81.46(9)
O1-Mn-N2	163.55(12)	O2-Mn-N2	92.15(12)	O2-Mn-O1#1	87.61(9)
O1-Mn-N3	96.15(12)	O2-Mn-N3	97.00(13)	N1-Mn-O1#1	82.78(10)
N1-Mn-N3	92.79(13)	O2-Mn-O1	94.65(10)	N2-Mn-O1#1	83.87(10)
Mn-N3-N4	127.8(3)	N2-Mn-N1	81.93(13)	N3-Mn-O1#1	174.99(11)
N3-N4-N5	177.9(5)	Mn-O1-Mn#1	98.55(4)	#1 –*x*+1, –*y*+1, –*z*+1	

Table 2.4 Selected bond lengths [Å] and angles [°] for $[Mn(acphpn)N_3]_2$ (**3**)

Mn-O1	1.8633(12)	Mn-N1	2.0148(13)	Mn-N3	2.1722(16)
Mn-O2	1.9124(11)	Mn-N2	2.0050(13)	Mn-O2#1	2.4929(12)
N3-N4	1.177(2)	N4-N5	1.157(3)		
O1-Mn-N1	89.51(5)	O2-Mn-N1	169.78(5)	O2-Mn-O2#1	78.77(5)
O1-Mn-N2	174.51(6)	O2-Mn-N2	85.63(5)	O1-Mn-O2#1	88.00(5)
O1-Mn-N3	91.59(6)	O2-Mn-N3	95.91(6)	N1-Mn-O2#1	91.84(5)
N1-Mn-N3	93.52(6)	O1-Mn-O2	94.16(5)	N2-Mn-O2#1	86.58(5)
Mn-N3-N4	130.80(14)	N2-Mn-N1	89.82(6)	N3-Mn-O2#1	174.61(5)
N3-N4-N5	178.5(2)	Mn-O2-Mn#1	101.23(5)	#1 –*x*, –*y*+2, –*z*	

Coming to the dimer formed by bridging the five-coordinate complex molecules, the plane of the Mn_2O_2 bridge is nearly perpendicular to the equatorial coordination plane: dihedral angle, 88.5º in **1**, 87.4º in **2**, 89.7º in **3**. The axial N atom deviates only slightly from the bridging plane (0.08 Å in **1**; 0.16 Å in **2**; 0.03 Å in **3**). The most important difference between the three dimers arises from the bridging bond lengths (Å) and angles (º): Mn–O, Mn···O, Mn–O···Mn are respectively, 1.92, 2.51, 100.6 in **1**; 1.90, 2.59, 98.5 in **2**; 1.91, 2.49, 101.2 in **3**. The Mn···Mn distance in the three dimers is 3.43 Å. In summary, the bridge geometry in compound **3** is characterized by a shorter Mn···O distance coupled with a wider Mn–O···Mn angle while the longer Mn···O* distance goes with a more acute Mn–O···Mn angle in compound **2**; compound **1** has a bridge geometry intermediate between those of **2** and **3**. These differences have an important bearing on the magnetic properties. Selected bond distances and angles are collated in Tables 2.2-2.4.

2.3.2. Spectral Studies

2.3.2a. FTIR Spectra

The IR spectra of compound **1** exhibits strong absorption in the range of 2100-2200 cm^{-1}, which is attributed to the asymmetric stretching vibration of N-bonded cyanate group. Compounds 2 and **3** exhibit strong absorption in the range of 2030-2040 cm^{-1}, which is attributed to the asymmetric stretching vibration of N-bonded azide group. All three compounds exhibit strong absorption at 1590-1630 cm^{-1}, which is assignable to the (-C=N) stretching vibration of Schiff-base. All these absorptions are with in the reported range.[30]

2.3.2b. Electronic Spectra

In all three complexes, the Mn^{III} (d^4) is a high-spin ion, and it has distorted octahedral geometry. For pure octahedral d^4 (^5D ground state term) system, only one electronic absorption ($^5T_{2g} \leftarrow {}^5E_g$) is possible, due to distorted octahedral geometry the complexes **1-3** have four broad absorption bands. The solution spectra of the compounds **1-3** were measured in methanol (Figure 2.2). The low intensity absorption bands in the range 18.23, 351 for complex **1**, 16.07, 322 for complex **2**

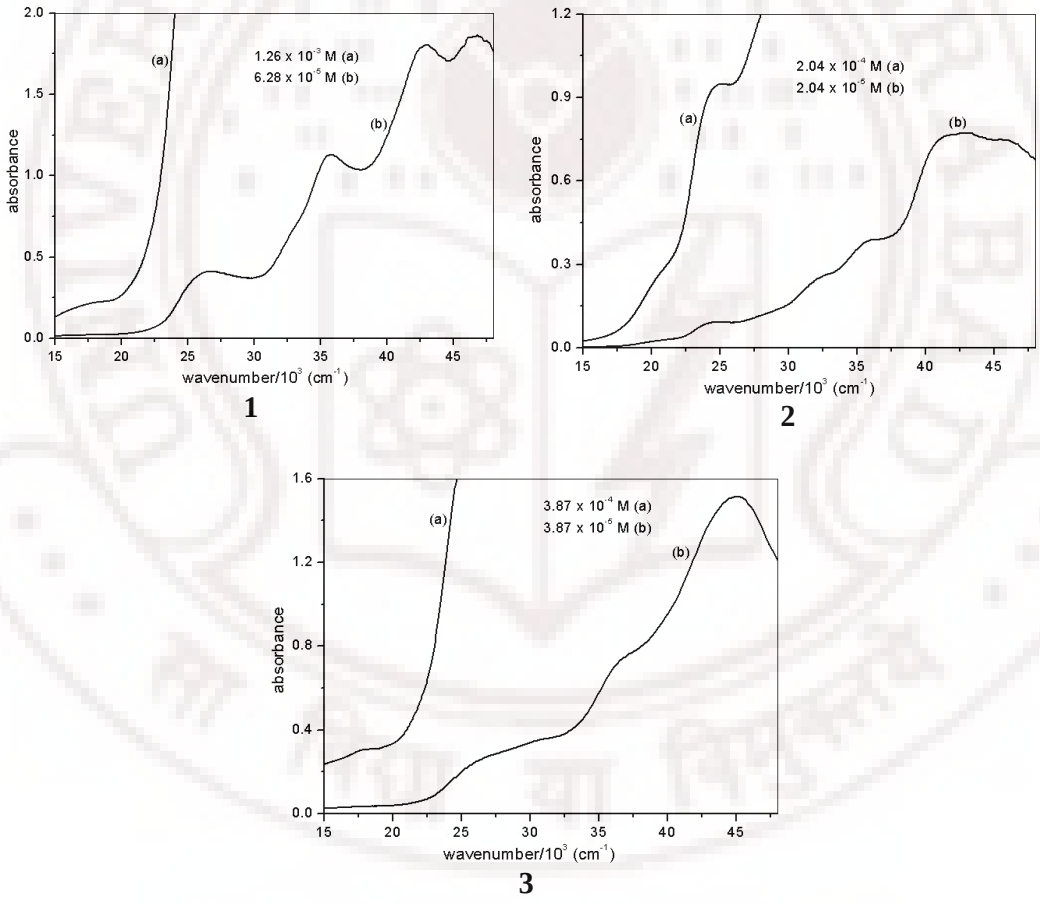

Figure 2.2 Electronic absorbance spectra of complex **1**, **2** and **3** in methanol.

and 18.93, 819 for complex **3** ($\bar{\nu}_{max}$ /10^3cm^{-1}, ε_{max}/cm^{-1}M^{-1}) respectively, which are assigned to d-d transition. The high intensity absorption bands in the range 26.72, 6487; 35.64, 17818; 42.73, 28614 for complex **1,** 24.27, 4637; 28.55, 6147; 32.22, 12230; 42.82, 38294 for complex **2**, and 26.77, 6899; 32.32, 9767; 45.12, 39069 for complex **3** ($\bar{\nu}_{max}$ /10^3cm^{-1}, ε_{max}/cm^{-1}M^{-1}) respectively, which are assigned to intraligand π-π* transitions in the complexes, the low intensity d-d transitions were masked in this range.

2.3.3. Magnetic Measurements

The variations of the molar magnetic susceptibility χ_m, and of the product $\chi_m T$ in the temperature range 1.98-300 K for the three complexes are shown in Figure 2.3. The room temperature $\chi_m T$ values (cm^3 mol^{-1} K) are nearly equal for the three dimers and comparable to the expected spin-only value of 6.00 cm^3 mol^{-1} K per dinuclear Mn^{III} unit: 6.19 for **1**; 5.99 for **2**; 5.90 for **3**. However, the three compounds behave differently when the temperature is lowered. In the case of compound **1**, $\chi_m T$ increases continuously to reach a value of 10.01 cm^3 mol^{-1} K at 1.98 K. Since the expected value for the S = 4 ground state is 10.00 cm^3 mol^{-1} K, the above result proves the ferromagnetic coupling within the dimer and the absence of significant competing effects from Mn^{III} single ion zero-field splitting and/or antiferromagnetic inter-dimer interactions. Compound **2** also shows an increase upon lowering the temperature. However a maximum $\chi_m T$ of 7.85 cm^3 mol^{-1} K is reached at 5.82 K. Further cooling leads to a rapid decrease to 6.34 cm^3 mol^{-1} K at 2 K. Therefore, while the intra-dimer interaction in compound **2** is ferromagnetic like in **1**, there are

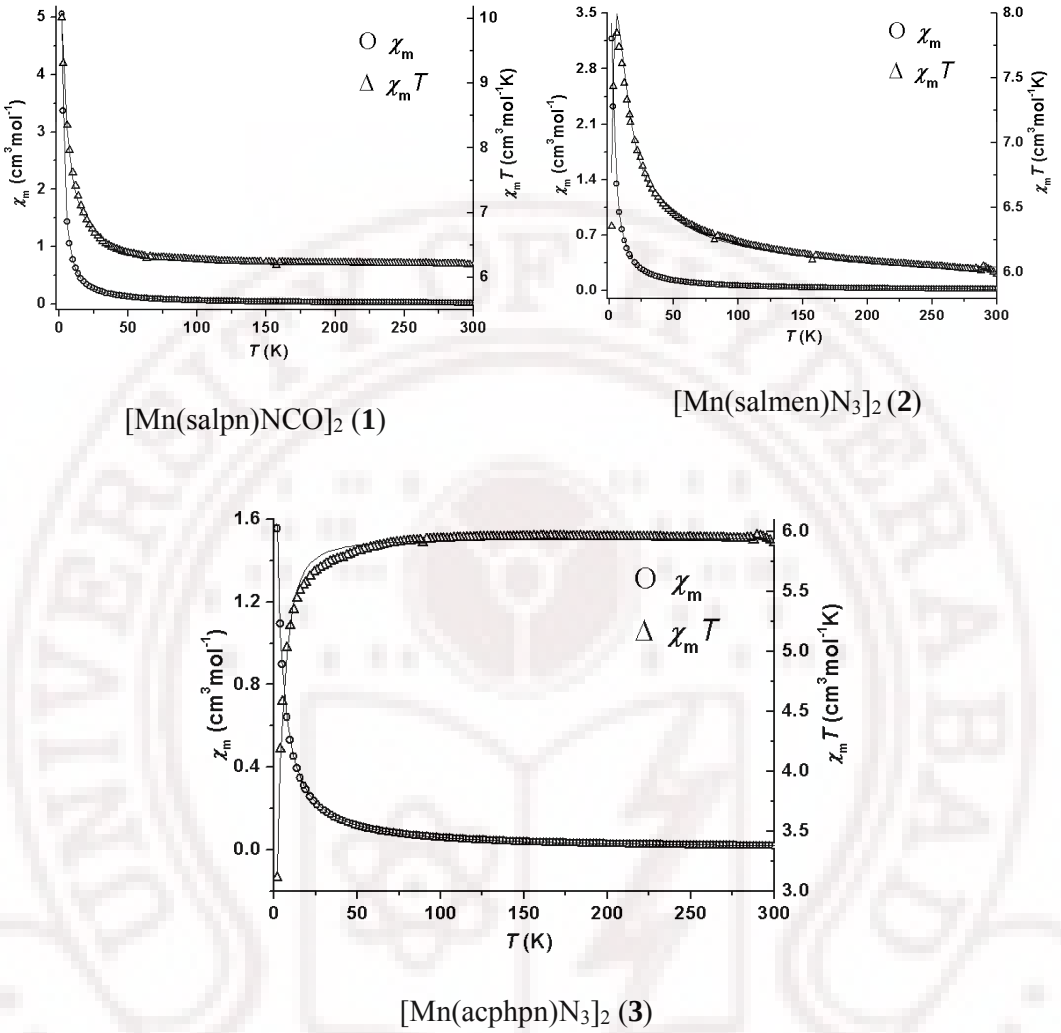

Figure 2.3. Temperature variation of the magnetic susceptibility χ_m and $\chi_m T$ product (per dimeric unit) for compounds **1** – **3**. Magnetic field strength used: 1000 Oe (**1**); 5000 Oe (**2**); 3000 Oe (**3**).

competing Mn^{III} single ion zero-field splitting (zfs) effects and/or antiferromagnetic inter-dimer interactions leading to a rapid fall in $\chi_m T$ below 6 K. In sharp contrast to **1** and **2**, compound **3** is clearly an antiferromagnetically coupled dimer with the $\chi_m T$

value decreasing continuously upon cooling from room temperature to reach a value of 3.11 cm^3 mol^{-1} K at 2 K.

The magnetic susceptibilities were therefore computed through exact diagonalisation of the spin Hamiltonian including Zeeman and zfs terms and isotropic exchange[25] and fitted to the experimental magnetic data by least-squares techniques.[26] The calculations employed the Hamiltonian, $\beta H \cdot g \cdot (S_1 + S_2) - 2JS_1 \cdot S_2 + D(S_{z1}^2 + S_{z2}^2)$. Although *g*-tensor was assumed to be axial, the difference between its parallel and perpendicular components was not significant. The single ion zero-field splitting parameter, *D* is identical for the two centrosymmetrically related Mn^{III} ions in the dimer. The best sets of parameters obtained by least square fitting were: **1**, J = 0. 42(2) cm^{-1}, D = 0.0006(2) cm^{-1}, g = 2.022(1), LSE (least squares error) = 0.00007; **2**, J = 0.58(1) cm^{-1}, D = – 2.32(4) cm^{-1}, g = 2.000(3), LSE = 0.0001; **3**, J = – 0.20(2) cm^{-1}, D = – 0.009(3) cm^{-1}, g = 1.997(2), LSE = 0.00003. The solid lines in the Figure 2.3 were computed using the above parameters. The differences between the three compounds are further illustrated in Figure 2.4, by plotting together their effective magnetic moments as a function of temperature. While the differences in *J* values are in agreement with the differences in bridge geometry in the molecular structures of **1**-**3**, the large zfs difference between **1** and **3** on the one hand, and **2** on the other hand, is difficult to explain in view of their very similar coordination geometries. This apparent discrepancy suggests that Mn^{III} zfs may not be the unique effect competing with the isotropic spin-spin interactions, but that possibly inter-dimer magnetic interactions also operate in these complexes. As a first step to check this hypothesis, we also

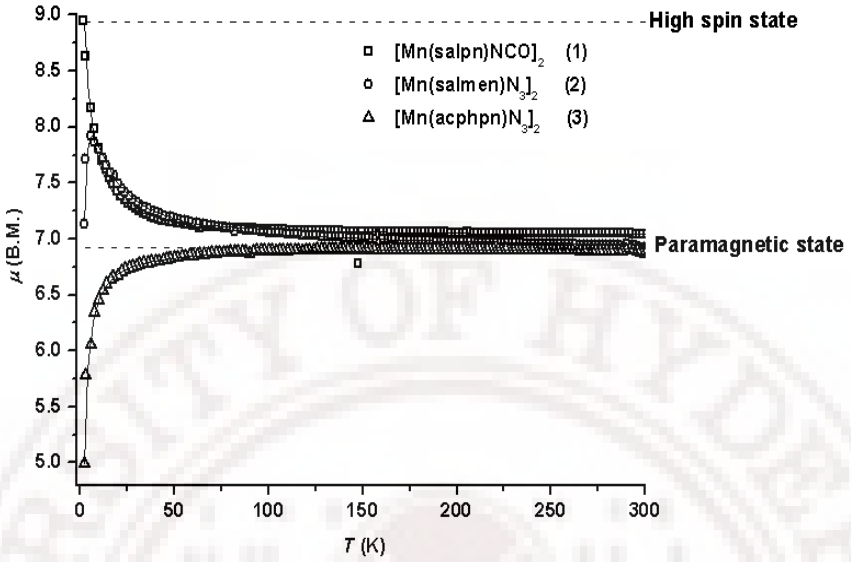

Figure 2.4. Temperature variation of magnetic moment (μ_{eff} per dimeric unit) for the three compounds (**1**, **2** and **3**)

computed the magnetic susceptibilities using the dimer model[24] including inter-dimer interactions within the molecular field approximation.[31] The best sets of parameters obtained by least square fitting were : **1**, J = 0.364(6) cm^{-1}, zj = 0.0020(3) cm^{-1}, g = 2.025(fixed), LSE = 0.002; **2**, J = 0.853(9) cm^{-1}, zj = – 0.0576(2) cm^{-1}, g = 1.99(fixed), LSE = 0.001; **3**, J = – 0.1385 (5) cm^{-1}, zj = – 0.0561 (5) cm^{-1}, g = 2.00(fixed), LSE = 0.0004. The quality of the fits, although satisfactory, was not as good as the previous ones, suggesting the operation of both Mn^{III} zfs and antiferromagnetic inter-dimer interactions, at least for **2** and **3**. As a further step, we also computed the magnetic susceptibilities through exact diagonalisation of the spin Hamiltonian including axial Zeeman and zfs terms, isotropic exchange, and inter-dimer interactions within the molecular field approximation. Although the quality of the fits was excellent, D and zj were correlated preventing us to safely estimate

independently the respective contribution of these two factors to the magnetic susceptibilities in this series of dimeric Mn^{III} compounds. Considering the similar Jahn-Teller elongation in complexes **1-3** the *D* is expected to be similar and negative in all the three compounds. Therefore, based on the observed temperature dependence of the magnetic moments and the fitting results, it is reasonable to conclude that the magnitude of *D* is very small for these compounds so that the variation of the magnetic moment at low temperatures is dominated by inter-dimer interactions.

It is worthwhile to examine the reason for the conspicuous difference in the inter-dimer interactions in compounds **1** and **2**. The intermolecular interactions between dimers are shown in Figure 2.5. The shortest Mn···Mn separation between dimers is nearly the same in both compounds: 8.86 Å in **1** and 8.68 Å in **2**. A close examination of the crystal packing shows that the important inter-dimer interactions present in both compounds are (i) =CH···N_c (2.52 Å in **1**; 2.47 Å in **2**), (ii) =CH···O_t / N_t (2.62 Å in **1**; 2.57 Å in **2**) and (iii) Ph-H···Cπ (2.83 Å in **1**; 2.66 Å in **2**) where, suffixes *c* and *t* refer to coordinated and terminal atom of the pseudohalide ion. The only difference between the two compounds is the presence of a π-stacking interaction (3.36 Å)[32] in **1** while such an interaction is blocked in **2** by the methyl group. Instead, a hydrogen atom of the methyl group in **2** is involved in a C-H···Phπ interaction (2.88 Å).[33] The above two contacts which distinguish the packing in the two compounds are shown by red dotted lines in Figure 2.5. Correlation of these observations with the magnetic data seems to suggest that the methyl group

interaction in **2** is responsible for the antiferromagnetic inter-dimer pathway, while the π-stacking in **1** is ferromagnetic and all other contacts common to both

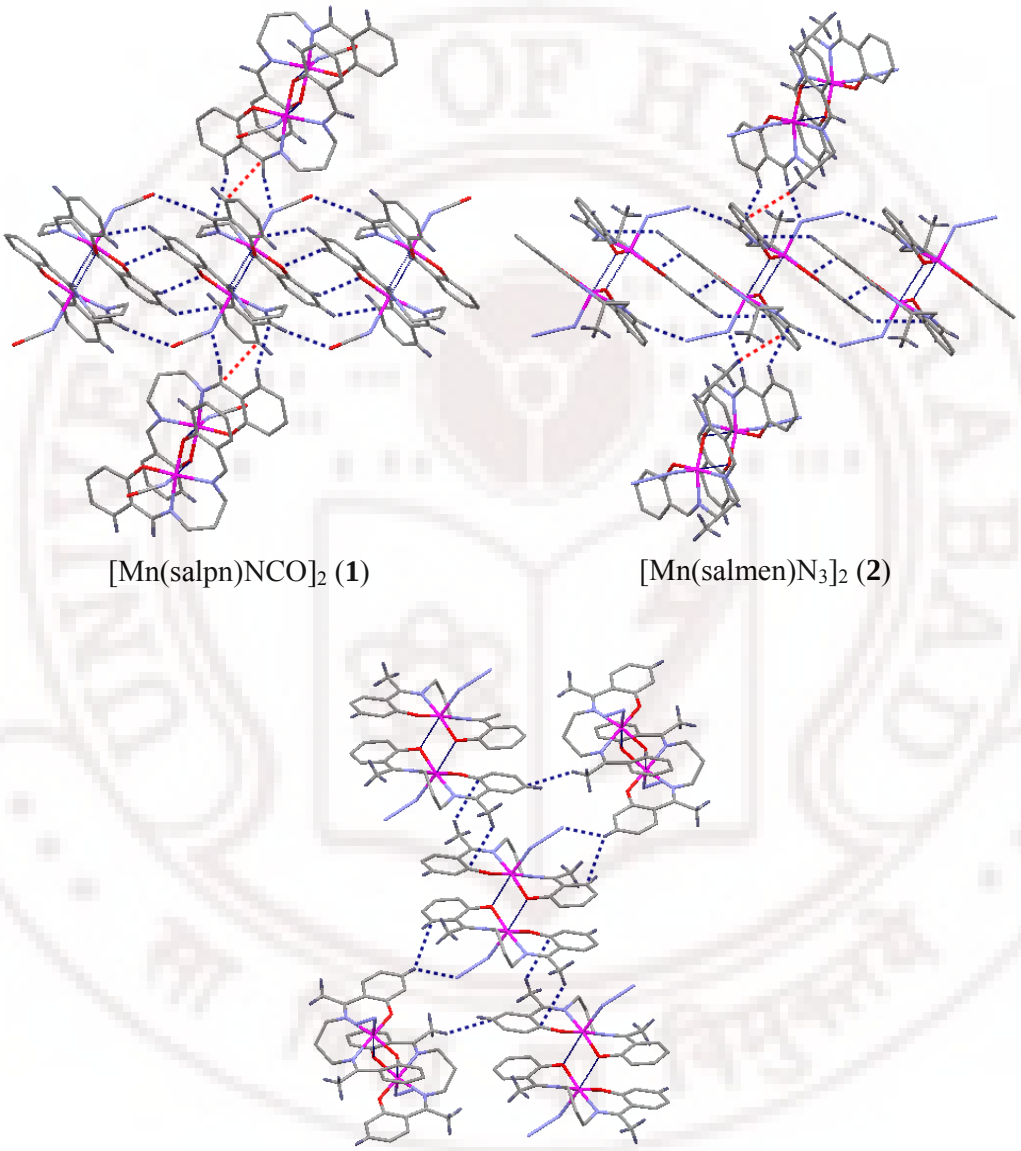

[Mn(salpn)NCO]$_2$ (**1**) [Mn(salmen)N$_3$]$_2$ (**2**)

[Mn(acphpn)N$_3$]$_2$ (**3**)

Figure 2.5. Intermolecular interactions between dimers in complexes **1**, **2** and **3**.

compounds may be of the antiferromagnetic type. This leads to a near-cancellation of the interdimer interactions so that the dimer in **1** remains ferromagnetically coupled down to 2K. The methyl C-H···Phπ interaction is also present in **3** (3.02, 3.13 Å) while the other interactions listed above are absent. The terminal azido in this compound is involved in a Ph-H···N interaction (2.59 Å). As noted above, the interdimer exchange interaction determined by the fitting of magnetic susceptibility is antiferromagnetic in this compound as well. DC-Magnetisation measurements were done for **1** and **2** mainly to check for hysteresis. Attempts to fit the magnetisation data (Figure 2.6) using the parameters previously derived from temperature variation of molar susceptibility gave satisfactory result only for **2**. It seems that a larger anisotropic term (D) will be needed for **1**. The reason for this discrepancy is not evident. The absence of hysteresis indicates that inter-dimer interactions do not lead to long range order in **1** and **2**, above 1.9 K.

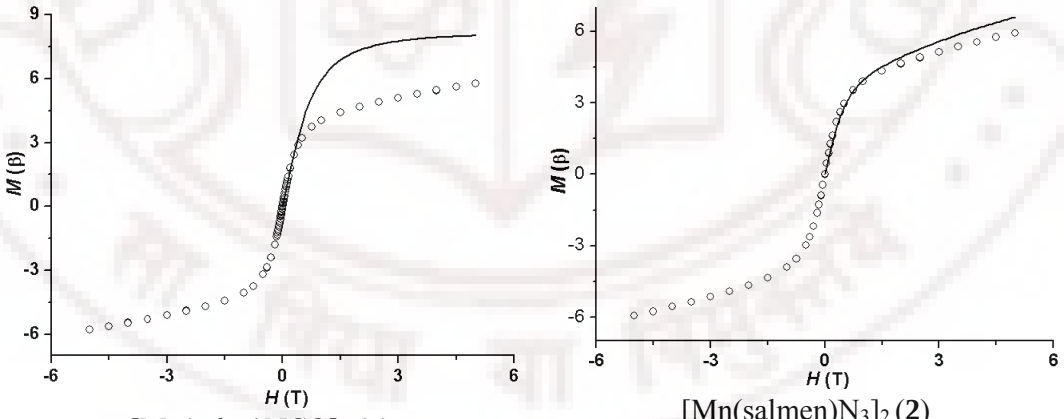

[Mn(salpn)NCO]$_2$ (**1**) [Mn(salmen)N$_3$]$_2$ (**2**)

Figure 2.6. Variation of magnetization with applied field at 2 K for complexes **1** and **2**. The solid lines represent simulations based on the parameters obtained by fitting the temperature dependent molar susceptibility data

A look at the twenty-odd phenoxo bridged dinuclear Mn^{III} compounds (Table 1.1) reported[2–19] to date shows that the exchange splitting, $2J$, falls in the range, –3.4 to 12.6 cm^{-1}, with only two instances of $2J > 4$ cm^{-1}. Further, the small magnitude of the interaction energy may reduce the precision with which it can be determined from least squares analysis when competing influences from zero-field splitting and inter-dimer interactions are present. Therefore, a precise correlation of exchange interactions with molecular structure is difficult to evaluate in this class of compounds. In the case of several dimers having water, thiocyanate or chloride as axial ligands and showing ferromagnetic interaction, it was found that the $2J$ value has a reciprocal correlation with the Mn···O bond distance (2.4-3.7 Å).[5] However, for the present compounds, the relationship is reversed, with the following respective Mn···O distances (Å) and $2J$ (cm^{-1}) values: 2.49, –0.4 (**3**); 2.51, 0.84 (**1**); 2.59, 1.16 (**2**). Because four magnetic orbitals are involved on each centre, it is unlikely that the exchange interaction may be controlled by just one structural parameter. In this respect, it is worth noting that the increase in $2J$ (cm^{-1}) parallels the decrease in Mn–O···Mn angle (º), with the following respective values: – 0.4, 101.2 in **3**; 0.84, 100.6 in **1**; 1.16, 98.5 in **2**.

In order to check whether compounds **1** and **2** behave as single molecule magnets (SMMs), their *ac* susceptibility was measured in the temperature range 2-10 K at two different frequencies (100 and 1000 Hz). The observation of frequency dependent in-phase (χ') and out-of-phase (χ'') magnetic susceptibilities (Figure 2.7) suggests an SMM behavior for both compounds. Even though no maxima were seen in the above data obtained with zero *dc* field, clear maxima appeared when a *dc* field

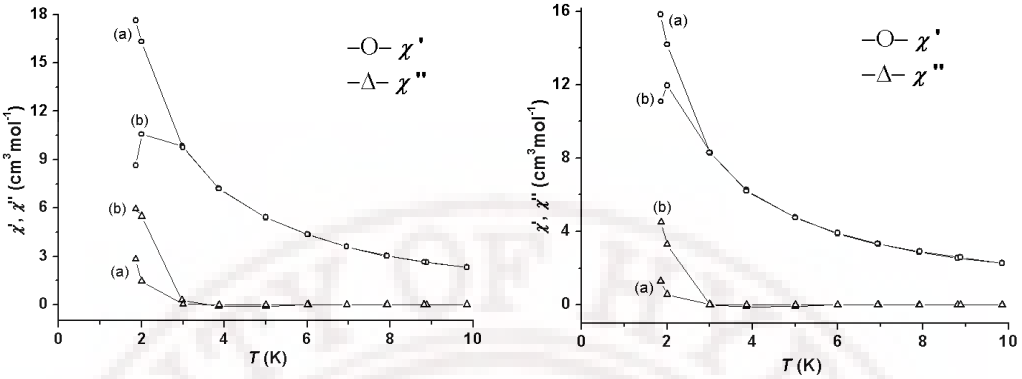

[Mn(salpn)NCO]$_2$ (**1**) [Mn(salmen)N$_3$]$_2$ (**2**)

Figure 2.7. Temperature variation of the in-phase (χ') and out-of-phase (χ'') components of the ac-magnetic susceptibility in zero static field for complexes **1** and **2** at, (a) 100Hz and (b) 1000Hz. Solid lines between the experimental data points are shown as a guide to the eye, they do not result from fitting.

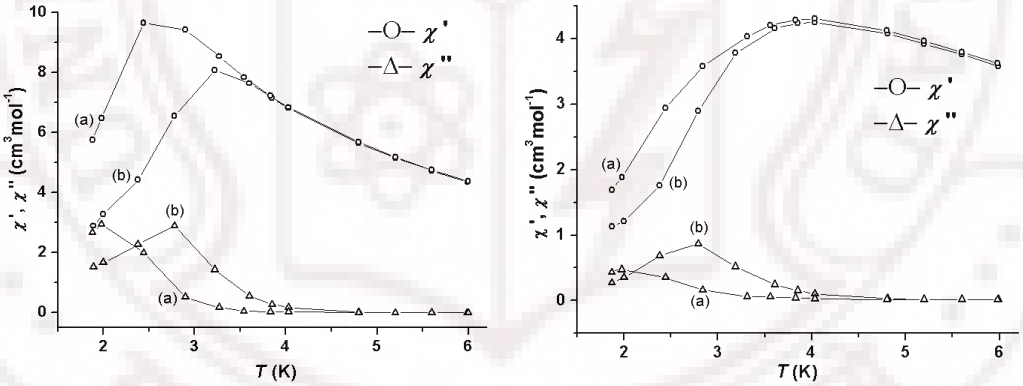

[Mn(salpn)NCO]$_2$ (**1**) [Mn(salmen)N$_3$]$_2$ (**2**)

Figure 2.8. Temperature variation of the in-phase (χ') and out-of-phase (χ'') components of the ac-magnetic susceptibility for complex **1** at a DC field of 0.1 T and for complex **2** at a DC field of 0.5 T. The AC field fluctuates at a frequency of (a) 100Hz and (b) 1000Hz. Solid lines between the experimental data points are shown as a guide to the eye, they do not result from fitting.

(0.1 and 0.5 T for complexes **1** and **2**, respectively) was applied (Figure 2.8). While the above results are in agreement with observation of an SMM behavior for other phenoxo bridged Mn^{III} dimers,[6] further detailed ac susceptibility measurements needed for evaluating the relaxation parameters of complexes **1** and **2** is not attempted in the present study.

2.4. Conclusions

The present results further demonstrate, in line with previous studies,[5,6] that a precise correlation of the magnetic exchange parameter with bridge geometry is difficult in the case of phenoxo-bridged dimers due to the weakness of the magnetic coupling and the involvement of several magnetic orbitals in the interaction. An important finding from the present study is that weak interdimer interactions like stacking or C-H$\cdots\pi$ can cause dramatic changes in the overall temperature dependence of the magnetic susceptibility as seen in the case of compounds **1** and **2**, both of which are ferromagnetically coupled dimers. Alkyl substituents on the Schiff base are effective in modulating the interdimer interactions causing differences in behavior at lower temperatures. The ferromagnetically coupled dimers, in spite of their very small magnitude of the zero field splitting do show evidence for single molecule magnetism.

2.5. References

1. *Review*: Wezenberg, S. J.; Kleij, A. W. *Angew. Chem. Int. Ed.* **2008**, *47*, 2.

2. Shyu, H.; Wei, H.; Wang, Y. *Inorg. Chim. Acta* **1999**, *290*, 8.

3. Karmakar, R.; Choudhury, C. R.; Bravic, G.; Sutter, J.-P.; Mitra, S. *Polyhedron* **2004**, *23*, 949.

4. Lecren, L.; Wernsdorfer, W.; Li, Y.-G.; Vindigi, A.; Miyasaka, H.; Clerac, R. *J. Am. Chem. Soc*. **2007**, *129*, 5045.

5. Miyasaka, H.; Clerac, R.; Ishii, T.; Chang, H.; Kitagawa, S.; Yamashita, M. *J. Chem. Soc., Dalton Trans*. **2002**, 1528.

6. Lu, Z.; Yuan, M.; Pan, F.; Gao, S.; Zhang, D.; Zhu, D. *Inorg. Chem.* **2006**, *45*, 3538.

7. Ko, H. H.; Lim, J. H.; Kim, H. C.; Hong, C. S. *Inorg. Chem*. **2006**, *45*, 8847.

8. Saha, S.; Mal, D.; Koner, S.; Bhattacherjee, A.; Gutlich, P.; Mondel, S.; Mukherjee, M.; Okamoto, K.-I. *Polyhedron*, **2004**, *23*, 1811.

9. Matsumoto, N.; Zhong, Z.; Okawa, H.; Kida, S. *Inorg. Chim. Acta* **1989**, *160*, 153.

10. Bermejo, M. R.; Castineiras, A.; Garcia-Montergudo, J. C.; Rey, M.; Sousa, A.; Watkinson, M.; McAuliffe, C. A.; Pritchard, R. G.; Beddose. R. I. *J. Chem, Soc., Dalton Trans.* **1996**. 2935.

11. Garcia-Deibe, A.; Sousa, A.; Bermejo, M. R.; MacRory, P. P.; McAuliffe, C. A.; Pritchard, R. G.; Hellowell, M. *J. Chem. Soc., Chem. Commun*. **1991**, 728.

12. (*a*) Mikuriya, M.; Yamato, Y.; Tokii, T. *Bull. Chem. Soc. Jpn*. **1992**, *65*, 1466. (*b*) Kennedy, B. J.; Murray, K. *Inorg. Chem*. **1985**, *24*, 152.

13. Sailaja, S.; Rajasekharan, M. V.; Hureau, C.; Riviere, E.; Cano, J.; Girerd, J.-J. *Inorg. Chem*. **200**3, *42*, 180.

14. (a) Mabad, B.; Luneau, D.; Theil, S.; Dahan, F.; Sarariault, J. M.; Tuchagues, J. P. *J. Inorg. Biochem.* **1991**, *43*, 373. (b) Kennedy, B. J.; Murray, K. S. *Inorg. Chem*. **1985**, *24*, 1552.

15. (a) Matsumoto, N.; Takemoto, N.; Ohyosi, A.; Okawa, H. *Bull. Chem. Soc. Jpn.* **1988**, *61*, 2984. (b) Mikuriya, M.; Yamato, Y.; Tokii, T. *Bull. Chem. Soc. Jpn.* **1992**, *65*, 1466.

16. Miyasaka, H.; Sugimoto, K.; Sugiura, K.; Ishii, T.; Yamashita, M. *Mol. Cryst. Liq. Cryst.* **2002**, *379,* 197.

17. Miyasaka, H.; Mizushima, K.; Furukawa. S.; Sugiura, K.; Ishii, T.; Yamasaka, H. *Mol. Cryst. Liq. Cryst.* **2002**, *379*, 171.

18. Sato, Y.; Miyasaka, H.; Matsumoto, N.; Okawa, H. *Inorg. Chim. Acta* **1996**, *247*, 57.

19. Miyasaka, H.; Saitoh, A.; Abe, S. *Coord. Chem. Rev.* **2007**, *251*, 2622.

20. Reddy, K. R.; Rajasekharan, M. V.; Tuchagues, J.-P. *Inorg. Chem.* **1998**, *37*, 5978.

21. Nastase, S.; Tuna, F.; Maxim, C.; Muryn, C. A.; Avarvari, N.; Winpenny, R. E. P.; Andruh, M. *Cryst. Growth Des.* **2007**, *7*, 1825.

22. Pascal, P. *Ann. Chim. Phys*. **1910**, *19*, 5.

23. Chandramouli, G. V. R.; Balagopalakrishna, C.; Rajasekharan, M. V.; Manoharan, P. T. *Comput. Chem.* **1996**, *20*, 353.

24. O'Connor, C. J. *Prog. Inorg. Chem.* **1982***, 29*, 203.

25. Garge, P.; Chikate, R.; Padhye, S.; Savariault, J.-M.; de Loth, P.; Tuchagues, J.-P. *Inorg. Chem*. **1990**, *29*, 3315.

26. James, F.; Roos, M. "*MINUIT Program*, a System for Function Minimization and Analysis of the Parameters Errors and Correlations"; *Comput. Phys. Commun.*, **1975**, *10*, 345.

27. SAINTPLUS, Bruker AXS Inc., Madison, Wisconsin, USA, 2003.

28. Sheldrick, G. M. SADABS, Program for Empirical Absorption Correction, University of Gottingen, Gottingen, Germany **1996**.

29. Sheldrick, G. M. SHELX-97, Programs for Crystal Structure Analysis, University of Gottingen, Gottingen, Germany **1997**.

30. Nakamoto, K. *Infrared and Raman Spectra of Inorganic and coordination Compounds*; 3 ed.; John Wiley & Sons, Inc.: New York, 1997, pp 270.

31. Ginsberg, A. P.; Lines, M. E. *Inorg. Chem.* **1972**, *11*, 2289.

32. Hunter, C. A. *Chem. Soc. Rev.* **1994**, 101.

33. Nishio, M. CrystEngComm **2004**, *6*, 130.

UNIVERSITY OF HYDERABAD

CHAPTER III

Antiferromagnetic interactions through phenoxo-bridges and lattice water. Synthesis, structure and magnetic properties of new Mn(III) Schiff base complexes in combination with thiocyanate ligand

3.1. Introduction

The five coordinate Mn^{3+} ion in Mn(SB)X, where SB is a tetradentate Schiff base[1] and X is a halide or pseudohalide, is known to attain six coordination in certain cases through the formation of a X-bridged one-dimensional chain or a phenoxo-bridged dimer.[2] There are also cases where the sixth coordination position is occupied by a solvent molecule, usually water.[3] In the case of phenoxo-bridged dimers, depending upon the Mn···O bond-length and Mn-O···Mn bond-angle, these complexes may show an intra-dimer ferro or antiferromagnetic interaction.[4-16] Dinuclear as well as larger assemblies formed by Mn(III) with tetradentate Schiff base ligands have been recently reviewed.[17] In the present work we report on two complexes, Mn(acphen)NCS and Mn(acphpn)(H_2O)NCS, where the ligands acphen and acphpn are obtained *in situ* by condensing 2-hydroxyacetophenone with 1,2-diaminoethane and 1,3-diaminopropane, respectively. The complex of acphen is a phenoxo-bridged dimer while the acphpn ligand yields a mononuclear aquo complex as a dihydrate. A previous preparation[3] using acphenH_2 had resulted in a mononuclear complex, Mn(acphen)(H_2O)NCS, even for acphen. An important result

from the present study is that both the compounds show weak antiferromagnetic coupling between Mn(III) centres. In the case of the mononuclear acphpn complex, the interaction arises from the presence of lattice water molecules, in sharp contrast to the above mentioned complex of acphen which forms only anhydrous crystals and displays no significant magnetic interaction.

3.2. Experimental Section

3.2.1. Synthesis

2-Hydroxyacetophenone, 1,2-diaminoethane and 1,3-diaminopropane were of reagent grade. The Schiff bases were formed *in situ* in the presence of the appropriate metal salt. Perchlorate salts are potentially explosive and should be prepared only in small quantities and handled with care.

$[Mn(acphen)NCS]_2$ (1): In a beaker open to the atmosphere, $Mn(CH_3COO)_2.4H_2O$ (0.245g, 1.00 mmol) and KSCN (0.194g, 2.00 mmol) were stirred in methanol (25 mL). 2-Hydroxyacetophenone(0.272g, 2.00 mmol) and 1,2-diaminoethane (0.060g, 1.0 mmol) were stirred in methanol (30 mL) and added to the above solution; stirring was continued for about 2h to complete the aerial oxidation of Mn^{2+} to Mn^{3+}. The filtered solution kept in a refrigerator (5 °C) yielded dark green crystals after 3 days. Yield: 0.252g (0.31 mmol, 62%). Anal. Cald. for $Mn_2C_{38}H_{36}N_8O_4S_2$: C, 56.02; H, 4.45; N, 10.31. Found: C, 56.18; H, 4.45; N, 10.78. Significant IR absorptions (cm^{-1}): 2054, 1599, 1535, 1433, 1325, 1140, 1084, 856, 750, 472.

$[Mn(acphpn)(H_2O)NCS]\cdot 2H_2O$ (2): In a beaker open to the atmosphere, 2-hydroxyacetophenone (0.272 g, 2.00 mmol) and 1,3-diaminopropane (0.071g 1.0

mmol) were stirred in methanol (40mL). $Mn(ClO_4)_2.6H_2O$ (0.361g, 1.00 mmol) was added, and the stirring was continued for about 1h. To the resulting solution, KSCN (0.194g, 2.00 mmol) dissolved in water (10 mL) was added, stirred for 5 minutes, and the filtered solution kept aside at room temperature for one day, over which time dark green crystals deposited. Yield: 0.289g (0.607 mmol, 60.7%). Anal. Calcd. for $MnC_{20}H_{26}N_3O_5S$: C, 50.53; H, 5.51; N, 8.84. Found: C, 50.48; H, 5.50; N, 9.03. Significant IR absorptions (cm^{-1}): 3344, 3200, 2085, 1643, 1597, 1433, 1319, 1150, 937, 854, 760, 599, 464.

3.2.2. Physical measurements

IR spectra were obtained in KBr pellets using Shimadzu FT-IR 8000 spectrometer. Elemental analysis of the complexes was performed on a FLASH EA SERIES CHNS analyzer. Absorption spectra for **1** and **2** in methanol were recorded on a Shimadzu UV-3100 PC spectrometer. The magnetic susceptibility was measured for **1** and **2** in a magnetic field of 5000 Oe and in the temperature range 1.98-300 K using a Quantum Design MPMS SQUID susceptometer. The samples were pressed into pellets to avoid orientation effects of the microcrystals during magnetic measurements. Diamagnetic corrections were applied using Pascal's constants. Fitting of the susceptibility data was initially done by using the program SUSCEP[18] based on the dimer equation[19a] for **1** and Curie-Weiss equation as well as chain equation[19b] for **2**. Final fittings for **1** were carried out through exact diagonalisation of the energy matrix including an axial zero field splitting (zfs) term,

Table 3.1. Crystallographic data and structure refinement for **1** and **2**

	1	**2**
Formula	$C_{38}H_{36}Mn_2N_6O_4S_2$	$C_{20}H_{26}MnN_3O_5S$
Formula weight	814.75	475.44
Crystal system	triclinic	orthorhombic
a (Å)	7.9128(6)	9.3234(8)
b (Å)	9.9970(7)	14.2756(12)
c (Å)	11.1144(8)	16.1270(14)
α (º)	92.7200(10)	90
β (º)	90.2690(10)	90
γ (º)	91.5390(10)	90
V (Å^3)	877.87(11)	2146.5(3)
Space group	$P\bar{1}$	*Pnma*
Z	1	4
T (K)	100(2)	100(2)
ρ_{calcd} (g cm^{-3})	1.541	1.471
μ (mm^{-1})	0.890	0.749
θ Range (º)	1.83 - 28.27	1.91 - 28.21
h/k/l indices	-10, 10/ -12, 13/ -14, 14	-12, 12/ -18, 18/ -21, 21
Reflections collected	10292	23625
Unique reflection, R_{int}	4094, 0.0367	2667, 0.0263
GooF	1.121	1.122
$R1[I > 2\sigma(I)]$	0.0478	0.0388
$wR2$[all data]	0.1083	0.0932
$\Delta\rho_{max}$, $\Delta\rho_{min}$ (e Å^{-3})	0.503, -0.298	0.792, -0.263
Weight. scheme (A, B)	0.0522, 0.30	0.0424, 2.26

D.[20] The isotropic Heisenberg exchange term used in the Hamiltonian is of the form $-2J\hat{S}_1\hat{S}_2$.

3.2.3. X-ray crystallography

X-ray data were collected for **1** and **2** on a Bruker SMART APEX CCD X-ray diffractometer, using graphite-monochromated Mo-Kα radiation (λ = 0.71073 Å). Data were reduced using SAINTPLUS[21] and a multi-scan absorption correction was applied using SADABS.[22] The structure was solved using SHELXS-97 and full matrix least squares refinement against F^2 was carried out using SHELXL-97.[23] All ring hydrogen atoms were assigned on the basis of geometrical considerations and were allowed to ride upon the respective carbon atoms with fixed U_{iso} values: $1.2U_{eq}$ of the parent atom (ring hydrogen atoms), $1.5U_{eq}$ for methyl and water hydrogen atoms. In **2**, one of the two lattice water molecules is disordered about the crystallographic mirror plane. Crystallographic data and structure refinement parameters are presented in Table 3.1.

3.3. Results and discussion

3.3.1. Synthesis

Both compounds were prepared by a similar procedure, except that compound **1** crystallized at 5º C, while **2** was obtained at about 25º C. Attempts to obtain other polymorphs of these complexes were not successful. Though in both cases the Schiff base was generated *in situ*, pure methanolic medium was used for the preparation of **1** while in the case of **2**, the crystals were obtained in a largely

aqueous medium. A previous preparation[3] using an acphenH_2 solution and Mn^{II} perchlorate hydrate resulted in the isolation of the mononuclear complex Mn(acphen)(H_2O)(NCS) as anhydrous crystals.

3.3.2. Crystal structure of [Mn(acphen)NCS]$_2$ (1)

Each unit of the phenoxo bridged dimer is made up of a tetradentate acphen ligand binding the Mn(III) ion in equatorial mode and an N-bonded terminal thiocyanato ion occupying the axial position (Figure 3.1). The structure has a crystallographic inversion centre at the mid point of the dimeric core. The Mn···O_p (where O_p is the oxygen atom of the phenoxo-bridge) bond distance is 2.411(2) Å and the bridge angle, Mn–O_p···Mn' is 102.14(7)º, both within the range of Type-1 out-of-plane dimers.[9] The Mn···Mn' distance is 3.374 Å. The basal atoms are approximately coplanar with deviations of 0.10 Å from the mean plane. The central Mn atom is displaced by 0.14 Å towards the thiocyanato ligand. The two halves of the acphen ligand, excluding the methylene and methyl groups are each nearly planar (rms deviations = 0.05, 0.07 Å) with an interplanar angle of 17.5º. The two halves of the ligand are unsymmetrically disposed about the basal coordination plane with interplanar angles of 12.7 and 29.0º. No short inter-dimer contacts are observed, the nearest intermolecular Mn···Mn' distance being 7.913 Å. The plane defining the $Mn_2(O_p)_2$ bridge makes an angle of 88.9º with the basal coordination plane, MnN_2O_2. The overall coordination geometry of each Mn(III) ion is distorted octahedral with the Jahn-Teller elongation along the SCN-Mn···O_p axis. Selected bond distances and angles are given in Table 3.2.

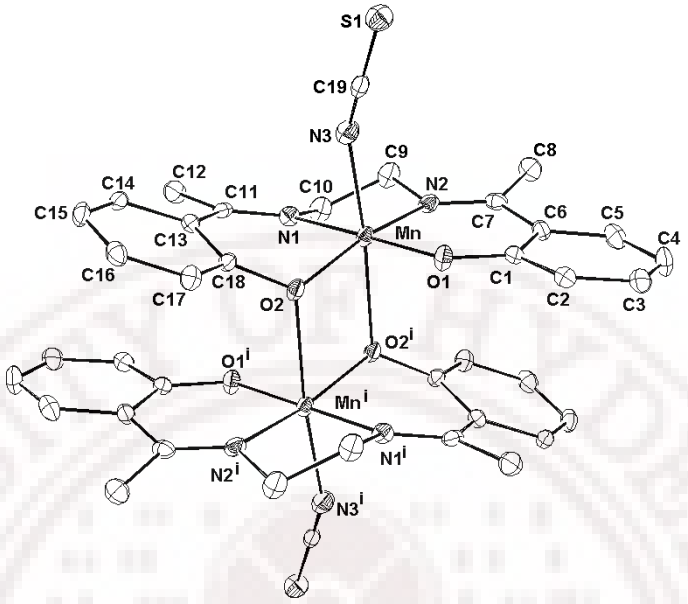

Figure 3.1 ORTEP view of the $[Mn(acphen)NCS]_2$ (**1**) with atom labeling. Atoms are shown as 30% thermal ellipsoids. Hydrogen atoms are omitted for clarity. (i) *–x*, *–y*, *–z*+1

Table 3.2 Selected bond lengths [Å] and angles [°] for $[Mn(acphen)NCS]_2$ (**1)**

Mn-O1	1.8572(16)	Mn-N1	1.992(2)	Mn-N3	2.169(2)
Mn-O2	1.9070(16)	Mn-N2	1.998(2)	Mn-O2#1	2.4109(17)
N3-C19	1.165(3)	C19-S1	1.631(3)		
O1-Mn-N1	91.58(8)	N1-Mn-N2	84.83(8)	O2-Mn-O2#1	77.86(7)
O1-Mn-N2	175.77(8)	N1-Mn-N3	98.24(8)	N1-Mn-O2#1	87.96(7)
O1-Mn-N3	91.41(8)	N2-Mn-N3	91.32(8)	O1-Mn-O2#1	89.99(7)
O1-Mn-O2	94.34(7)	O2-Mn-N1	164.61(8)	N2-Mn-O2#1	87.65(7)
O2-Mn-N3	95.80(8)	O2-Mn-N2	88.59(7)	N3-Mn-O2#1	173.60(7)
Mn-N3-C19	152.5(2)	N3-Mn-S1	179.2(2)	Mn-O2-Mn#1	102.14(7)

#1 *-x*, *-y*, *-z*+1

3.3.3. Structure of $[Mn(acphpn)(H_2O)NCS]\cdot 2H_2O$ (2)

The structure is entirely different from the previous one, the formation of dimer/polymer being prevented by the coordinated water molecule. As shown in Figure 3.2, the Mn(III) coordination has a distorted octahedral geometry. The tetradentate acphpn ligand chelates the Mn atom in the equatorial mode, the apical positions being occupied by an N-bonded terminal thiocyanato and a water molecule. The coordination of the thiocyanato ion is nearly linear, the Mn–N–C angle being 177.7º. The equatorial donors N1, N1', O1 and O1' are exactly in a plane and the manganese atom is displaced by 0.065 Å towards the coordinated water molecule. However, the ligand as a whole is grossly non-planar, even after excluding the methylene groups, the angle between the mean planes of the two halves being 71.6º. The two halves are thereby greatly bent towards the water ligand and away from the thiocyanato. The non-methylated ligand is known to form two polymorphs[2b], a phenoxo bridged dimer in which the above mentioned inter-planar angle is 10º and a helical chain in which the angle is 37º. Selected bond distances and angles are given in Table 3.3. Two solvent water molecules are present in the lattice, which are hydrogen bonded to the complex molecule to build a one dimensional chain as shown in Figure 3.3. The hydrogen bonding parameters are presented in Table 3.4.

There are some features worth noting in the crystal structure of **2**. Regarding the molecular structure, the Mn–N–C–S atoms are arranged in a closely linear mode, at variance with most other structures where the terminal thiocyanato and Mn(III) are bonded in a bent mode.[2b,3,9,12b,24-29] A notable exception is a five coordinate complex

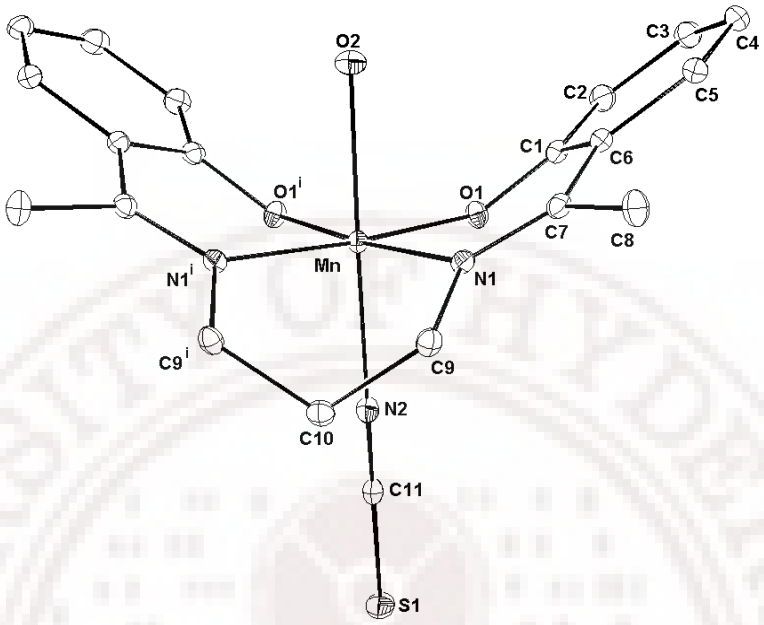

Figure 3.2 ORTEP view of [Mn(acphpn)(H_2O)(NCS)].2H_2O (**2**) with atom labelling. Atoms are shown as 30% thermal ellipsoids. All hydrogen atoms and lattice water molecules are omitted. Symmetry: (i) *x*, *–y*+1/2, *z*.

Table 3.3 Selected bond lengths [Å] and angles [°] for [Mn(acphpn)(H_2O)(NCS)].2H_2O (**2**)

Mn-O1	1.8869(12)	Mn-N1	2.0402(14)	Mn-O1#1	1.8869(12)
Mn-O2	2.2349(18)	Mn-N2	2.247(2)	Mn-N1#1	2.0402(14)
N2-C11	1.152(3)	C11-S1	1.647(3)		
O1-Mn-N1	87.97(5)	N1-Mn-N2	96.62(5)	O1#1-Mn-O1	89.40(7)
O1-Mn-O2	89.01(5)	O2-Mn-N1	87.23(5)	O1#1-Mn-N1	175.44(6)
O1-Mn-N2	86.95(5)	O2-Mn-N2	174.31(7)	N1#1-Mn-N1	94.41(8)
Mn-N2-C11	177.7(2)	N2-C11-S1	179.4(2)	#1 *x, –y* +1/2, *z*	

where the thiocyanato and Mn are located on a crystallographic two fold axis, and hence strictly linear.[30] Alike in that structure, the linear coordination results in a shorter N–C bond for **2** compared to **1**. The C–N stretching frequencies seen in the IR spectra are also significantly different: 2054 cm^{-1} in **1** and 2085 cm^{-1} in **2**. These observations are in line with the expectation of a bond order higher than two for a linearly coordinated thiocyanato. Concerning the three water molecules, the coordinated one is situated fully on the mirror plane while one of the lattice water molecules is bisected by the mirror plane and the other one is disordered about this plane. These features related to the mirror symmetry element can be rationalized by the coordination and hydrogen bonding requirements. While the bisecting mode is unsuitable for a coordinated water molecule, it creates no problem for a lattice water molecule. The fact that these two water molecules attain saturation with regard to hydrogen bonding (Figure 3.3) seems to "protect" them from being disordered. The second water molecule has only one acceptor so that the entropy driven disorder about the mirror plane operates for it.

Table 3.4 Hydrogen bonding parameters for [Mn(acphpn)(H_2O)(NCS)].2H_2O (**2**)

D-H···A	D-H (Å)	H···A (Å)	D···A (Å)	D-H···A (º)
O2-H2A···O3	0.826	1.950	2.775	175.12
O2-H2B···O4#1	0.716	2.059	2.689	147.22
O3-H3B···O1#2	0.871	2.059	2.812	144.19
O4-H4B···O3#3	0.893	2.114	2.912	148.42

#1 *x*, –*y*+1/2, *z*; #2 *x*+1/2, *y*, –*z*+1/2; #3 *x*+1, *y*, *z*

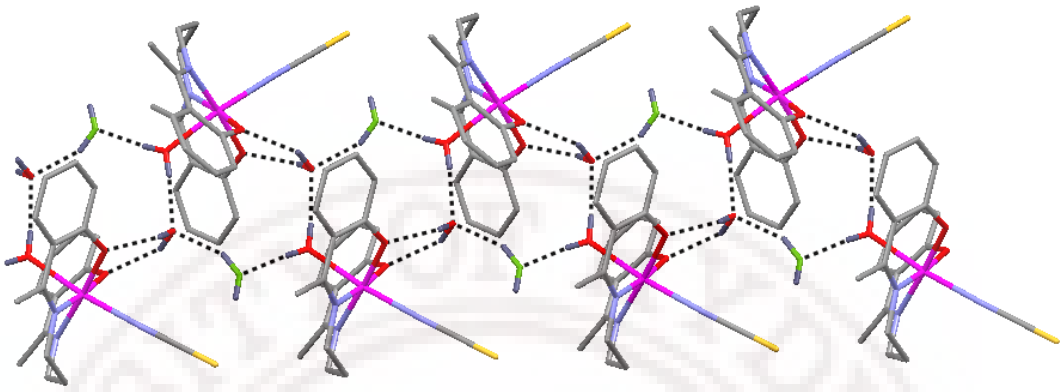

Figure 3.3 One-dimensional hydrogen bonded chains in complex **2**. The lattice water molecule with one free hydrogen atom is disordered about the crystallographic mirror plane. For the purpose of illustration it has been moved to the mirror plane.

3.3.4. Spectral Studies

3.3.4a. FTIR Spectra

The IR spectra of compound **1** and **2** exhibit strong absorption in the range of 2040-2090 cm^{-1}, which is attributed to the asymmetric stretching vibration of N-bonded thiocyante group and the strong absorption at 1590-1645 cm^{-1}, which is assignable to the (-C=N) stretching vibration of Schiff-base. Compound **2** exhibits broad absorption bands at 3344, 3200 cm^{-1}, which is attributed stretching vibration (O-H) of water molecules. All these absorptions are with in the reported range.[31]

3.3.4b. Electronic Spectra

The solution spectra of the compounds **1** and **2** were measured in methanol (Figure 3.4). The low intensity absorption bands in the range 16.67, 425(sh) for

complex **1** and 16.67, 551(sh) for complex **2** ($\bar{\nu}_{max}$ /10^3cm^{-1}, ε_{max}/cm^{-1}M^{-1}) respectively, which are assigned to d-d transition. The high intensity absorption bands in the range 17.62, 522; 25.86, 5589; 35.64, 17721 for complex **1** and 17.62, 588; 26.91, 8162; 35.97, 17292 for complex **2** ($\bar{\nu}_{max}$ /10^3cm^{-1}, ε_{max}/cm^{-1}M^{-1}) respectively, which are assigned to intraligand π-π* transitions in the complexes, the low intensity d-d transitions were masked in this range.

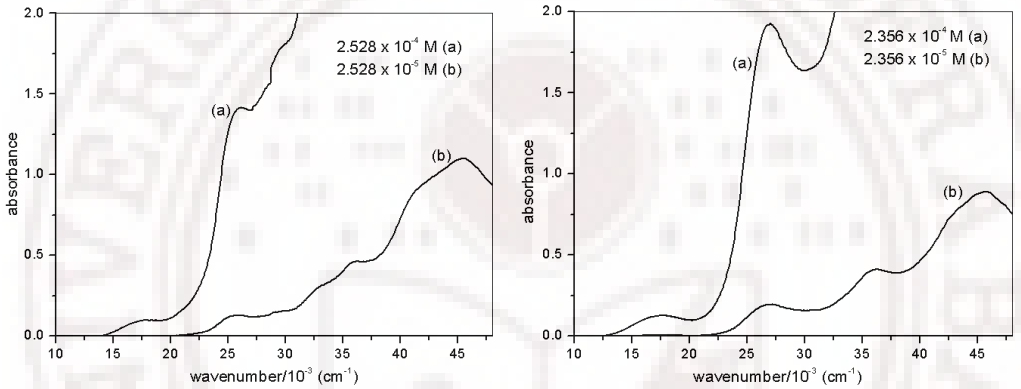

(1) **(2)**

Figure 3.4 Electronic absorption spectra Solution spectra of complex **1** and **2** in methanol.

3.4. Magnetic Properties

The temperature-dependence of the magnetic susceptibility χ_m, of **1** and **2** was measured in the temperature range 1.98-300 K (Figures 3.5 and 3.6). The $\chi_m T$ value of **1** per magnetic ion is 2.97 cm^3 mol^{-1} K at 300 K (close to the expected spin-only value, 3.00 cm^3 mol^{-1} K per Mn(III)). While decreasing the temperature, there is no significant change up to about 80 K, from where $\chi_m T$ decreased to 1.30 cm^3 mol^{-1} K per Mn(III) at 5.8 K and 0.414 cm^3 mol^{-1} K per Mn(III) at 2.0 K. The decrease is characteristic of an antiferromagnetic exchange interaction between the two high-

spin Mn(III) ions. The best fit to the dimer equation[18a] yielded the parameters values $J = -0.79(1)$ cm^{-1}, $zJ' = -0.017(1)$ cm^{-1}, $g = 2.00$, L.S. Error = 0.000470. The weakness of the inter-dimer interaction (small magnitude of zJ'), which is in agreement with the absence of significant inter-dimer contacts in the crystal, suggests operation of single ion zero-field splitting. Exact diagonalisation of the spin Hamiltonian including axial Zeeman and zfs terms in addition to isotropic exchange led to the following best fit parameters: $J = -0.7(1)$ cm^{-1}, $D = -0.6(1)$ cm^{-1}, $g = 2.017(5)$, L.S. Error = 0.00013.

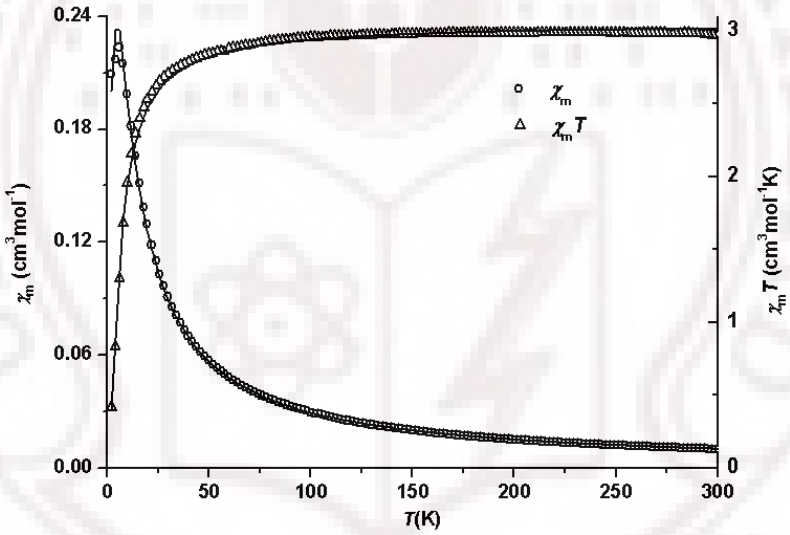

Figure 3.5 Temperature variation of magnetic susceptibility (per magnetic ion) for compound **1**. The solid lines result from a least-squares fit to the data of the theoretical values calculated through exact diagonalisation of the spin Hamiltonian including axial Zeeman, zfs and isotropic exchange terms as explained in the text.

The fitting is unique, and in particular, a positive value for *D* leads to divergence. This is satisfying because, a Jahn-Teller elongated Mn(III) complex is expected to have a small negative *D*.[32] Finally, the geometry of the bridge (Mn–O, 1.91, 2.41Å; Mn–O–Mn, 102.1º) is in the range usually reported[9] for phenoxo-bridged complexes characterized by antiferromagnetic interactions.

The $\chi_m T$ value of **2** at 300K is 3.38 $cm^3\ mol^{-1}$ K, slightly higher than the spin-only value of 3.00 $cm^3\ mol^{-1}$ K per Mn^{III}. With decreasing temperature, $\chi_m T$ also decreased and reached a value of 1.27 $cm^3\ mol^{-1}$ K per Mn(III) at 1.98 K, indicating weak intra-chain antiferromagnetic interactions. The data were fitted to both the Curie-Weiss equation[18a] as well as the Heisenberg chain equation[18b] with the following results: Curie-Weiss: g = 2.12(fixed), θ = – 3.76 (5) K, L.S. Error = 0.00623; chain, g = 2.12(fixed), J = – 7.82(2) cm^{-1}, θ = 1.18(2) K, L.S. Error = 0.00008. A comment on the validity of the above parameters is in order. A *g*-value significantly greater than 2 and a ferromagnetic interchain coupling as implied by the positive θ are difficult to explain. Moreover, it is found that J and θ are strongly correlated. If g is fixed at 2.0, it is possible to get equally good fit for two sets of parameters: J = – 5.59(9) cm^{-1}, θ = 1.07(2) K, L.S. Error = 0.003; J = +0.7(1) cm^{-1}, θ = – 4.2(2) K, L.S. Error = 0.004. If θ is not included, the best fit is obtained with J = – 2.40 cm^{-1}, g = 1.95 with a relatively high L.S. Error of 0.01. Omitting θ but including the interchain interactions through the mean-field leads to divergence. Only the Curie-Weiss fit is included in Fig. 5. The only valid conclusion that can be drawn from the data is that there is weak antiferromagnetic interaction in the crystals of this mononuclear Mn(III) complex characterized by *J*-value of about – 2 cm^{-1}.

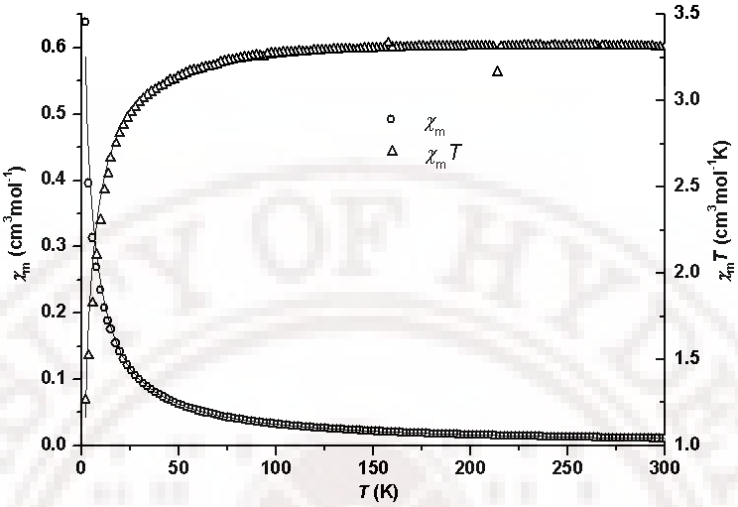

Figure 3.6 Temperature variation of magnetic susceptibility (per magnetic ion) for compound **2**. The solid line results from a least-squares fit to the data of the theoretical values calculated with the Curie-Weiss equation.

It is instructive to compare the above result for compound **2** with the magnetic properties of the homologous complex [Mn(acphen)(H_2O)NCS], the crystals of which contain no lattice water.[3] However, it is first necessary to analyze the possible exchange pathways in **2,** all of which involve hydrogen bonding among coordinated water (CW), lattice water (LW) and coordinated Schiff base oxygen (SBO) atoms. If for a moment the disordered lattice water (the one with a free hydrogen atom in Figure 3.3) is ignored, one gets a zig-zag chain in which the adjacent Mn(III) centers are connected by a 5-atom CW–LW–SBO bridge. The second lattice water molecule, though disordered, introduces two additional bridges in the 1-dimensional system: CW–LW–LW–SBO and CW–LW–LW–CW, both involving seven atoms. If one considers the topology of these bridges with reference

to the Mn(III) centers, two types can be recognized: Type-I, z – (x, y), which connects a ligand in the axial position (water, in this compound) to one or more ligands in the equatorial plane (the two Schiff base oxygen atoms) and Type-II, z – z, in which two axial ligands are inter-connected. The magnetic orbitals for a d^4 ion in an axially elongated octahedral complex are d_{xy}, d_{xz}, d_{yz}, and d_{z2}. Super-exchange involving these orbitals will be weak because, the first three are essentially π-bonding while the last one is σ-bonding but its overlap with the axial ligand is small. Nevertheless, the relative strengths of these pathways can be inferred by comparing with the above mentioned homologous complex of acphen. The crystal structure of this complex[3] is also built from 1-dimensional hydrogen bonded chains generating just one CW–SBO (3-atom, Type-I) bridge, there being no lattice water in the crystals of this compound. Remarkably, the acphen complex has a constant μ_{eff} value of 4.96 B.M. in the temperature range 6-300 K indicating that there is no intermolecular magnetic interaction. It is therefore reasonable to conclude that the 7-atom Type-II bridge is responsible for the weak antiferromagnetic coupling observed in compound **2** (Figure 3.7).

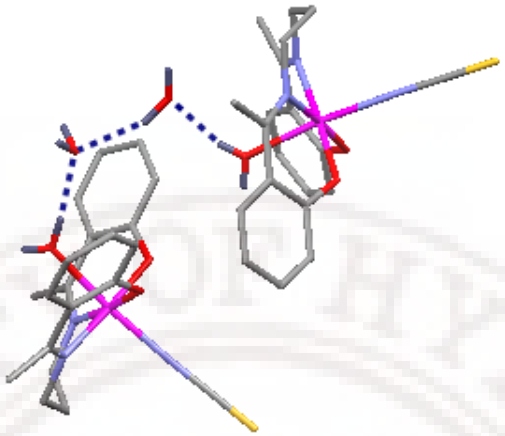

Figure 3.7 Antiferromagnetic exhange pathway via lattice water in compound **2**.

3.5. Conclusions

The weak antiferromagnetic interaction in $[Mn(acphen)NCS]_2$ and $[Mn(acphpn)(H_2O)NCS]\cdot 2H_2O$ has different origins. In the case of the acphen complex, two phenoxo bridges are involved. According to the classification given above, these are single atom Type-I bridges. For the acphpn complex, the exchange pathway is made up of multi atom bridges involving hydrogen bonded lattice water, the dominant contribution being attributed to a 7-atom Type-II bridge. The similar magnitudes of the Heisenberg exchange parameter (J) for these two structurally very different systems do not mean that the pathways are equally efficient. The small negative value of J for the phenoxo dimer may result from near cancellation of moderately strong ferro and antiferromagnetic contributions from the four different magnetic orbitals on each Mn(III) centre. The most significant result from the present study arises from comparison of the acphpn aquo complex with the previously

studied similar mononuclear Mn(III) complex of acphen, the only important difference being the absence of lattice water in its crystals. It is shown that hydrogen bonding through lattice water provides a pathway for exchange in the present complex while the previous compound, though consisting of hydrogen bonded chains, has no significant magnetic interaction. A definitive characterization of the role of lattice water in transmitting magnetic coupling across multi-atom bridges has been previously reported for a Cu(II) complex.[33] Measurement and understanding of the role of solvent molecules in transmitting magnetic information across long distances is important in the context of, among other things, bio-inorganic chemistry and quantum computing.

3.6. References

1. For an early study of Mn(III) tetradentate Schiff base crystals, See: Joseph, A. B.; Martin L. K.; Myoung, S. L.; Dimitri, P. K.; William, E. H.; Vincent L. P. *Inorg. Chem.* **1989**, *28*, 180.
2. (a) Reddy, K. R.; Rajasekharan, M. V.; Tuchagues, J.-P. *Inorg. Chem.* **1998**, *37*, 5978. (b) Sailaja, S.; Rajasekharan, M. V.; Hureau, C.; Riviere, E.; Cano, J.; Girerd J.-J. *Inorg. Chem*. **2003**, *42*, 180.
3. Chakraborty, J.; Brajagopal, S.; Pilet, G.; Mitra, S. *Struct. Chem.* **2006**, *17*, 585.
4. Lecren, L.; Wernsdorfer, W.; Li, Y. -G.;Vindigni, A.; Miyasaka, H.; Clerac, R. *J. Am. Chem. Soc*. **2007**, *129*, 5045.

5. Lu, Z.; Yuan, M.; Pan, F.; Gao, S.; Zhang, D.; Zhu, D. *Inorg. Chem.* **2006**, *45*, 3538 (and references therein).

6. Karmakar, R.; Choudhury, C. R.; Bravic, G.; Sutter, J.-P.; Mitra, S. *Polyhedron* **2004**, *23*, 949.

7. Shyu, H.; Wei, H.; Wang, Y. *Inorg. Chim. Acta* **1999**, *290*, 8.

8. (a) Mabad, B.; Luneau, D.; Theil, S.; Dahan, F.; Savariault, J. M.; Tuchagues, J. - P. *J. Inorg. Biochem.* **1991**, *43*, 373. (b) Kennedy, B. J.; Murray, K. S. *Inorg. Chem*. **1985**, *24*, 1552.

9. Miyasaka, H.; Clerac, R.; Ishii, T.; Chang, H.; Kitagawa, S.; Yamashita, M. *J. Chem. Soc., Dalton Trans*. **2002**, 1528.

10. Bermejo, M. R.; Castineiras, A.; Garcia-Montergudo, J. C.; Rey, M.; Sousa, A.; Watkinson, M.; McAuliffe, C. A.; Pritchard, R. G.; Beddose, R. I. *J. Chem, Soc., Dalton Trans.* **1996**. 2935.

11. Matsumoto, N.; Zhong, Z.; Okawa, H.; Kida, S. *Inorg. Chim. Acta* **1989**, *160*, 153.

12. (a) Matsumoto, N.; Takemoto, N.; Ohyosi, A.; Okawa, H. *Bull. Chem. Soc. Jpn.* **1988**, *61*, 2984. (b) Mikuriya, M.; Yamato, Y.; Tokii, T. *Bull. Chem. Soc. Jpn.* **1992**, *65*, 1466.

13. Garcia-Deibe, A.; Sousa, A.; Bermejo M, R.; MacRory, P. P.; McAuliffe, C. A.; Pritchard, R. G.; Helliwell, M. *J. Chem. Soc., Chem. Commun.* **1991**, 728.

14. Miyasaka, H.; Sugimoto, K.; Sugiura, K.; Ishii, T.; Yamashita, M. *Mol. Cryst. Liq. Cryst.* **2002**, *379,* 197.

15. Miyasaka, H.; Mizushima, K.; Furukawa, S.; Sugiura, K.; Ishii, T.; Yamashita, M. *Mol. Cryst. Liq. Cryst.* **2002**, *379*, 171.

16. Sato, Y.; Miyasaka, H.; Matsumoto, N.; Okawa, H. *Inorg. Chim. Acta* **1996**, *247*, 57.

17. Miyasaka, H.; Saitoh, A.; Abe, S. *Coord. Chem. Rev.* **2007**, *251*, 2622.

18. Chandramouli, G. V. R.; Balagopalakrishna, C.; Rajasekharan, M. V.; Manoharan, P. T. *Comput. Chem.* **1996**, *20*, 353.

19. (a) O'Connor, C. J. *Prog. Inorg. Chem.* **1982***, 29*, 203. (b) Koenig, E.; Desai, V. P.; Kanallakopulos, B; Klenze, R. *Chem. Phys.* **1980**, *54*, 109.

20. Garge, P.; Chikate, R.; Padhye, S.; Savariault, J.-M.; de Loth, P.; Tuchagues, J.-P. *Inorg. Chem*. **1990**, *29*, 3315.

21. *SAINTPLUS*, Bruker AXS Inc., Madison, Wisconsin, USA 2003.

22. Sheldrick, G. M. *SADABS, Program for empirical absorption correction*, University of Gottingen, Gottingen, Germany 1996.

23. Sheldrick, G. M. *SHELX-97*, *Programs for crystal structure analysis*, University of Gottingen, Gottingen, Germany 1997.

24. Nastase, S.; Tuna, F.; Maxim, C.; Muryn, C. A.; Avarvari, N.; Winpenny, R. E. P.; Andruh, M. *Cryst. Growth Des*. **2007**, *7*, 1825.

25. Biswas, S.; Mitra, k.; Schwalbe, C.H.; Lucas, C. R.; Chattopadhyay, S. K.; Adhikary. B. *Inorg. Chim. Acta* **2005**, *358*, 2473.

26. Li, H.; Zhong, Z. J.; Duan, C. -Y.; You, X. -Z.; Mak, T. C. W.; Wu, B. *J. Coord. Chem.* **1997**, *41*, 183.

27. Yun-Long, F.; Shi-Xiong, L. *Chin. J. Struct. Chem.* **1996**, *15*, 47.

28. (a) Feng, Y. -L.; Liu, S. -X. *J. Coord. Chem.* **1998**, *44*, 81. (b) Shou-Bin, W.; Kun, T.; Bao-Hua, Y.; Sheng, L. *Acta Crystallogr.* **2008**, *E64*, m543.

29. Bertoncello, K.; Fallon, G. D.; Murray, K. S.; Tiekink, E. R. T. *Inorg. Chem.* **1991**, *30*, 3562.

30. Weiss, M. C.; Goedken, V. L. *Inorg. Chem.* **1979**, *18*, 274.

31. Nakamoto, K. *Infrared and Raman Spectra of Inorganic and coordination Compounds*; 3 ed.; John Wiley & Sons, Inc.: New York, 1997, pp 270.

32. (a) Kennedy, B. J.; Murray, K. S. *Inorg. Chem*. **1985**, *24*, 1557. (b)Whittaker, J. W.; Whittaker, M. M. *J. Am. Chem. Soc*. **1991**, *113*, 5528. (c) Zhang, Z.-Y.; Brouca-Cabarrecq, C.; Hemmert, C.; Dahan, F.; Tuchagues, J.-P. *J. Chem. Soc. Dalton Trans*. **1995**, 1453.

33. Balagopalakrishna, C.; Rajasekharan, M. V. *Phys. Rev. B* **1990**, *42*, 7794.

UNIVERSITY OF HYDERABAD

CHAPTER IV

Antiferromagnetic interactions in a zig-zag end-on polymer bridged by a *trans*-μ-(1,1) azide. Synthesis, structure and magnetic properties of $[Mn(5\text{-}Clsalpn)N_3]_n$ and phenoxo bridged $[Mn(5\text{-}Clsalpn)N_3]_2$.

4.1. Introduction

In $[Mn(SB)N_3]$, the N_3^- ion may remain terminal often resulting in phenoxo bridged dimers,[1-3] or more commonly it can function as a bridging ligand. Commonly observed bridging modes are *trans*-μ-(1,3),[4-7] and *trans*-μ-(1,1/1,3),[8] leading to 1-D coordination polymers. These complexes exhibit different kinds of magnetic exchange interactions depending on the bridging geometry. By changing the side group of the teradentate Schiff base, very few phenoxo bridged dimers and *trans*-μ-$(1,3)N_3$ bridged $[Mn(SB)N_3]_n$ polymers have been reported.[9] In this chapter, we present the structural and magnetic details of two polymorphs of *trans*-μ-$(1,1)N_3$ bridged $[Mn(5\text{-}Clsalpn)N_3]_n$ (**1**) polymer and one phenoxo bridged dimer with N-bonded terminal azide $[Mn(5\text{-}Clsalpn)N_3]_2$ (**2**). The complex **2** is within the range of phenoxo bridged dimers.[1-3, 9] The compound **1** is the first Mn^{3+} complex with *trans*-μ-$(1,1)N_3$ bridged polymer. The unsymmetrical bond distance of azide ion in *trans*-μ-$(1,1)N_3$ bridged polymeric complex **1** is similar to reported bibridged [*trans*-μ-$(1,1)N_3]_2$ and mixed bridged [*trans*-μ-(1,1/1,3)] polymeric complexes.[8,10-13] The

compound **1** is less symmetrical than *trans*-μ-(1,3)N_3 bridged polymers.[4-7] The Schiff base (5-Clsalpn) involved is depicted in Scheme 1.4.

4.2. Experimental Section

4.2.1. Synthesis

All chemicals used for synthesis were reagent grade. The Schiff base was formed *in situ* in the presence of the appropriate metal salt. **Caution:** Azide compounds are potentially explosive and should be prepared only in small quantities and handled with care.

Preparation of [Mn(5-Clsalpn)N_3] (1): In a beaker open to the atmosphere, $Mn(CH_3COO)_2.4H_2O$ (0.245g, 1.00 mmol) and NaN_3 (0130g, 2.00 mmol) were stirred into 25 mL of methanol. 5-Chlorosalicyladehyde (0.313g, 2.00 mmol) and 1,3-diaminoethane (0.071g, 1.0 mmol) were stirred in 30 mL methanol and added to the above solution and stirring continued for about 40 minutes to complete the aerial oxidation of Mn^{II}. The green coloured precipitate formed was separated by filtration and dried. Yield: 0.361g (0.809 mmol, 80.9%). It was recrystallized from CH_3OH to obtain green X-ray quality crystals. Anal. Calcd. for $MnC_{17}H_{14}Cl_2N_5O_2$: C, 45.76; H, 3.16; N, 15.71. Found: C, 45.76; H, 3.12; N, 15.96. Important IR absorptions of precipitate (cm^{-1}): $\nu_a(N_3)$ 2048(s), $\nu_s(N_3)$ 1377(s), $\delta(N_3)$ 707(s), $\nu_{schiff\ base}$(C=N) 1620(s). Important IR absorptions of crystal (cm^{-1}): $\nu_a(N_3)$ 2046(s), $\nu_s(N_3)$ 1377(s), $\delta(N_3)$ 707(s), $\nu_{schiff\ base}$(C=N) 1620(s). X-ray examination revealed that the crystals consist of two polymeric forms.

(**1a**) Monoclinic, space group, *C*2/*c*.

(**1b**) Monoclinic, space group, $P2_1/c$.

[Mn(5-Clsalpn)N_3]$_2$ (2): The precipitate of [Mn(5-Clsalpn)N_3] obtained as in the preparation of **1** was dissolved in methanol and vapor diffused with n-hexane in desiccator. Dark-green X-ray quality crystals were collected after three weeks. Anal. Calcd. Mn_2C_{34} $H_{28}Cl_4N_{10}O_4$: C, 45.76; H, 3.16; N, 15.71. Found: C, 45.69; H, 3.18; N, 15.81. Important IR absorptions of crystal (cm^{-1}): $\nu_a(N_3)$ 2035(s), $\nu_s(N_3)$ 1373(s), $\delta(N_3)$ 707(s), $\nu_{schiff\ base}$(C=N) 1620(s).

4.2.2. Physical measurements

IR spectra were obtained in KBr pellets using Shimadzu FT-IR 8000 spectrometer. Elemental analysis of the complexes was performed on a FLASH EA SERIES CHNS analyzer. The magnetic susceptibility was measured for **1** and **2** in the 1.98-300 K temperature range using a Quantum Design MPMS SQUID susceptometer. The sample was pressed into pellet to avoid orientation effects of the microcrystals during magnetic measurements. Diamagnetic corrections were applied using Pascal's constants.[14] Fitting of the susceptibility data was done using the program SUSCEP[15] based on the Heisenberg chain equation of Koenig et al[16] for **1**. The magnetic susceptibilities have been computed both with the program SUSCEP[15] based on the expression derived from the isotropic spin-exchange Hamiltonian $H = -2JS_1S_2$ ($S_1 = S_2 = 2$) and van Vleck's equation,[17] and by exact calculations of the energy levels associated to the spin Hamiltonian through diagonalization of the full matrix with a general program for axial symmetry.[18] In the latter case, least-squares

Table 4.1 Crystallographic data and structure refinement for $[Mn(5\text{-}Clsalpn)N_3]_n$ (**1**)

	1a	**1b**
Formula	$C_{17}H_{14}Cl_2MnN_5O_2$	$C_{17}H_{14}Cl_2MnN_5O_2$
Formula weight	446.17	446.17
Crystal system	monoclinic	monoclinic
a (Å)	24.035(4)	12.5241(8)
b (Å)	8.5326(14)	17.6241(11)
c (Å)	19.386(3)	8.4720(5)
α (°)	90	90
β (°)	114.162(8)	107.7210(10)
γ (°)	90	90
V (Å^3)	3627.4(10)	1781.26(19)
Space group	*C*2/*c*	*P* 2_1/*c*
Z	8	4
T (K)	100(2)	100(2)
ρ_{calcd} (g cm^{-3})	1.634	1.664
μ (mm^{-1})	1.046	1.065
θ range (°)	1.86 - 28.25	1.71 - 28.25
h/*k*/*l* indices	-31, 32/ -11, 11/	-16, 16/ -22, 22/
	-25, 25	-11, 11
Reflections collected	20426	20425
Unique reflection, R_{int}	4344, 0.0273	4268, 0.0433
GooF	1.053	1.117
*R*1[$I > 2\sigma(I)$]	0.0381	0.0477
*wR*2[all data]	0.0968	0.1140
Weight. scheme (A, B)	0.0491, 3.50	0.0574, 1.11

fittings were accomplished with an adapted version of the function-minimization program MINUIT.[19]

4.2.3. X-ray Crystallography

X-ray data were collected for **1** and **2** on a Bruker SMART APEX CCD X-ray diffractometer, using graphite-monochromated Mo-Kα radiation (λ = 0.71073 Å). Data were reduced using SAINTPLUS[20] and a multi-scan absorption correction using SADABS[21] was performed. The structure was solved using SHELXS-97 and full matrix least squares refinement against F^2 was carried out using SHELXL-97.[22] All ring hydrogen atoms were assigned on the basis of geometrical considerations and were allowed to ride upon the respective carbon atoms. All hydrogen atoms were assigned fixed U_{iso} values, equal to $1.2U_{eq}$ of the parent atom for ring hydrogen atoms. Crystallographic data presented for complex **1a**, **1b** and **2** in Tables 4.1 - 4.4.

4.3. Results and discussion

4.3.1 Structure of $[Mn(5\text{-}Clsalpn)N_3]_n$ (1a, 1b)

The molecular structure obtained in the polymorphs **1a** and **1b** differ only very marginally in the geometrical parameters. Therefore, the two structures are described together. The Mn^{III} ion assumes a distorted octahedral geometry in which the Mn^{III} ion binds to one 5-Clsalpn in equatorial mode and two azide ions in an axial positions as shown in Figure 4.1(Figure 4.2) for **1a** (**1b)**. Each azide ion functions as a *trans*-μ-(1,1) bridge, resulting in a one-dimensional polymeric zig-zag chain along the *b*-axis as shown in Figure 4.3 for **1a** and along the *c*-axis as shown in Figure 4.4 for **1b**. The corresponding bond distances in the Mn(III) octahedral for **1a** and **1b**

differ at most by 0.01 Å, except for the long axial Mn-N bonds which differ by 0.04 Å. The bond angles differ by less than 1.33º. In the following discussion, the structural parameters for **1b** are given in the parenthesis after the corresponding values for **1a**. The basal atoms (N_2O_2) are coplanar (with rms deviation = 0.13(0.15) Å) even though central manganese atom is displaced by 0.11(0.11) Å towards the azide ligand. The two halves of the 5-Clsalpn ligand, excluding the methylene groups and chlorine atoms are individually planar (rms deviations = 0.051(0.062), 0.047(0.039) Å), with the Mn deviating by 0.80(0.83) Å and 0.75(0.74) Å from these planes. The two halves of the Schiff base 5-Clsalpn are inclined towards each other by 73º (74º). Along the chain the dihedral angle between the equatorial N_2O_2 planes of adjacent molecules is 48º (47º). The overall coordination geometry of each Mn^{III} ion is distorted octahedral with the Jahn-Teller elongation seen along the N3-Mn···N3 axis, with bond distances Mn-N3, 2.22(2.21) Å, Mn···N3 2.47(2.46) Å and bridge angle Mn-N3···Mn 131° (132°). The coordination of the azide bridge is unsymmetrical and the bond angles of Mn-N3-N4 and $Mn\text{-}N3^{i}\text{-}N4^{i}$ are 123º (122º) and 106º (106º). The intrachain and the shortest interchain Mn---Mn distances are 4.27(4.24) Å and 9.52(9.53) Å. The intra chain Cl---Cl distances are 6.60(6.58) Å, 6.71(6.62) Å, and the inter chain Cl---Cl distances are 4.93(6.31) Å, 5.28(7.30) Å respectively, which are longer than the sum of the van der Walls radii (3.5 Å). The *trans*-μ-(1,1)-azide is less symmetrical than that of *trans*-μ-(1,3)-azides.[4-7] Selected bond distances and angles are listed in Table 4.2 (Table 4.3). Packing diagram of the compound **1a** (**1b**) is shown in Figure 4.5.

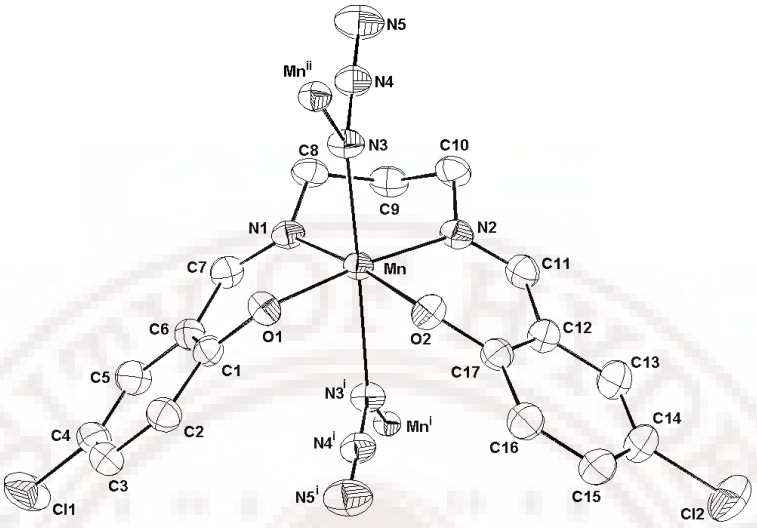

Figure 4.1 ORTEP view of one complex along the 1D chains of $[Mn(5\text{-}Clsalpn)]_n$ in **1a**. Hydrogen atoms are omitted for clarity, and the thermal ellipsoids are represented at the 50% probability level [i = -*x*+1/2, *y*+1/2, -*z*+1/2; ii = -*x*+1/2, *y*-1/2, -*z*+1/2].

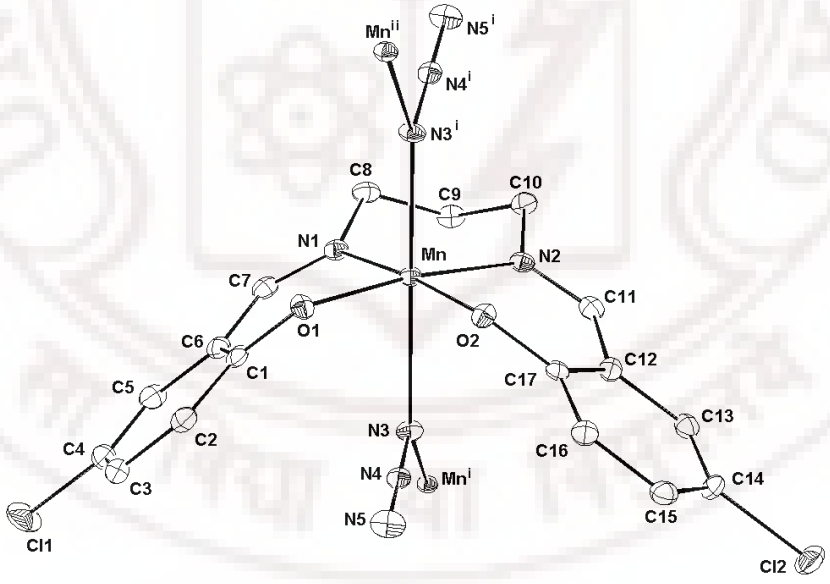

Figure 4.2 ORTEP view of one complex along the 1D chains of $[Mn(5\text{-}Clsalpn)]_n$ in **1b**. Hydrogen atoms are omitted for clarity, and the thermal ellipsoids are represented at the 50% probability level [i = *x*, -*y*+1/2, *z*+1/2; ii = *x*, -*y*+1/2, *z*-1/2].

Table 4.2 Selected bond lengths [Å] and angles [°] for $[Mn(5\text{-}Clsalpn|)N_3]_n$ (**1a**)

Mn-O1	1.8821(12)	Mn-N1	2.0398(15)	Mn-N3	2.2161(15)
Mn-O2	1.8970(12)	Mn-N2	2.0328(15)	Mn-N3^{i}	2.4715(15)
N3-N4	1.204(2)	N4-N5	1.149(2)		
O1-Mn-O2	89.81(6)	O2-Mn-N1	172.62(6)	O1-Mn-N3^{i}	85.53(5)
O1-Mn-N2	174.10(6)	O2-Mn-N2	88.79(6)	O2-Mn-N3^{i}	85.08(5)
O1-Mn-N1	88.66(6)	O2-Mn-N3	93.60(6)	N1-Mn-N3^{i}	87.60(6)
O1-Mn-N3	91.78(6)	N2-Mn-N1	92.00(6)	N2-Mn-N3^{i}	88.64(6)
N2-Mn-N3	94.03(6)	N1-Mn-N3	93.67(6)	N3-Mn-N3^{i}	177.00(3)
Mn-N3- N4	122.85(12)	Mn-N3^{i}-N4^{i}	105.86(11)	Mn-N3-Mn^{ii}	131.29(7)
N3-N4- N5	178.5(2)	(i) -*x*+1/2, *y*+1/2, -*z*+1/2. (ii) -*x*+1/2, *y*-1/2, -*z*+1/2.			

Table 4.3 Selected bond lengths [Å] and angles [°] for $[Mn(5\text{-}Clsalpn|)N_3]_n$ (**1b**)

Mn-O1	1.8975(16)	Mn-N1	2.0326(19)	Mn-N3	2.2112(18)
Mn-O2	1.8862(16)	Mn-N2	2.0369(19)	Mn-N3^{i}	2.4359(18)
N3-N4	1.209(3)	N4-N5	1.154(3)		
O1-Mn-O2	89.64(7)	O2-Mn-N1	174.45(7)	O1-Mn-N3^{i}	84.76(7)
O1-Mn-N2	172.77(7)	O2-Mn-N2	88.91(7)	O2-Mn-N3^{i}	85.76(7)
O1-Mn-N1	88.74(7)	O2-Mn-N3	91.38(7)	N1-Mn-N3^{i}	88.80(7)
O1-Mn-N3	93.61(7)	N2-Mn-N1	92.03(8)	N2-Mn-N3^{i}	88.07(7)
N2-Mn-N3	93.50(7)	N1-Mn-N3	94.02(7)	N3-Mn-N3^{i}	176.71(5)
Mn-N3- N4	122.3(2)	Mn-N3^{i}-N4^{i}	106.0(1)	Mn-N3-Mn^{ii}	131.69(9)
N3-N4- N5	178.5(2)	#i, *x*, -*y*+1/2, *z*+1/2. #ii, *x*, -*y*+1/2, *z*-1/2.			

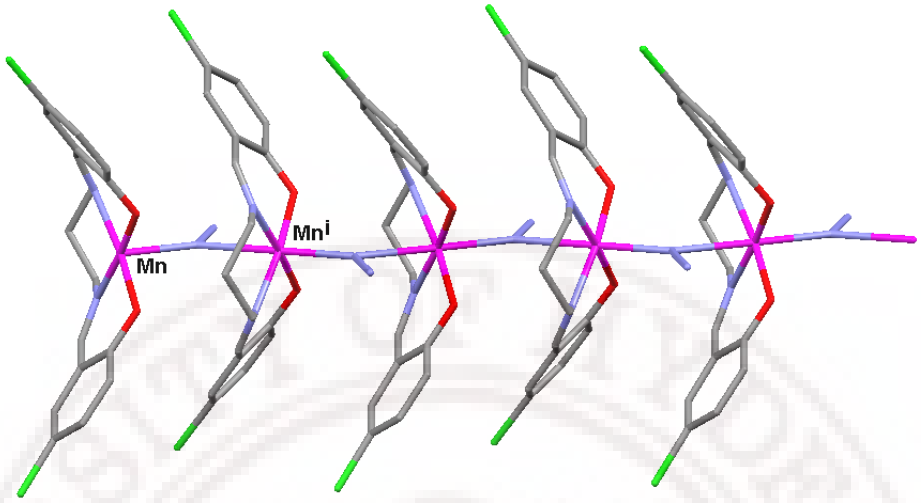

Figure 4.3 Perspective view of zig-zag 1D-polymeric chain of compound $[Mn(5\text{-}Clsalpn|)N_3]_n$ (**1a**) along the *b*-axis (i = -*x*+1/2, *y*+1/2, -*z*+1/2). Colour code for atoms: blue, N; red, O; grey C; purple, Mn, green Cl.

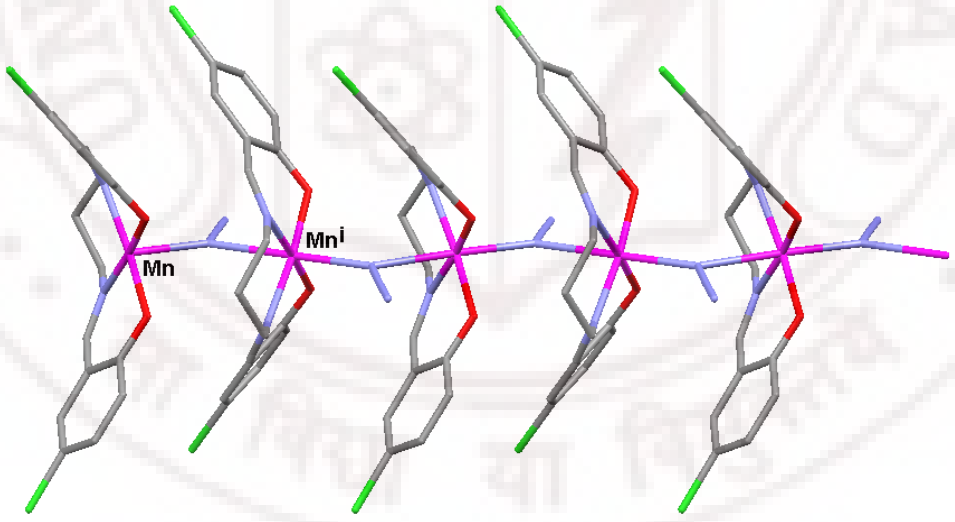

Figure 4.4 Perspective view of zig-zag 1D-polymeric chain of complex **1b** along the *c*-axis (i = *x*, -*y*+1/2, *z*+1/2). Colour code for atoms: blue, N; red, O; grey C; purple, Mn, green Cl.

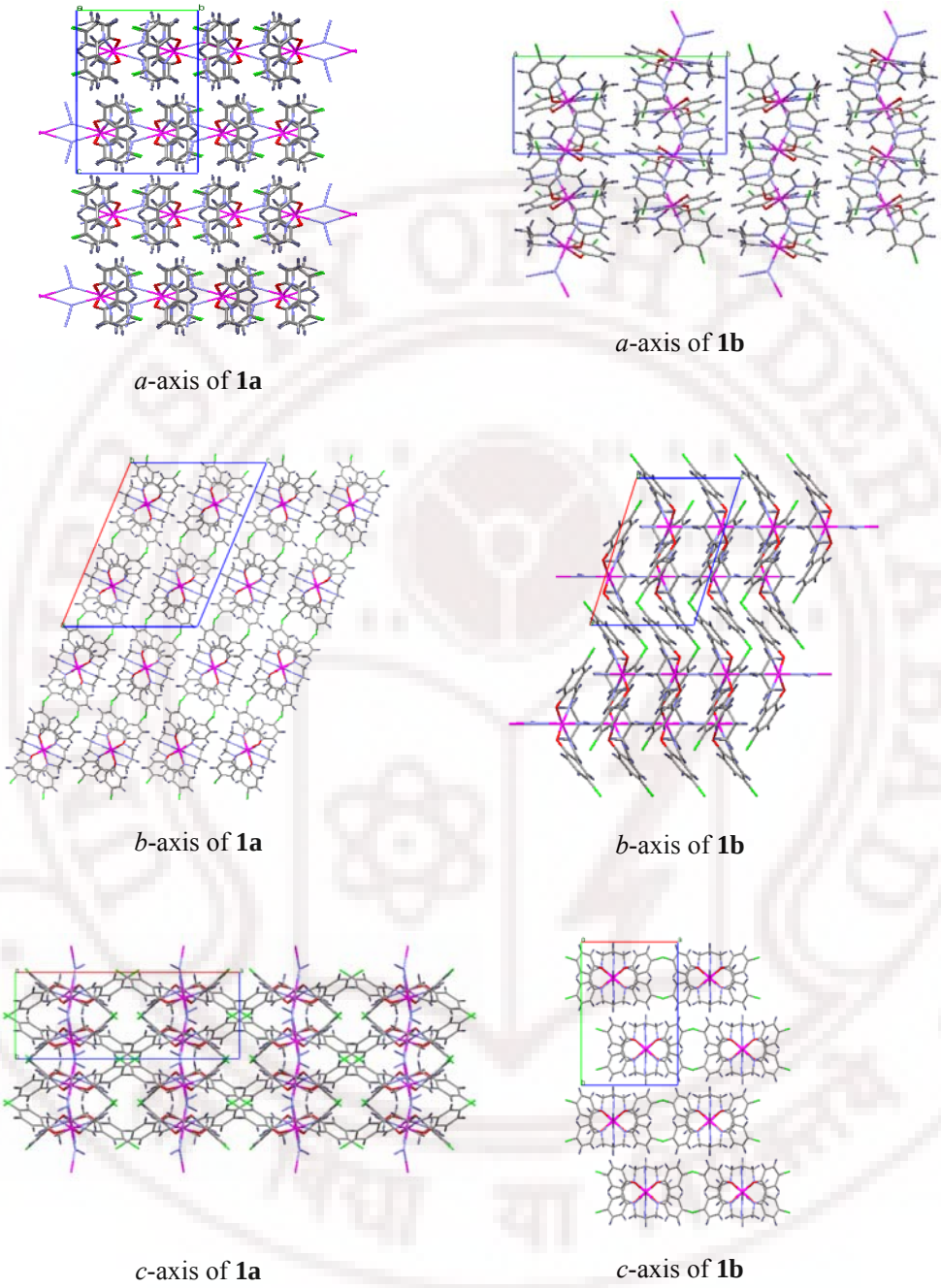

Figure 4.5 Packing views of the compound $[Mn(5\text{-}Clsalpn|)N_3]_n$ **1a (1b)** along the (a) *a*-axis, (b) *b*-axis and (c) *c*-axis. Colour code for atoms: blue, N; red, O; grey C; purple, Mn, green Cl.

Table 4.4 Crystallographic information data for complex $[Mn(5\text{-}Clsalpn|)N_3]_2$ (**2**)

Formula	$C_{34}H_{28}Cl_4Mn_2N_{10}O_4$
Formula weight	892.34
Crystal system	monoclinic
a (Å)	8.6558(6)
b (Å)	14.9144(11)
c (Å)	13.8532(10)
α (°)	90
β (°)	106.5470(10)
γ (°)	90
V (Å^3)	1714.3(2)
Space group	$P2_1/n$
Z	2
T (K)	298(2)
ρ_{calcd} (g cm^{-3})	1.729
μ (mm^{-1})	1.107
θ range (°)	2.05 - 26.04
$h/k/l$ indices	-10, 10/ -18, 18/ -17, 17
Reflections collected	17551
Unique reflection, R_{int}	3383, 0.0632
GooF	1.019
$R1[I > 2\sigma(I)]$	0.0487
$wR2$[all data]	0.1139
Weight. scheme (A, B)	0.0544, 0.86

4.3.2. Structure of $[Mn(5\text{-}Clsalpn)N_3]_2$ (2)

The complex is structurally characterized as a phenoxo-bridged dimer. Each unit of the phenoxo-bridged dimer is made up of a tetradentate 5-Clsalpn binding the Mn^{III} ion in equatorial mode and an N-bonded terminal azide ion occupying the axial position (Figure 4.6). The structure has a crystallographic inversion centre at the mid point of the dimeric core. The equatorial bond lengths Mn-$O(N)_{ave}$ are 1.90(2.01) Å and the axial Mn-N_{azide} bond length is 2.14 Å. The Mn···O_p (where O_p is the oxygen atom of the phenoxo bridge) bond distance is 2.49 Å and the bridge angle, Mn-O_p···Mn is 101.5º, both within the range of out-of-plane dimers.[1-3,9] The basal atoms of **2** (N_2O_2) are coplanar (with rms deviation = 0.26Å) even though central manganese atom is displaced by 0.15 Å towards the azide ligand. The two halves of the 5-Clsalpn ligand, excluding the methylene groups and chlorine atoms are nearly planar (rms deviations = 0.06, 0.04 Å) with an interplanar angle of 11º. The two halves of the ligand are unsymmetrically disposed about the basal coordination plane with interplanar angles 37 and 26º. The intra dimer Mn…Mn distance is 3.44 Å, and the nearest inter dimer Mn…Mn distance is 8.29 Å. The shortest intra-dimer distance between two Cl atoms is 4.14 Å, which is 0.25 Å, longer than the complex $[Mn(5\text{-}Chlorosalen)N_3]_2$,[8] and shortest inter-dimer distance between two Cl atoms is 10.0 Å. The plane defining the $Mn_2(O_p)_2$ bridge makes an angle of 86.6º with the basal coordination plane, MnN2O2. The overall coordination geometry of each Mn(III) ion is distorted octahedral with the Jahn-Teller elongation seen along the N3-Mn···O_p axis. The packing view of the dimer is shown in Figure 4.7. In the crystal packing of

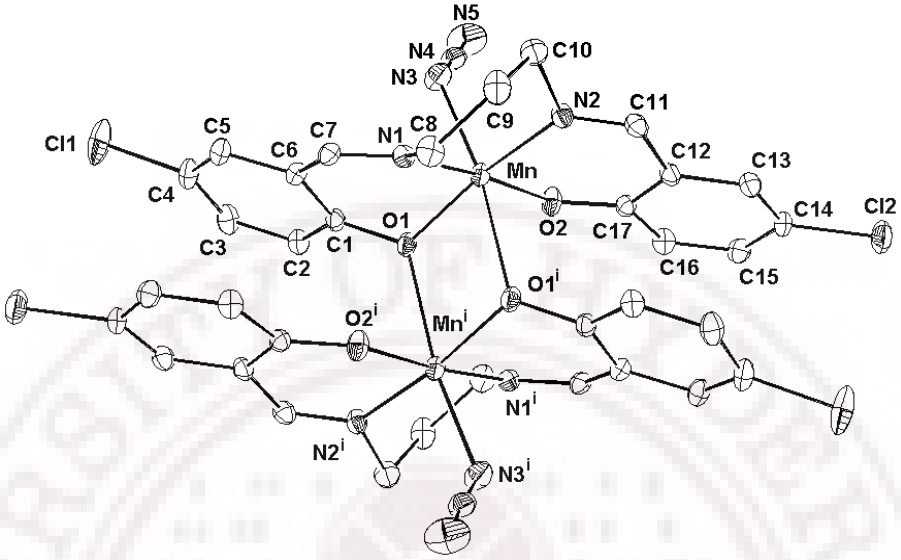

Figure 4.6 ORTEP view of the $[Mn(5\text{-}Clsalpn)N_3]_2$ in **2** with atom labeling. Atoms are shown as 30% thermal ellipsoids. Hydrogen atoms are omitted for clarity. i = *-x*, *-y*, *-z*+1.

Table 4.5 Selected bond lengths [Å] and angles [°] for $[Mn(5\text{-}Clsalpn|)N_3]_2$ (**2**)

Mn-O1	1.922(2)	Mn-N1	2.032(3)	Mn-N3	2.136(3)
Mn-O2	1.880(2)	Mn-N2	1.991(3)	Mn-O1#1	2.492(2)
N3-N4	1.190(4)	N4-N5	1.151(4)		
O1-Mn-O2	92.12(9)	O2-Mn-N1	172.9(1)	O1-Mn-O1#1	78.53(9)
O1-Mn-N2	169.3(1)	O2-Mn-N2	90.2(1)	O2-Mn-O1#1	89.87(9)
O1-Mn-N1	87.53(1)	O2-Mn-N3	96.3(1)	N1-Mn-O1#1	83.06(9)
O1-Mn-N3	95.4(1)	N2-Mn-N1	88.9(1)	N2-Mn-O1#1	91.04(9)
N2-Mn-N3	94.8(1)	N1-Mn-N3	90.8(1)	N3-Mn-O1#1	171.5(1)
Mn-N3- N4	127.5(2)	N3-N4-N5	178.0(4)	Mn-O1-Mn#1	101.5(1)

#1, *x*, *-y*, *-z*+1.

complex **2**, there are strong interdimer interactions between N5 from the coordinated terminal azide ion with C7(=CH···N5) and Cl1 with C3 atom of the 5-Clsalpn with bond distances 2.65 and 2.83 Å respectively. The Cl atoms are also participating in inter dimer interaction and the bond distance Cl1···Cl2 3.47Å, which is with in the range of van der Walls radii (3.5 Å). Finally the complex **2** leads a 2D-net work because of these inter-dimer interactions. The 2D-net work of the complex **2** is shown in the Figure 4.8. Selected bond distances and angles are listed in Tables 4.5

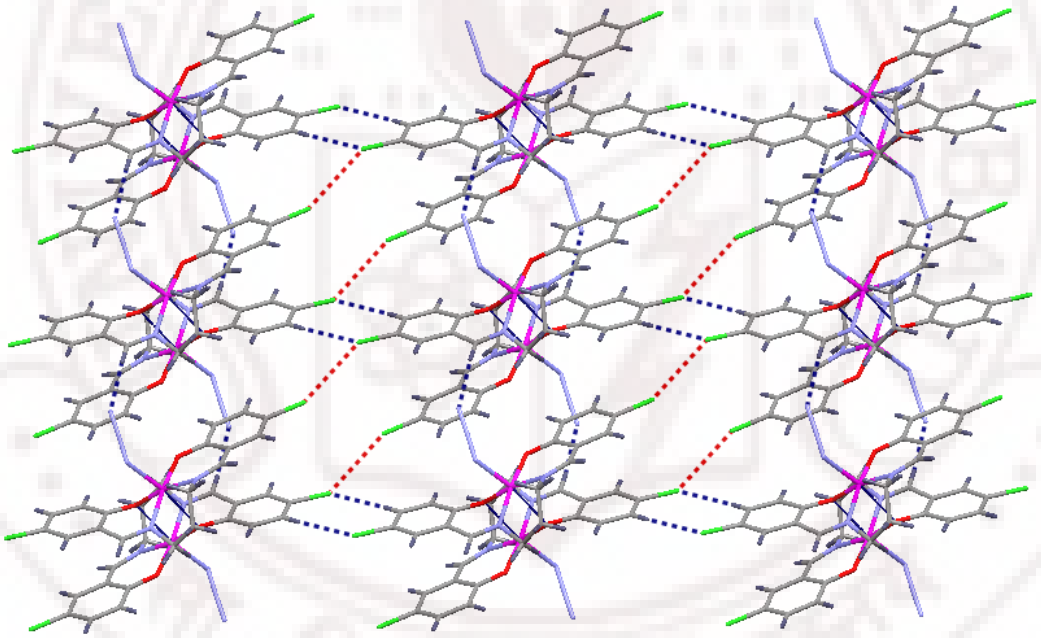

Figure 4.7 2D-network view of $[Mn(5\text{-}Clsalpn)N_3]_2$ (2) through interdimer interactions. Terminal azide ion, Cl atom inter dimer interaction with 5-Clsalpn were represented with blue doted lines and Cl atoms interactions were in red doted line.

4.3.3. FTIR Spectra

The IR spectra of the precipitate [Mn(5-Clsalpn)N_3], compounds **1** and **2** exhibit strong absorption in the range of 2030-2050 cm^{-1}, which is attributed to the asymmetric starching vibration of azide group in the range of reported. The sharp asymmetric stretching vibration (2048 cm^{-1}) of azide in precipitate [Mn(5-Clsalpn)N_3] is similar to the asymmetric stretching vibration (2046 cm^{-1}) of azide ion **1a** and **1b** crystals. The asymmetric stretching vibration of azide ion in compound **2** is (2035 cm^{-1}) is different from precipitate and compound **1**, such difference arising from the different coordination modes of the N_3^- ion. The strong absorption at 1620 cm^{-1}, assignable to the (-C=N) starching vibration of Schiff-base. The rest of the IR (3000-400 cm^{-1}) is almost identical for the precipitate and compounds **1** and **2**. All these absorptions are with in the reported range.[23]

4.3.4. Magnetic measurements

The temperature-dependence of the magnetic susceptibility χ_m, of **1** and **2** was measured in the temperature range 1.98-300 K (Figures 4.8 and 4.9). The room temperature $\chi_m T$ (cm^3 mol^{-1} K) value of the complex **1** per magnetic ion is 2.84 cm^3 mol^{-1} K at 300 K (close to the expected spin-only value, 3.00 cm^3 mol^{-1} K). While decreasing temperature, there is no significant change up to about 75 K, from where $\chi_m T$ decreased to 1.10 cm^3 mol^{-1} K at 9.8 K and to 0.433 cm^3 mol^{-1} K at 2.00 K. The decrease in $\chi_m T$ is characteristic of an antiferromagnetic exchange interaction between the two high-spin Mn^{III} ions. The data were fitted by using the Heisenberg chain equation[12] with the following results: g = 1.99 (fixed), J = -15.9 (2) cm^{-1}, θ =

1.19 (2) K and L.S. Error = 0.00559. The *J* value obtained for **1** is comparatively higher than *trans*-μ-(1,3) azide briged 1D-polymeric compound.[4-7]

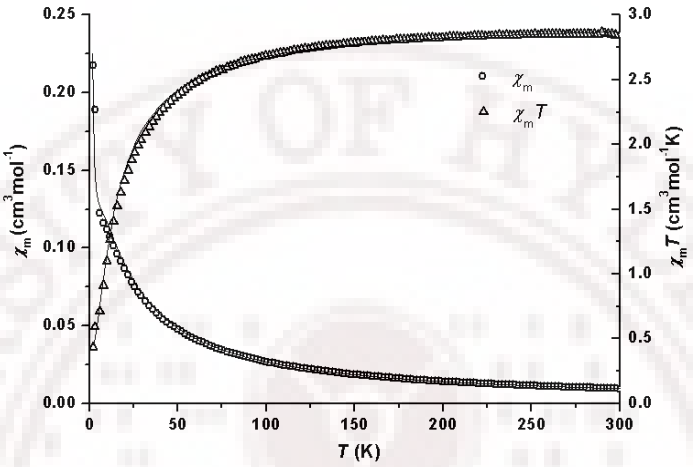

Figure 4.8 Temperature variation of magnetic susceptibility (per magnetic ion) for compound $[Mn(5\text{-}Clsalpn)N_3]_n$ (**1**). The solid lines result from a least-square fit to the data of the theoretical values calculated with the Heisenberg chain equation.

The room temperature $\chi_m T$ value of the dinuclear compound **2** is 6.13 cm^3 mol^{-1} K, which is comparable to the expected spin-only value of 6.00 cm^3 mol^{-1} K per dinuclear Mn^{III} unit. When temperature is lowered, in the case of compound **2**, $\chi_m T$ increases continuously to reach a maximum value of 13.59 cm^3 mol^{-1} K at 2.8 K further cooling leads to a decrease to 12.76 cm^3 mol^{-1} K at 1.99 K. Since the expected value for the $S = 4$ ground state is 10.00 cm^3 mol^{-1} K, this result proves the ferromagnetic coupling within the dimer. The data were fitted by using the dimer moldel[17] including inter dimer interactions with in the molecular field approximation shown in Figure 4.9. The best fit parameters obtained for the dimer equation are: J =

1.263(2) cm^{-1}, zj = 0.0263(6) cm^{-1}, g = 2.00 (fixed), LSE = 0.06354.

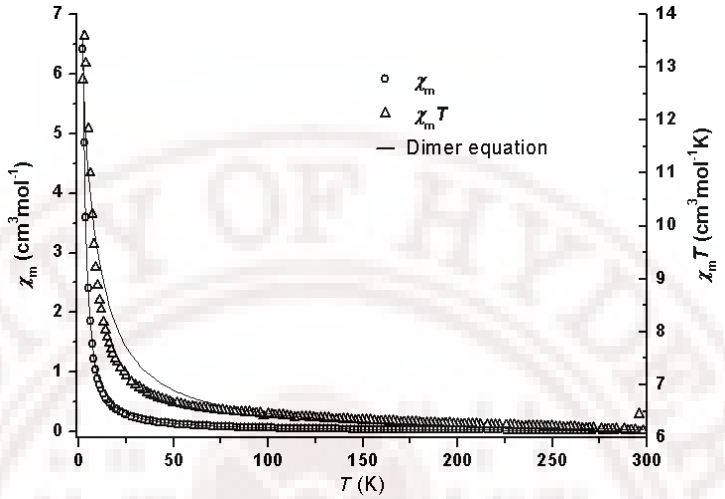

Figure 4.9 Temperature variation of the magnetic susceptibility χ_m and $\chi_m T$ product (per dimeric unit) for compound $[Mn(5\text{-}Clsalpn)N_3]_2$ (**2**). The solid lines result from a least-square fit to the data of the theoretical values calculated with the dimer equation.

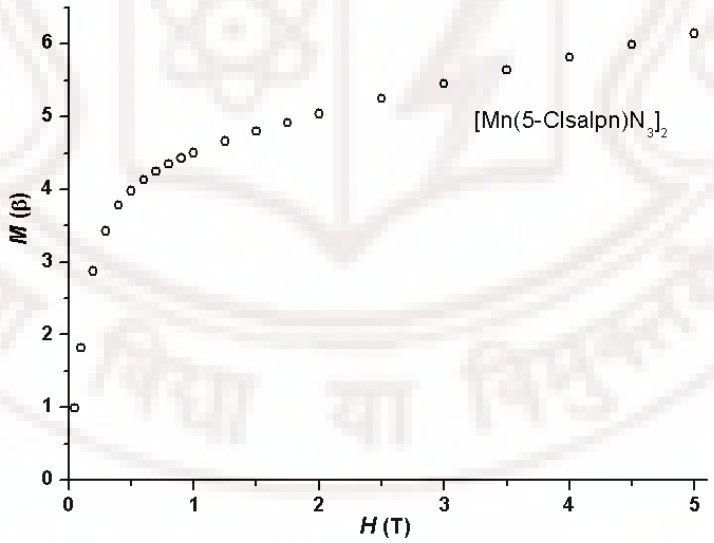

Figure 4.10 Variation of magnetization with applied field at 2 K for complex **2**.

The magnetic susceptibilities also fitted through exact diagonalisation of the spin Hamiltonian including axial Zeeman and zfs terms and isotropic exchange[18] and fitted to the experimental magnetic data by least-squares techniques.[19] The best sets of parameters obtained by least square fitting are : $J = 0.88$ cm^{-1}, $D = -0.025$ cm^{-1}, $g = 2.01$. Magnetization with applied field at 2K is shown in the Figure 4.10.

In order to check whether compound **2** behaves as single molecule magnet

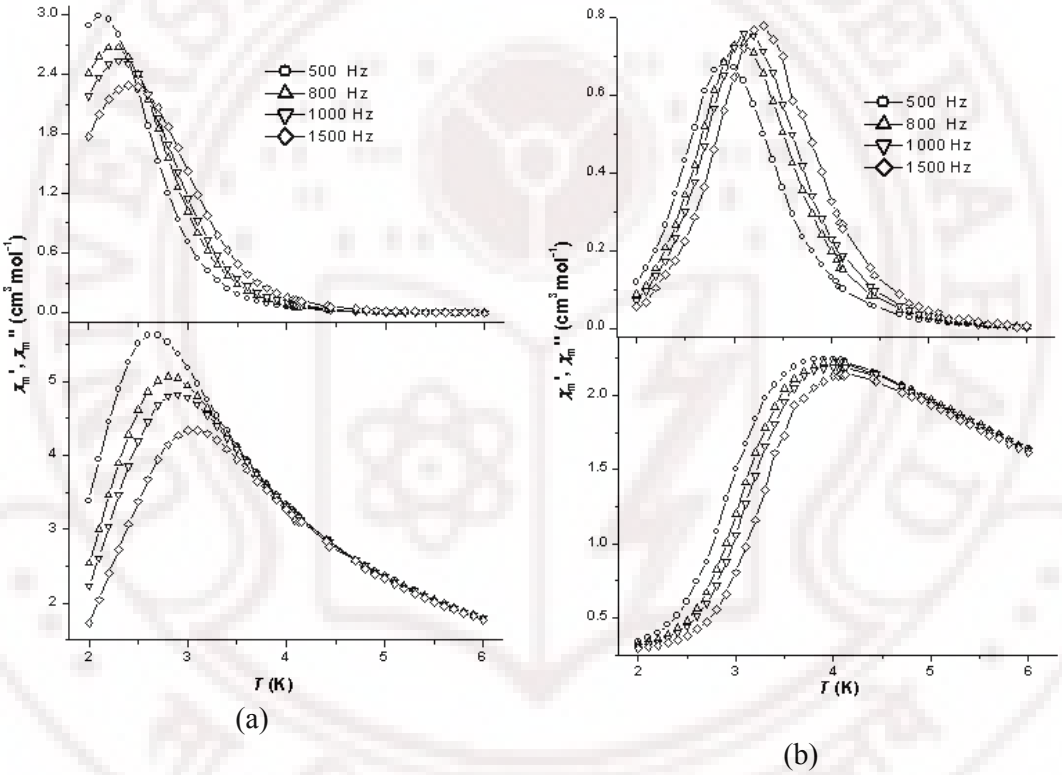

Figure 4.11 Temperature variation of the in-phase (χ', bottom) and out-of-phase (χ'', top) components of the ac-magnetic susceptibility for complex **2** at a DC field of (a) zero T and (b) 0.3 T. Solid lines between the experimental data points are shown as a guide to the eye, they do not result from fitting.

(SMM), the AC susceptibility was measured in the temperature range 2-10 K at different frequencies. The observation of frequency dependent in-phase (χ') and out-of-phase (χ'') magnetic susceptibilities are shown in Figure 4.11.

Arrhenius type plot is shown in Figure 4.12, constructed as explained in Chapter 1 (Section 1.4.2). The fit leads to a value of 17.7 K for the activation energy (T_0) and 4.6x10^{-7} s for τ_0, respectively at zero field. The corresponding values at a field of 0.3 T are 26.0 K and 2.4x10^{-7} s, respectively. These values are comparable to those obtained for the first dinuclear Mn(III) complex showing SMM, *viz.*, [Mn(saltmen)(ReO$_4$)]$_2$.[24]

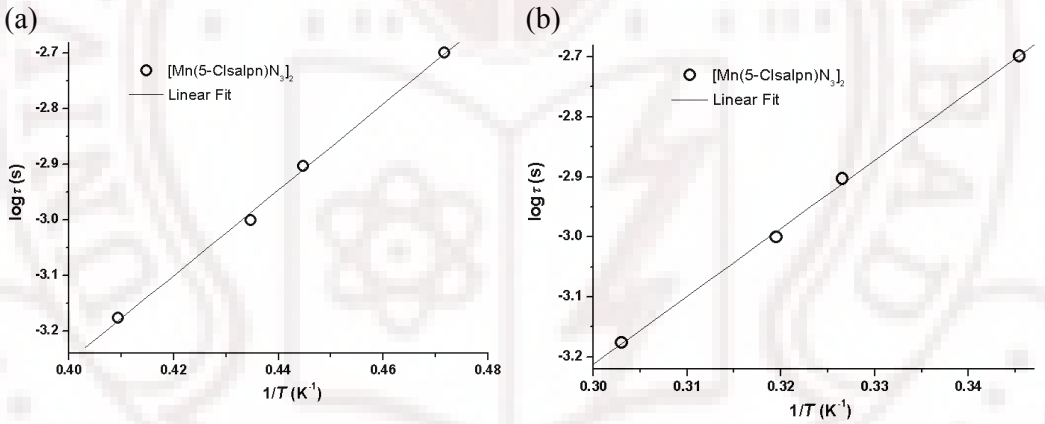

Slope = 7.710, intercept = –6.338

Slope = 11.308, intercept = –6.604

Figure 4.12 Plot of the relaxation time τ versus 1/T for **2** at (a) zero field and (b) 0.3 T.

It is difficult to explain the correlation between the structural parameters of phenoxo-bridged Mn(III) out-of-plane-bridged complex with magnetic parameters due to the small range of the observed *J* values, which are themselves quite small. The important bond distance (Å) and bond angle (º) of the dimeric core is Mn-O,

Mn···O_p, Mn…Mn, Mn-O_p···Mn; 1.92, 2.43, 3.44, 101.5 respectively. These parameters are comparable with $[Mn(saltmen)(H_2O)]_2(ClO_4)_2$[3] intradimer ferromagnetic complex (Mn-O, Mn···O_p, Mn…Mn, Mn-O_p···Mn; 1.91 Å, 2.43 Å, 3.38 Å, 101.6º and the best fitted magnetic parameters J = 1.79 cm^{-1}, D = –2.53 cm^{-1}, g = 1.93 and zJ' = –0.79 cm^{-1}), except that in the present complex both the intradimer as well as the interdimer pathways are ferromagnetic leading to a $\chi_m T$ value greater than 10 cm^3 mol^{-1} K at the lowest temperature.

4.4. Conclusions

The first end-on trivalent Mn^{III}(5-Clsalpn)-μ-(1,1)azide bridged compounds **1a** and **1b** are the polymorphs of the $[Mn(5\text{-}Clsalpn)N_3]$. The crystal structure of complexes **1a** and **1b** are similar to that of the *trans*-μ-(1,3)azide bridged polymeric complex $[Mn(salpn)N_3]_n$.[4] and analogous to other azide-bridged $[Mn(SB)N_3]_n$, (where SB is salen-type schiff base) polymers.[5-7] The simple $[Mn(salpn)N_3]$ is 1D-*trans*-μ-(1,3)azide helical polymer, but the replacement of salpn with 5-Clsalpn, the [Mn(5-Clsalpn)N3] is a one dimensional *trans*-μ-(1,1)azide zig-zag polymer. The magnetued of exchange exchange parameter J of this complex is higher (–15 cm^{-1}) than the observed J values[4-7] (–3 to –5 cm^{-1}). The Jahn-Teller axis is unsymmetrical in compound **1a** (**1b**). The compound **2** is a phenoxo-bridged dimer and having ferromagnetic coupling and shows SMM property.

4.5. References

1. (a) Lu, Z.; Yuan, M.; Pan, F.; Gao, S.; Zhang, D.; Zhu, D. *Inorg. Chem.* **2006**, *45*, 3538 (and references therein). (b) Lecren, L.; Wernsdorfer, W.; Li, Y.-G.; Vindigi, A.; Miyasaka, H.; Clerac, R. *J. Am. Chem. Soc*. **2007**, *129*, 5045.
2. Miyasaka, H.; Clerac, R.; Ishii, T.; Chang, H.; Kitagawa, S.; Yamashita, M. *J. Chem. Soc., Dalton Trans*. **2002**, 1528.
3. Saha, S.; Mal, D.; Koner, S.; Bhattacherjee, A.; Gutlich, P.; Mondel, S.; Mukherjee, M.; Okamoto, K.-I. *Polyhedron*, **2004**, *23*, 1811.
4. (a) Reddy, K. R.; Rajasekharan, M. V.; Tuchagues, J. -P. *Inorg. Chem*. **1998**, *37*, 5978. (b) Li, H.; Zhong, Z. J.; Duan, C. Y.; Yu, X. Z.; Mak, T. C. W.; Wu, B. *Inorg. Chim. Acta* **1998**, *271*, 99.
5. (a) Panja, A.; Shaikh, N.; Vojtısek, P.; Gao, S.; Banerjee, P. *New J. Chem.* **2002**, *26*, 1025. (b) Kennedy, B. J.; Murray, K. S. *Inorg. Chem.***1985**, *24*, 1552.
6. Ko, H. H.; Lim, J. H.; Kim, H. C.; Hong, C. S. *Inorg. Chem.* **2006**, *45*, 8847.
7. Yuan, M.; Zhao, F.; Zhang, W.; Wang, Z. -M.; Gao, S. *Inorg. Chem.* **2007**, *46,* 11235.
8. Darensbourg, D, J.; Frantz, E, B. *Inorg. Chem.* **2007**, *46*, 5967.
9. Miyasaka, H.; Saitoh, A.; Abe, S. *Coord. Chem. Rev.* **2007**, *251*, 2622.
10. Liu, T,-F.; Fu, D.; Gao, S.; Zhang, Y, -Z.; Sun, H, -L.; Su, G.; Liu, Y.-J. *J. Am. Chem. Soc.* **2003**, *125*, 13976.

11. Yue, Y.-F.; Gao, E. -Q.; Fang, C. -J.; Zheng, T.; Liang, J.; Yan, C. -H. *Crys. Growth. Des.* **2008**, *8*, 3295.

12. Liu, F. -C.; Zeng, Y. -F.; Zhao, J. -P.; Hu, B. -W.; Bu, X. -H.; Ribas, J.; Cano, J. *Inorg. Chem.* **2007**, *46*, 1520.

13. Abu-Youssef, M. A. M.; Drillon, M.; Escuer, A.; Goher, M. A. S.; Mautner, F. A.; Vicente. R. *Inorg. Chem.* **2007**, *39*, 5022.

14. Pascal, P. *Ann. Chim. Phys*. **1910**, *19*, 5.

15. Chandramouli, G. V. R.; Balagopalakrishna, C.; Rajasekharan, M. V.; Manoharan, P. T. *Comput. Chem.* **1996**, *20*, 353.

16. Koenig, E.; Desai, V. P.; Kanallakopulos, B.; Klenze, R. *Chem. Phys.***1980**, *54*, 109.

17. O'Connor, C. J. *Prog. Inorg. Chem.* **1982***, 29*, 203.

18. Garge, P.; Chikate, R.; Padhye, S.; Savariault, J.-M.; de Loth, P.; Tuchagues, J.-P. *Inorg. Chem*. **1990**, *29*, 3315.

19. James, F.; Roos, M. "*MINUIT Program*, a System for Function Minimization and Analysis of the Parameters Errors and Correlations"; *Comput. Phys. Commun.*, **1975**, *10*, 345.

20. SAINTPLUS, Bruker AXS Inc., Madison, Wisconsin, USA, **2003**.

21. Sheldrick, G. M. SADABS, Program for Empirical Absorption Correction, University of Gottingen, Gottingen, Germany **1996**.

22. Sheldrick, G. M. SHELX-97, Programs for Crystal Structure Analysis, University of Gottingen, Gottingen, Germany 1997.

23. Nakamoto, K. *Infrared and Raman Spectra of Inorganic and coordination Compounds*; 3 ed.; John Wiley & Sons, Inc.: New York, 1997, pp 270.

24. Miyasaka, H.; Clerac, R.; Wernsdorfer, W.; Lecren, L.; Bonhomme, C.; Sugiura, K.; Tamashita, M. *Angew. Chem. Int. Ed.* **2004**, *43*, 2801.

UNIVERSITY OF HYDERABAD

CHAPTER V

Synthesis, Crystal Structure and Electronic spectra of $[Mn(salmen)NCO]_2$, $[Mn(salmen)NCS]_2$, $[Mn(5\text{-}Clsalen)NCO]_2$, $[Mn(4\text{-}MeOsalen)(H_2O)N_3]$, $[Mn(4\text{-}MeOsalen)N_3]_n$ and $[Mn(4\text{-}MeOsalen)(H_2O)NCS]$

5.1. Introduction

Many coordination compounds of Mn(III) with the combination of a tetradentate Schiff base (SB) ligand and a pseudo-halide ion (N_3^-, NCS^-, NCO^-) have been synthesized and characterized. These compounds have general formula [Mn(SB)X], where X is a pseudohalide ion. To achieve six coordination, these Mn(III) compounds may be mononuclear with neutral solvent molecule in the six position,[1-4] phenoxo-bridged dimers,[5-7] or end-to-end pesudohalide bridged 1D-polymers.[8-12] Depending upon the bridging geometry, these complexes exhibit a variety of magnetic interactions and behave like ferro or antiferro magnetic compounds. In this chapter we report on three new phenoxo bridged complexes, $[Mn(salmen)NCO]_2$ (**1**), $[Mn(salmen)NCS]_2$ (**2**), $Mn(5\text{-}Clsalen)NCO]_2$ (**3**) and three new Mn(III) complexes with 4-MeOsalen ligand and pseudohalide ion $[Mn(4\text{-}MeOsalen)(H_2O)N_3]$ (**4**), $[Mn(4\text{-}MeOsalen)N_3]_n$ (**5**) and $[Mn(4\text{-}MeOsalen)(H_2O)NCS]$ (**6**). Compounds **4** and **6** are simple mononuclear complexes.[1-4] The compound $[Mn(4\text{-}MeOsalen)N_3]_n$ (**5**) is *trans*-μ-(1,3)-azide bridged zig-zag 1D-polymer.[8-12]

5.2. Experimental Section

5.2.1 Synthesis

All chemicals used for synthesis were reagent grade. The Schiff bases were formed *in situ* in the presence of the appropriate metal salt.

[Mn(salmen)NCO]$_2$ (1): In a beaker open to the atmosphere, salicylaldehyde (0.244 g, 1.00 mmol) and 1,2-diaminopropane (0.074 g, 1.0 mmol) were stirred in 40 mL of methanol. $Mn(CH_3COO)_2.4H_2O$ (0.245 g, 1.00 mmol) was added, and stirring was continued for about 1 h. To the resulting solution, KOCN (0.162 g, 2.00 mmol) dissolved in a minimum amount of water was added. The solution was allowed to stand for about 3 h to complete the aerial oxidation of Mn^{II}. The filtered solution was kept at room temperature for three days to obtain dark brown crystals. Yield: 0.270 g (0.318 mmol, 31.8 %). Anal. Calcd. for $MnC_{18}H_{16}N_3O_3$: C, 57.1; H, 4.27; N, 11.14. Found: C, 57.20; H, 4.23; N, 11.23. Important IR absorptions (cm^{-1}): ν_a(NCO) 2160, ν_s(NCO) 1313, δ(NCO) 615, $\nu_{schiff\ base}$(C=N) 1620.

[Mn(salmen)NCS]$_2$ (2): In a beaker open to the atmosphere, salicylaldehyde (0.244 g, 1.00 mmol) and 1,2-diaminopropane (0.074 g, 1.0 mmol) were stirred in 40 mL of methanol. $Mn(CH_3COO)_2.4H_2O$ (0.245 g, 1.00 mmol) was added, and stirring was continued for about 1 h. To the resulting solution, KSCN (0.194 g, 2.00 mmol) dissolved in a minimum amount of water was added. The solution was allowed to stand for about 2 h to complete the air oxidation of Mn^{II}. The filtered solution was kept in a refrigerator (5º C) for four days when dark green crystals deposited. Yield: 0.306 g (0.389 mmol, 38.9 %). Anal. Calcd. for $MnC_{18}H_{16}N_3O_2S$: C, 54.96; H, 4.10;

N, 10.68. Found: C, 54.68; H, 4.13; N, 10.44. Important IR absorptions (cm^{-1}): ν_a(NCS) 2050, ν_s(NCS) 1307, δ(NCS) 615, $\nu_{schiff\ base}$(C=N) 1614.

[Mn(5-Clsalen)NCO]$_2$ (3): In a beaker open to the atmosphere, KOCN (0.162 g, 2.00 mmol) and $Mn(CH_3COO)_2.4H_2O$ (0.245 g, 1.00 mmol) were stirred for 30 minutes in 30 mL methanol and filtered. 5-Chlorosalicylaldyde (0.313 g, 2.00 mmol) was taken in 60 mL methanol, to this ethylenediamine (0.067 g, 1.0 mmol) was added. This Schiff base (5-Clsalen) solution was then microwave irradiated for 1 minute at 160 W cooled to room temperature and then filtered. The two solutions were mixed and allowed to stand for about 2 h to complete the aerial oxidation of Mn^{II}. The filtered solution was kept at room temperature for four days to obtain dark brown crystals. Yield: 0.289 g (0.335 mmol, 33.5 %). Anal. Calcd. for $MnC_{17}H_{14}N_3O_3Cl_2$: C, 47.11; H, 3.26; N, 11.08. Found: C, 47.02; H, 3.19; N, 10.99. Important IR absorptions (cm^{-1}): ν_a(NCO) 2168, ν_s(NCO) 1298, δ(NCO) 610, $\nu_{schiff\ base}$(C=N) 1628.

[Mn(4-MeOsalen)(H_2O)N_3] (4): In a beaker open to the atmosphere, 2-hydroxy-4-methoxybanzaldehyde (0.152 g, 1.00 mmol) and ethylenediamine (0.034 ml, 0.50 mmol, 0.030 g) were stirred for 10 minutes in 40 mL of methanol. $Mn(ClO_4)_2.6H_2O$ (0.181 g, 0.50 mmol) and solid NaOH (0.040g, 1.0 mmol) were added and stirring was continued for about 1 h. To the resulting solution, NaN_3 (0.065 g, 1.00 mmol) dissolved in 5 mL water was added. The solution was allowed to stand for about 3 h to complete the aerial oxidation of Mn^{II}. The precipitated sodium perchlorate was removed by filtration and the solution was kept at room temperature for four days to obtain dark brown crystals. Yield: 0.108 g (0.23 mmol, 46 %). Anal. Calcd. for

$MnC_{18}H_{20}N_5O_5$: C, 48.99; H, 4.57; N, 15.87. Found. C, 48.69; H, 4.46; N, 15.73. Important IR absorptions (cm^{-1}): ν_s(O-H) 3379, $\nu_a(N_3)$ 2056, $\nu_s(N_3)$ 1435, $\delta(N_3)$ 646, $\nu_{schiff\ base}$(C=N) 1595.

$[Mn(4\text{-}MeOsalen)N_3]_n$ (5): In a beaker open to the atmosphere, 2-hydroxy-4-methoxybanzaldehyde (0.152 g, 1.00 mmol) and ethylenediamine (0.034 ml, 0.50 mmol, 0.030 g) were stirred for 10 minutes in 40 mL of methanol. $Mn(CH_3COO)_2.4H_2O$ (0.123 g, 0.50 mmol) was added, and stirring was continued for about 1 h. To the resulting solution, NaN_3 (0.065 g, 1.00 mmol) dissolved in 5 mL water was added. The solution was allowed to stand for about 3 h to complete the aerial oxidation of Mn^{II}. The filtered solution was kept at room temperature for four days yielding a crystalline precipitate. The precipitate was separated and dried. Yield: 0.101g (0.24 mmol, 48%). It was recrystallized from methanol to obtain dark-brown X-ray quality crystals. Anal. Calcd. for $MnC_{18}H_{18}N_5O_4$: C, 51.07; H, 4.29; N, 16.54. Found. C, 51.13; H, 4.23; N, 16.31. Important IR absorptions (cm^{-1}): $\nu_a(N_3)$ 2031, $\nu_s(N_3)$ 1304, $\delta(N_3)$ 644, $\nu_{schiff\ base}$(C=N) 1608.

$[Mn(4\text{-}MeOsalen)(H_2O)NCS]$ (6): In a beaker open to the atmosphere, 2-hydroxy-4-methoxybanzaldehyde (0.152 g, 1.00 mmol) and ethylenediamine (0.034 ml, 0.50 mmol, 0.030 g) were stirred for 10 minutes in 40 mL of methanol. $Mn(CH_3COO)_2.4H_2O$ (0.123 g, 0.50 mmol) was added, and stirring was continued for about 1 h. To the resulting solution, KSCN (0.094 g, 1.00 mmol) dissolved in 12 mL of methanol was added. The solution was allowed to stand for about 3 h to complete the aerial oxidation of Mn^{II}. The filtered solution was kept at room temperature for four days to obtain dark brown crystals. Yield: 0.110 g (0.24 mmol,

48 %). Anal. Calcd. for $MnC_{19}H_{20}N_3O_5S$: C, 49.89; H, 4.41; N, 9.19. Found. C, 48.72; H, 4.40; N, 9.08. Important IR absorptions (cm^{-1}): ν_s(O-H) 3439, ν_a(NCS) 2065, ν_s(NCS) 1439, δ(NCS) 642, $\nu_{schiff\ base}$(C=N) 1597.

5.2.2. Physical measurements

IR spectra were obtained in KBr pellets using Shimadzu FT-IR 8000 spectrometer. Elemental analysis of the complexes was performed on a FLASH EA SERIES CHNS analyzer. Absorption spectra for **1-6** in methanol were measured on a Shimadzu UV-3100 PC spectrometer.

5.2.3. X-ray crystallography

X-ray data were collected for **1-6** on a Bruker SMART APEX CCD X-ray diffractometer, using graphite-monochromated Mo-Kα radiation (λ = 0.71073 Å). Data were reduced using SAINTPLUS[13] and a multi-scan absorption correction using SADABS[14] was performed. The structure was solved using SHELXS-97 and full matrix least squares refinement against F^2 was carried out using SHELXL-97.[15] All ring hydrogen atoms were assigned on the basis of geometrical considerations and were allowed to ride upon the respective carbon atoms. All hydrogen atoms were assigned fixed U_{iso} values, equal to $1.2U_{eq}$ of the parent atom for ring and $1.5U_{eq}$ for methyl and solvent water molecule hydrogen atoms. Crystallographic data are presented in Tables 5.1- 5.8.

Table 5.1 Crystallographic data and structure refinement for **1**, **2** and **3**

	1	**2**	**3**
Formula	$C_{36}H_{32}Mn_2N_6O_6$	$C_{36}H_{32}Mn_2N_6O_4S_2$	$C_{34}H_{24}Cl_4Mn_2N_6O_6$
Formula weight	754.56	786.70	864.27
Crystal system	Monoclinic	monoclinic	monoclinic
a (Å)	8.642(6)	8.8810(7)	8.5460(4)
b (Å)	13.663(9)	13.9064(11)	14.9459(7)
c (Å)	14.139(9)	14.7884(11)	13.4739(7)
α (º)	90	90	90
β (º)	104.558(10)	107.0930(10)	106.7790(10)
γ (º)	90	90	90
V (Å^3)	1615.9(18)	1745.7(2)	1647.72(14)
Space group	*P* $2_1/n$	*P* $2_1/n$	*P* $2_1/n$
Z	2	2	2
T (K)	100	100	100
ρ_{calcd} (g cm^{-3})	1.551	1.497	1.742
μ (mm^{-1})	0.840	0.892	1.150
θ Range (º)	2.11-26.34	2.05-26.00	2.09-26.02
h/*k*/*l* indices	-10, 10/ -17, 16/ -17, 17	-10, 10/ -17, 17/ -18, 18	-10, 10/ -17, 16/ -16, 16
Reflections collected	15739	17592	16722
Unique reflection, R_{int}	3215, 0.0847	3413, 0.0571	3247, 0.0367
GooF	1.068	1.052	1.047
$R1[I > 2\sigma(I)]$	0.0587	0.0652	0.0311
wR_2[all data]	0.1664	0.1821	0.0757
$\Delta\rho_{max}$, $\Delta\rho_{min}$ (e.Å^{-3})	1.175, -0.574	1.898, -0.689	0.403, -0.235
Weight. scheme (A, B)	0.0745, 1.56	0.1001, 2.37	0.0375, 1.10

5.3. Results and discussion

5.3.1. Synthesis: The compounds **1** and **2** were prepared by using a similar procedure, except for crystallization temperature. The Schiff base (salmen) was prepared *in situ* in methanol and compound **1** was crystallized at 25º C, while **2** was obtained at about 5º C. For these two complexes the reaction was done in aqueous methanolic medium. The same procedure when used for compound **3** gave no crystals but only powdery material. So to get compound **3**, the Schiff base (5-Clsalen) was prepared by using microwave irradiation at 160 W, for 1 minute and then the Schiff base was cooled to room temperature (pure mathanolic medium was used throughout). To get compound **4**, Schiff base (4-MeOsalen) was prepared *in situ*, in the presence of $Mn(ClO_4)_2.6H_2O$ and NaOH. The crystals of compound **4** were recrystallized from methanol. Based on IR spectra it was concluded that this recrystallization does not convert compound **4** to **5**. For complex **5,** $Mn(CH_3COO)_2.4H_2O$ instead of $Mn(ClO_4)_2.6H_2O$ in the absence of NaOH is used and the precipitate formed was recrystallized in methanol at room temperature. The IR of the precipitate and crystals are virtually identical and entirely different from that of **4**. The compound **6** is prepared in pure methanolic media with the same procedure described for **1** and **2**. To check for other (pseudo) polymorphs of complex **6**, the crystallization temperature was changed from 25º C to 5º C and the microcrystalline precipitate that formed after one week was collected and checked with IR spectra. The IR of the complex **6** crystallized at different temperatures are identical.

5.3.2. Structure of [Mn(salmen)NCO]$_2$ (1): The complex crystallizes in $P2_1/n$ space group. This dinuclear Mn(III) complex, contains two five-coordinated units, which are held by weak phenoxo-bridges is shown in Figure 5.1. Within each five coordinate unit, the tetradentate Schiff base ligand salmen coordinates in the equatorial plane, while the axial position is coordinated by a terminal N-bonded cyanate ion, in a bent mode. The complex has an inversion centre at the mid point of the dimeric core. The equatorial atoms (O2N2) are very nearly coplanar even though the manganese atom deviates from this plane by 0.23 Å (with rms deviation = 0.030 Å). The mean planes of the two halves of the Schiff base ligand (excluding the methylene groups) are inclined to each other by 15º. The significant equatorial Mn-(O,N)$_{av}$ and the axial Mn-N$_{ax}$ distances (Å) are 1.88, 1.98, and 2.11 respectively. The overall coordination geometry of each Mn^{III} ion is thus distorted octahedral with the Jahn-Teller elongation along the OCN-Mn···O axis. The phenoxo-bridged plane (Mn2O2) is nearly perpendicular to the equatorial coordination plane (dihedral angle 87.7º). The important bond distances (Å) and bond angle (º) of the dimeric core are: Mn-O, 1.90, Mn···O, 2.61, Mn-O···Mn, 97.9º. The Mn···Mn distance in the dimer is 3.43 Å. Selected bond distances and bond angles are shown in the Table 5.2. The important inter-dimer interactions in this complex are (i) =CH···N$_c$ (2.54 Å), (ii) =CH···O$_t$ (2.61 Å) and (iii) Ph-H···Cπ (2.64 Å) where, suffixes *c* and *t* refer to coordinated and terminal atom of the pseudohalide ion NCO^-. The free methyl group of the salmen is involved in a C-H···Phπ interaction (2.78 Å) which is shown in red dotted line in Figure 5.2.

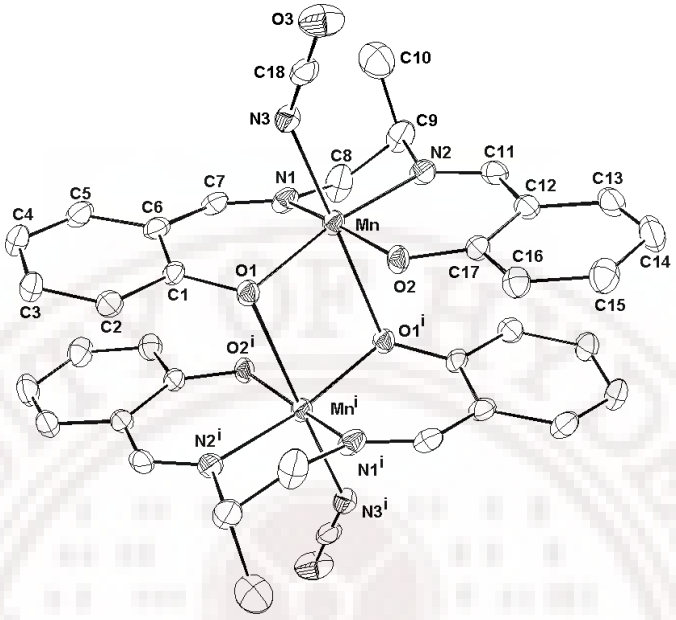

Figure 5.1 ORTEP view of the $[Mn(salmen)NCO]_2$ (**1**), Hydrogen atoms are omitted for clarity, and the thermal ellipsoids are represented at the 50% probability level. i = -*x*, -*y*+2, -*z*+1.

Table 5.2 Selected bond lengths [Å] and angles [°] for $[Mn(salmen)NCO]_2$ (1)

Mn-O1	1.898(3)	Mn-N1	1.991(4)	Mn-N3	2.115(4)
Mn-O2	1.860(3)	Mn-N2	1.977(3)	Mn-O1#1	2.608(3)
N3-C18	1.177(6)	C18-O3	1.196(6)	C9-C10	1.426(8)
O2-Mn-O1	93.62(12)	O1-Mn-N1	89.08(13)	O1-Mn-O1#1	82.06(11)
O2-Mn-N1	167.3(1)	O1-Mn-N2	162.8(1)	O2-Mn-O1#1	86.19(11)
O2-Mn-N2	92.41(14)	O1-Mn-N3	97.86(13)	N1-Mn-O1#1	82.07(12)
O2-Mn-N3	96.31(14)	N2-Mn-N1	81.66(15)	N2-Mn-O1#1	82.31(12)
N1-Mn-N3	95.55(15)	N2-Mn-N3	97.44(15)	N3-Mn-O1#1	177.5(1)
Mn-N3-C18	138.8(3)	N3-C18-O3	178.8(5)	Mn-O1-Mn#1	97.94(4)

#1 -*x*, -*y*+2, -*z*+1

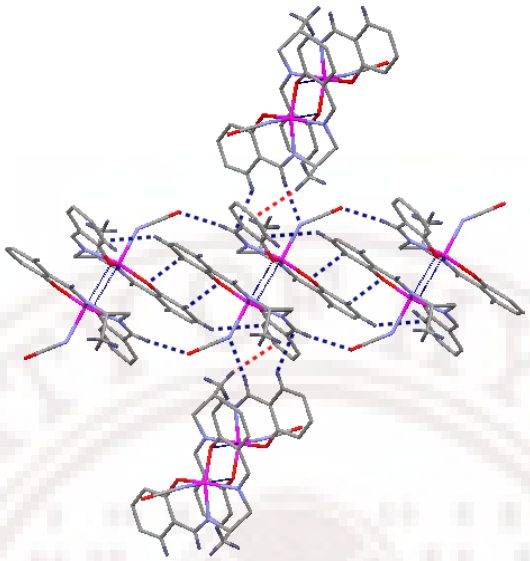

Figure 5.2 Intermolecular interactions between dimers in complex $[Mn(salmen)NCO]_2$ (**1**). Colour code for atoms: blue, N; red, O; grey C; purple, Mn.

5.3.3. Structure of $[Mn(salmen)NCS]_2$ (2): The complex crystallizes in $P2_1/n$ space group. This dinuclear Mn(III) complex, contains two five-coordinated units, which are held by phenoxo-bridges is shown in Figure 5.3. Within each five coordinate unit, the tetradentate Schiff base ligand salmen coordinates in the equatorial plane, while the axial position is coordinated by a terminal N-bonded thiocyanate ion, in a bent mode. The complex has an inversion centre at the mid point of the dimeric core. The equatorial atoms (O2N2) are very nearly coplanar even though the manganese atom deviates from this plane by 0.15 Å (with rms deviation = 0.046 Å). The mean planes of the two halves of the Schiff base ligand (excluding the methylene groups) are inclined to each other by 15º. The significant equatorial Mn-$(O,N)_{av}$ and the axial Mn-N_{ax} distances (Å) are 1.89, 1.97 and 2.17 respectively.

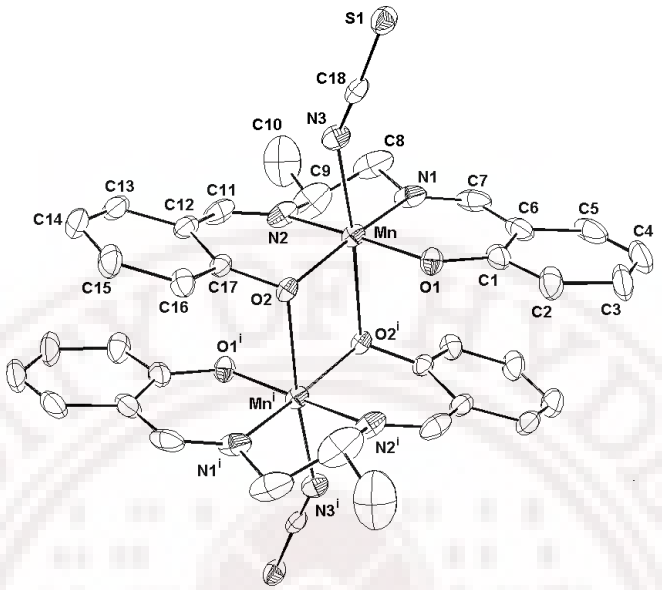

Figure 5.3 ORTEP view of the $[Mn(salmen)NCS]_2$ (**2**), Hydrogen atoms are omitted for clarity, and the thermal ellipsoids are represented at the 50% probability level. i = -*x*, -*y*+1, -*z*+1.

Table 5.3 Selected bond lengths [Å] and angles [°] for $[Mn(salmen)NCS]_2$ (2)

Mn-O1	1.865(3)	Mn-N1	1.973(4)	Mn-N3	2.166(4)
Mn-O2	1.907(3)	Mn-N2	1.975(4)	Mn-O2#1	2.456(3)
N3-C18	1.151(6)	C18- S1	1.636(5)	C9-C10	1.388(12)
O1-Mn-O2	95.22(13)	O2-Mn-N1	165.8(2)	O1-Mn-O2#1	89.36(12)
O1-Mn-N1	92.31(18)	O2-Mn-N2	89.64(16)	O2-Mn-O2#1	80.33(11)
O1-Mn-N2	171.6 (2)	O2-Mn-N3	95.48(14)	N1-Mn-O2#1	87.69(14)
O1-Mn-N3	93.99(15)	N1-Mn-N2	81.6(2)	N2-Mn-O2#1	84.75(14)
N1-Mn-N3	96.03(16)	N2-Mn-N3	92.31(16)	N3-Mn-O2#1	174.9(1)
Mn-N3-C18	150.0(4)	N3-C18-S1	177.4(4)	Mn-O2-Mn#1	99.67(11)

#1 -*x*, -*y*+1, -*z*+1

The overall coordination geometry of each Mn^{III} ion is thus distorted octahedral with the Jahn-Teller elongation along the SCN-Mn···O axis. The phenoxo-bridged plane (Mn2O2) is nearly perpendicular to the equatorial coordination plane, the dihedral angle is 87.7º. The important bond distances (Å) and bond angle (º) of the dimeric core are: Mn-O, 1.87, Mn···O, 2.46, Mn–O···Mn, 99.7º. The Mn···Mn distance in the dimers is 3.35 Å. Selected bond distances and bond angles are shown in the Table 5.3. The important inter-dimer interactions in this complex (i) =CH···N_c (2.83 Å), which is 0.29 Å more than complex **1**, (ii) =CH···S_t (2.84 Å) and (iii) Ph-H···S (2.91 Å) where, suffixes *c* and *t* refer to coordinated and terminal atom of the pseudohalide ion NCS^-. The methyl group of the salmen is involved in a C-H···S interaction (2.97 Å) which are shown in Figure 5.4.

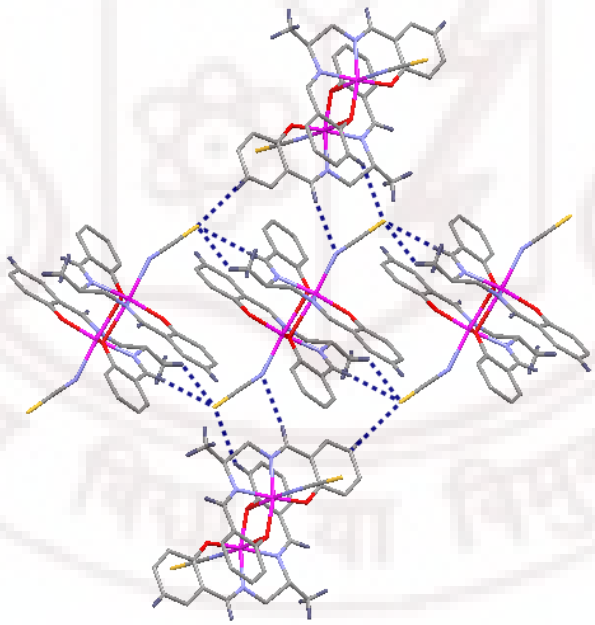

Figure 5.4 Intermolecular interactions between dimers in complex $[Mn(salmen)NCS]_2$ (**2**). Colour code for atoms: blue, N; red, O; grey C; purple, Mn, yellow S.

5.3.4. Structure of [Mn(5-Clsalen)NCO]$_2$ (3): The complex crystallizes in $P2_1/n$ space group. This dinuclear Mn(III) complex, contains two five-coordinated units, which are held by weak phenoxo-bridges is shown in Figure 5.5. Within each five coordinate unit, tetradentate Schiff base ligand 5-Clsalen coordinates in the equatorial plane, while the axial position is coordinated by a terminal N-bonded cyanate ion, in a bent mode. The complex has an inversion centre at the mid point of the dimeric core. The equatorial atoms (O2N2) are very nearly coplanar even though the manganese atom deviates from this plane by 0.22 Å (with rms deviation = 0.082 Å). The mean planes of the two halves of the Schiff base ligand (excluding the methylene groups) are inclined to each other by 8.8º. The significant equatorial Mn-$(O,N)_{av}$ and the axial Mn-N_{ax} distances are 1.91, 1.99 Å, and 2.11 Å respectively. The overall coordination geometry of each Mn^{III} ion is thus distorted octahedral with the Jahn-Teller elongation along the OCN-Mn···O axis. The phenoxo-bridged plane (Mn2O2) is nearly perpendicular to the equatorial coordination plane (dihedral angle 85.3º). The important bond distances (Å) and bond angle (º) of the dimeric core are: Mn-O, 1.91, Mn···O, 2.59, Mn–O···Mn 100.4º. The Mn···Mn distance in the dimer is 3.49 Å. Selected bond distances and bond angles are shown in the Table 5.4. In the crystal packing of the complex **3**, there are strong interdimer interactions between O3 from the coordinated terminal cyanate ion with C7(=CH···O3) with bond distance 2.49 Å. The Cl atoms are also participating in inter dimer interactions and the bond distance Cl1···Cl2 and Cl2···Cl2 are 3.40, 3.41 Å respectively, which are with in the range of van der Walls radii (3.5 Å). Finally the complex **3** leads a 2D-net work

because of these inter-dimer interactions. The packing diagram of the complex 3 is shown in Figure 5.6.

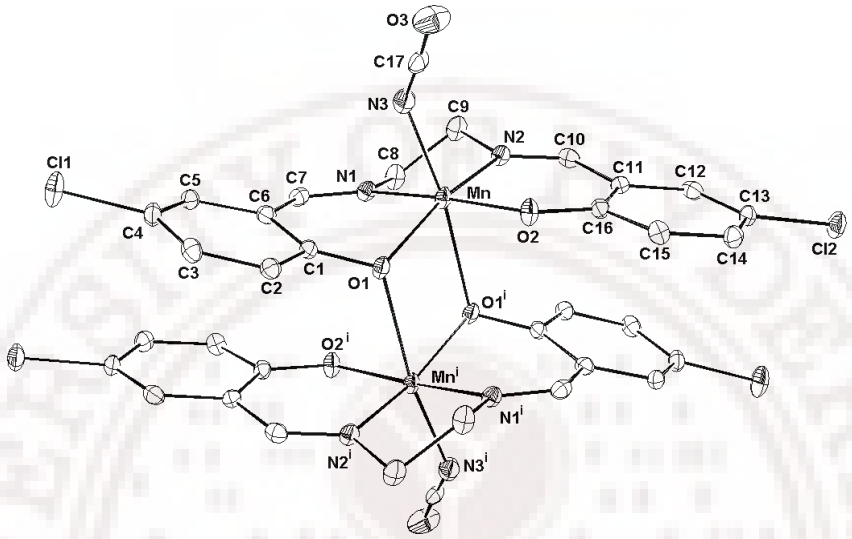

Figure 5.5 ORTEP view of the $[Mn(5\text{-}Clsalen)NCO]_2$ (**3**), Hydrogen atoms are omitted for clarity, and the thermal ellipsoids are represented at the 50% probability level. i = *-x*, *-y*+2, *-z*.

Table 5.4 Selected bond lengths [Å] and angles [°] for $[Mn(5\text{-}Clsalen)NCO]_2$ (3)

Mn-O1	1.9142(14)	Mn-N1	1.9947(17)	Mn-N3	2.115(2)
Mn-O2	1.8715(14)	Mn-N2	1.9857(17)	Mn-O1#1	2.586(2)
N3-C17	1.182(3)	O3-C17	1.203(3)		
O2-Mn-O1	95.46(6)	O1-Mn-N1	88.34(6)	O2-Mn-O1#1	90.36(6)
O2-Mn-N1	170.19(7)	O1-Mn-N2	160.11(7)	O1-Mn-O1#1	79.57(6)
O2-Mn-N2	91.74(7)	O1-Mn-N3	95.63(7)	N1-Mn-O1#1	81.41(6)
O2-Mn-N3	95.71(7)	N1-Mn-N3	92.91(7)	N2-Mn-O1#1	81.87(6)
Mn-N3- C17	139.0(2)	N2-Mn-N3	102.09(7)	N3-Mn-O1#1	172.62(6)
N3-C17-O3	177.8(2)	N2-Mn-N1	81.86(7)	Mn-O1-Mn#1	100.4 (3)

#1 *-x*, *-y*+2, *-z*

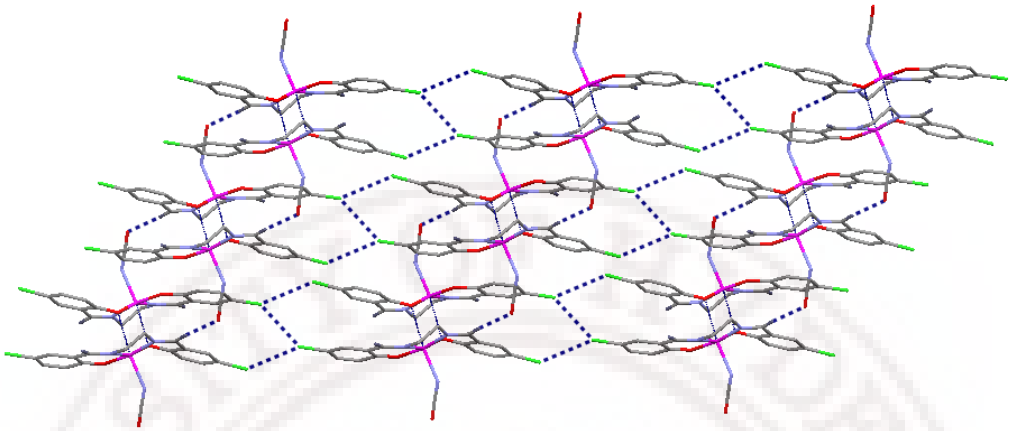

Figure 5.6 2D-network view of $[Mn(5\text{-}Clsalen)NCO]_2$ (**3**) through interdimer interactions. Colour code for atoms: blue, N; red, O; grey C; purple, Mn, green Cl.

5.3.5. Structure of $[Mn(4\text{-}MeOsalen)(H_2O)N_3]$ (4): The complex is mononuclear and crystallographically characterized in the orthorhombic system, space group *Pbca*, with 8 molecules present in the unit cell. The asymmetric unit is shown in Figure 5.7. The tetradentate Schiff base 4-MeOsalen coordinated to the Mn^{III} in equatorial plane with the bond length Mn-O(N)$_{ave}$, 1.89(1.98) Å. The apical positions are occupied by N-bonded terminal azide ion with bond length 2.21 Å and solvent water molecule with bond length 2.33 Å. The equatorial atoms (O2N2) are nearly coplanar even though the manganese atom deviates from this plane by 0.060 Å (with rms deviation = 0.025 Å). The mean planes of the two halves of the Schiff base ligand (excluding the methylene groups) are inclined to each other by 5.6º The overall coordination geometry of each Mn^{III} ion is thus distorted octahedral with the Jahn-Teller elongation along the N3–Mn···O5 axis. The coordinated water molecule

Table 5.5 Crystallographic data and structure refinement for **4**, **5** and **6**

	4	**5**	**6**
Formula	$C_{18}H_{20}MnN_5O_5$	$C_{18}H_{18}MnN_5O_4$	$C_{19}H_{20}MnN_3O_5S$
Formula weight	441.33	423.31	457.38
Crystal system	orthorhombic	orthorhombic	Monoclinic
a (Å)	14.349(3)	12.722(4)	11.4514(8)
b (Å)	12.634(3)	12.439(4)	13.1674(9)
c (Å)	21.153(4)	11.591(3)	14.0926(9)
α (º)	90	90	90
β (º)	90	90	109.9850(10)
γ (º)	90	90	90
V (Å^3)	3834.6(14)	1834.3(9)	1997.0(2)
Space group	*Pbca*	*Pbc*2$_1$	*P*2$_1$/*c*
Z	8	4	4
T (K)	298(2)	298(2)	298(2)
ρ_{calcd} (g cm^{-3})	1.529	1.533	1.521
μ (mm^{-1})	0.730	0.756	0.802
θ Range (º)	1.93-25.00	1.60-26.07	1.89-26.03
h/k/l indices	-17, 12/ -14, 15/ -25, 23	-15, 15/ -15, 15/ -14, 14	-14, 14/ -16, 16/ -17, 17
Reflections collected	17193	13587	20419
Unique reflection, R_{int}	3374, 0.0382	3587, 0.0313	3934, 0.0435
GooF	1.442	1.061	1.042
$R1[I > 2\sigma(I)]$	0.0746	0.0397	0.0440
wR_2[all data]	0.1378	0.0960	0.1090
$\Delta\rho_{max}$, $\Delta\rho_{min}$ (e.Å^{-3})	0.452, -0.370	0.349, -0.231	0.370, -0.193
Weight. scheme (A, B)	0.0220, 8.23	0.0465, 0.86	0.0573, 0.37

forms hydrogen bonds with coordinated phenoxo oxygen atoms of the Schiff base (4-MeOsalen) and resulting in a dimer as shown in Figure 5.8 with interatomic distances O1···H5B, O2···H5B, O5···O1(2) 2.14, 2.66 and 2.96(3.25) Å respectively. The intradimer Mn···Mn distance is 5.18 Å. The N5 atom of the N-bonded terminal N_3^- ion is also participating in forming hydrogen bond with O5 atom of the coordinated water molecule with bond length N5···O5 2.87 Å, which builds the monomeric units into a 1D-dimentional zig-zag polymeric chain along the *b*-axis (Figure 5.9). Finally the complex **4** leads to a 2D-net work because of the hydrogen bonds are shown in Figure 5.10. The molecular structure of this complex is similar to complex [Mn(3-OCH_3salen)(H_2O)NCS][1]. The shortest intrachain and interchain Mn···Mn bond lengths are 6.89 and 5.18 Å.

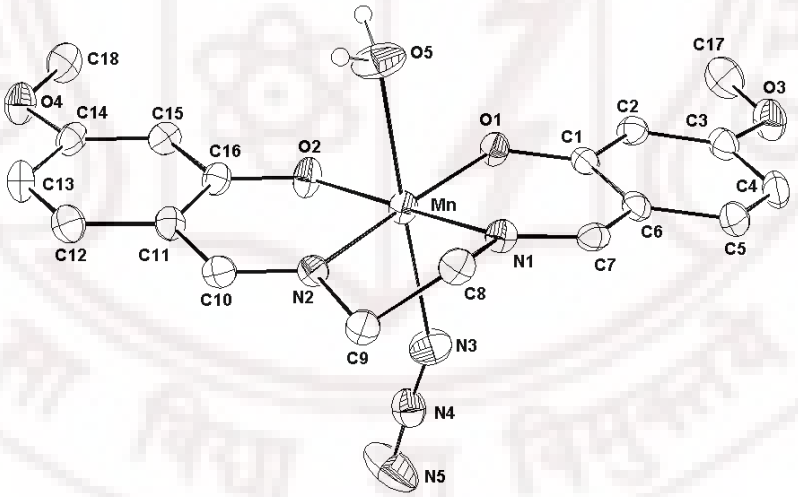

Figure 5.7 ORTEP view of the [Mn(4-MeOsalen)(H_2O)N_3] (**4**). Hydrogen atoms of the Schiff base are omitted for clarity, and the thermal ellipsoids are represented at the 30 % probability level.

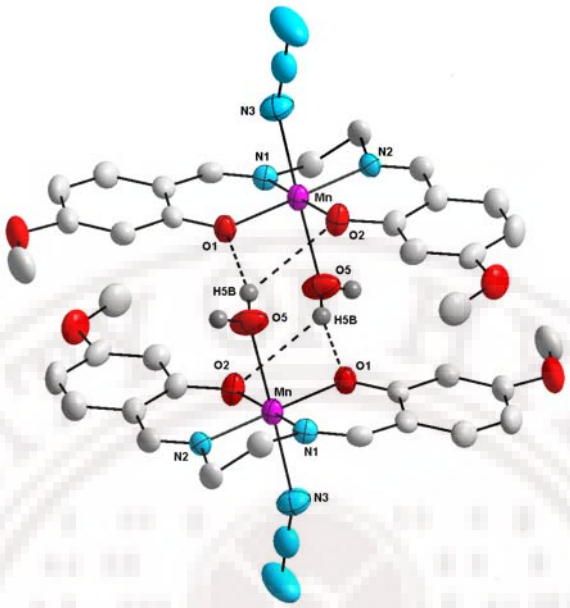

Figure 5.8 Dimeric view of [Mn(4-MeOsalen)(H_2O)N_3] (**4**) coordinated water molecule. For clarity Schiff base 4-MeOsalen hydrogens are omitted. Colour code for atoms: blue, N; red, O; grey C; purple, Mn.

Table 5.6 Selected bond lengths [Å] and angles [°] for [**Mn(4-MeOsalen)(H_2O)N_3**] (**4**)

Mn-O1	1.905(3)	Mn-N1	1.984(3)	Mn-O5	2.330(4)
Mn-O2	1.881(3)	Mn-N2	1.971(3)	Mn-N3	2.215(5)
N3-N4	1.161(6)	N4-N5	1.159(7)		
O1-Mn-N1	91.58(14)	O2-Mn-N1	172.76(14)	O1-Mn-O2	93.49(13)
O1-Mn-N2	173.33(14)	O2-Mn-N2	92.75(14)	O1-Mn-O5	89.77(15)
O1-Mn-N3	93.94(16)	O2-Mn-N3	96.23(17)	O2-Mn-O5	90.23(16)
N1-Mn-N2	82.00(15)	N1-Mn-N3	88.57(17)	N2-Mn-N3	87.71(17)
N1-Mn-O5	84.62(15)	N2-Mn-O5	87.86(15)	N3-Mn-O5	172.3(2)
Mn-N3-N4	151.9(4)	N3-N4-N5	177.6(6)		

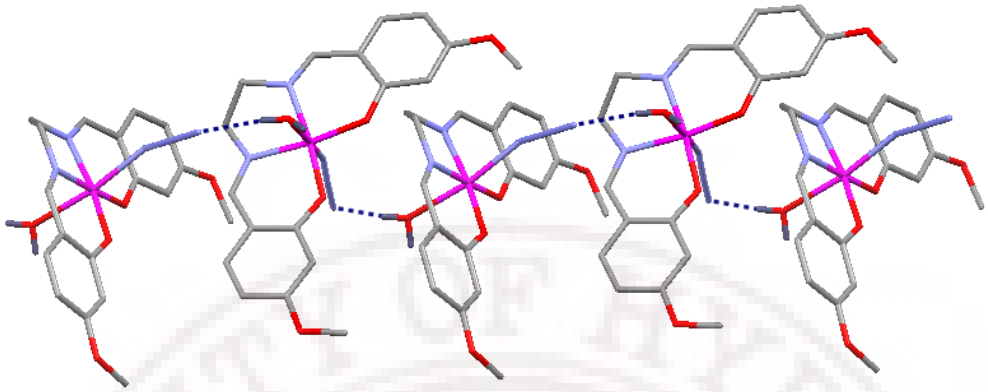

Figure 5.9 Perspective view of 1D-zig-zag polymeric chain in [Mn(4-MeOsalen)(H_2O)N_3] (**4**). For clarity Schiff base 4-MeOsalen hydrogens are omitted. Colour code for atoms: blue, N; red, O; grey C; purple, Mn.

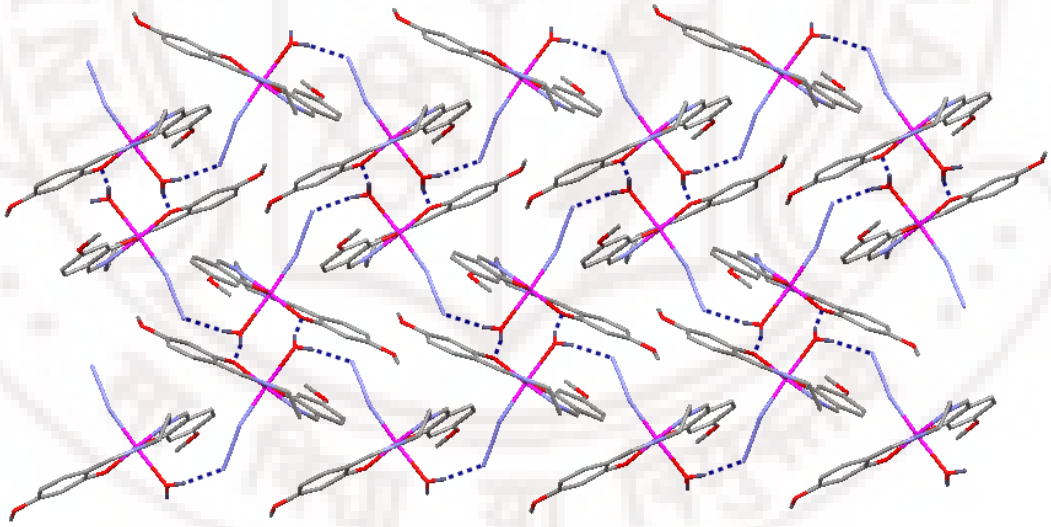

Figure 5.10 View of 2D-network in [Mn(4-MeOsalen)(H_2O)N_3] (**4**) through hydrogen bonds. For clarity Schiff base 4-MeOsalen hydrogens are omitted.

5.3.6. Structure of [Mn(4-MeOsalen)N_3]$_n$ (5): The asymmetric unit of **5** contains one Mn^{III} ion, and the coordination of Mn^{III} is to one tetradentate 4-MeOsalen ligand coordinating in the equatorial mode and two azide ions in axial positions (Figure 5.11). Each azide functions as a *trans*-μ-(1,3) bridge, resulting a one dimensional polymer. Each monomeric unit is related to its adjacent ones by a 2-fold screw axis, leading to a zig-zag propagation along the crystallographic *c*-axis (Figure 5.12). In the equatorial plane the bond lengths of Mn-$O_{(av)}$ and Mn-$N_{(av)}$ are 1.96, 1.99 Å respectively, which are comparable to those observed in other [Mn(SB)N_3]$_n$ compound.[4-7] The equatorial donor atoms (O_2N_2) are nearly coplanar (with rms deviation = 0.07 Å) even though the manganese atom deviates significantly from this plane 0.043 Å. The mean planes of the two halves of the Schiff base ligand, excluding the methylene group, are also individually planar (rms deviation = 0.02 Å), with the Mn deviating by 0.22 and 0.23 Å from this planes. The two halves of the Schiff base excluding the methylene group are inclined with respect to each other by 24º. The overall coordination geometry of each Mn^{III} ion is thus distorted octahedral with the Jahn-Teller elongation along the N3–Mn···N5 axis. Due to Jahn-Teller distortion the symmetrical elongated axial Mn-N3 and Mn-N5 lengths are 2.26 and 2.30 Å. The coordination of the azide bridge is almost symmetrical and the bond angles of Mn-N3-N4 and Mn-N5-N4 are 123 and 124º. As for N_3^- itself, N3-N4 (1.16 Å) and N4-N5 (1.19 Å) bond lengths are symmetrical and N3-N4-N5 bond angle is 179.6º.

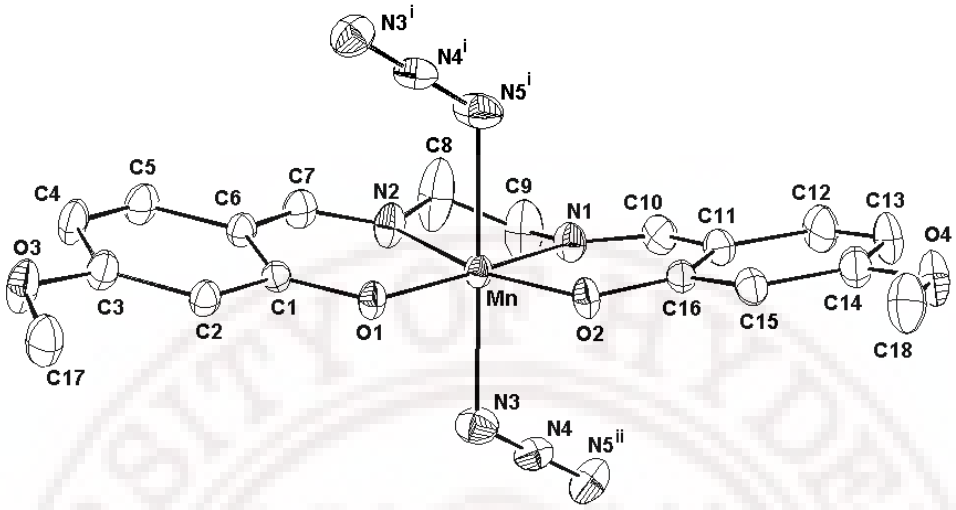

Figure 5.11 ORTEP view of one complex cation and its two bonded azide anions along the 1D chains of $[Mn(4\text{-}MeOsalen)N_3]_n$ in **5**. Hydrogen atoms are omitted for clarity and the thermal ellipsoids are represented at the 30% probability level (i = *x*, -*y*+1/2, *z*-1/2, ii = *x*, -*y*+1/2, *z*+1/2).

Table 5.7 Selected bond lengths [Å] and angles [°] for [**Mn(4-MeOsalen)N$_3$**]$_n$ (**5**)

Mn-O1	1.893(2)	Mn-N1	1.982(3)	Mn-N3	2.260(3)
Mn-O2	1.914(2)	Mn-N2	1.989(3)	Mn-N5#1	2.297(3)
N3-N4	1.165(5)	N4-N5	1.187(5)		
O1-Mn-O2	96.62(9)	O2-Mn-N1	168.63(11)	O1-Mn-N5#1	88.53(12)
O1-Mn-N1	92.59(10)	O2-Mn-N2	90.66(10)	O2-Mn-N5#1	87.56(13)
O1-Mn-N2	172.61(11)	O2-Mn-N3	91.36(12)	N1-Mn-N5#1	86.03(14)
O1-Mn-N3	89.75(12)	N1-Mn-N3	95.34(13)	N2-Mn-N5#1	93.08(13)
N1-Mn-N2	80.34(12)	N2-Mn- N3	88.79(13)	N3-Mn-N5#1	177.9(1)
Mn-N3-N4	122.8(3)	N3-N4-N5	179.6(4)	N4-N5-Mn#2	124.5(3)

#1 *x*,-*y*+1/2, *z*-1/2 #2 *x*,-*y*+1/2, *z*+1/2

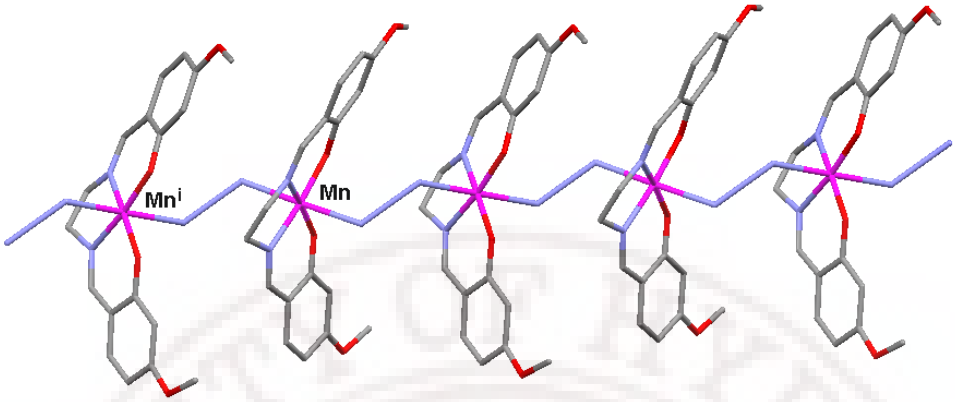

Figure 5.12 Perspective view of zig-zag ploymeic chains in complex **5**. (i = *x*, -*y*+1/2, *z*-1/2). Colour code for atoms: blue, N; red, O; grey C; purple, Mn.

5.3.7. Structure of [Mn(4-MeOsalen)(H_2O)NCS] (6): The complex is mononuclear and crystallographically characterized in the monoclinic system, space group $P2_1/c$, with 4 molecules present in the unit cell. The asymmetric unit is shown in Figure 5.13. The tetradentate Schiff base 4-MeOsalen coordinated to the Mn^{III} in equatorial plane with the bond length Mn-O(N)$_{ave}$, 1.88(1.97) Å. The apical positions are occupied by N-bonded terminal thiocyanate ion with bond length 2.23 Å and solvent water molecule with bond length 2.38 Å. The equatorial atoms (O2N2) are nearly coplanar even though the manganese atom deviates from this plane by 0.093 Å (with rms deviation = 0.022 Å). The mean planes of the two halves of the Schiff base ligand (excluding the methylene groups) are inclined to each other by 7.8º The overall coordination geometry of each Mn^{III} ion is thus distorted octahedral with the Jahn-Teller elongation along the N3–Mn···O5 axis. The coordinated water molecule forms hydrogen bonds with coordinated phenoxo oxygen atoms of the Schiff base (4-MeOsalen) and resulting in a dimer as shown in Figure 5.14 with interatomic

distances O1···H5A, O2···H5A, O5···O1(2), 2.40, 2.58 and 3.01(3.12) Å respectively. The intradimer Mn···Mn distance is 5.28 Å. The S1 atom from N-bonded terminal NCS^- ion is also participating in forming hydrogen bond with O5 atom of the water molecule with S1···O5 2.77 Å, which builds the monomeric units into a 1D-dimentional zig-zag polymeric chain along the *c*-axis (Figure 5.14). Finally the complex **6** leads to a 2D-net work because of the hydrogen bonds are shown in Figure 5.10. The molecular structure of this complex is analogues to complex [Mn(3-OCH_3salen)(H_2O)NCS][1]. The shortest intrachain and interchain Mn···Mn bond lengths are 6.89 and 5.18 Å.

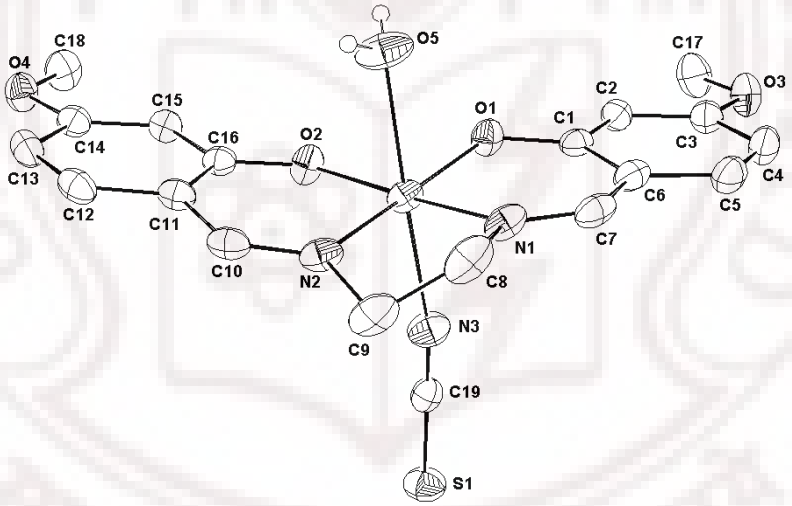

Figure 5.13 ORTEP view of the [Mn(4-MeOsalen)(H_2O)NCS] (**6**). Hydrogen atoms of the Schiff base are omitted for clarity, and the thermal ellipsoids are represented at the 30 % probability level.

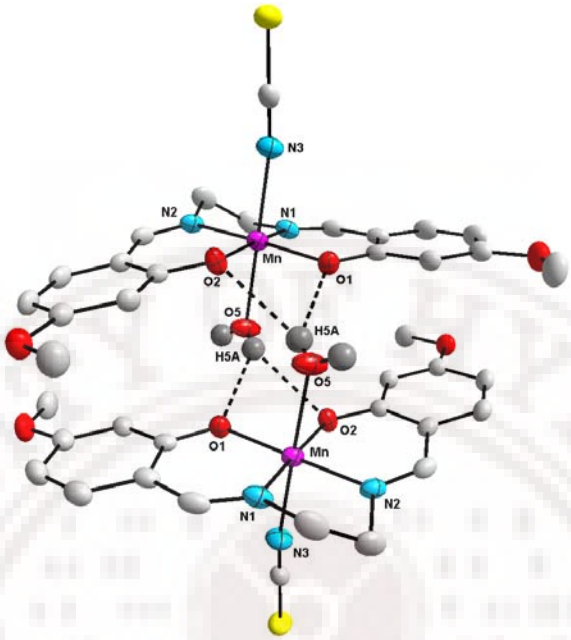

Figure 5.14 Dimeric view of [Mn(4-MeOsalen)(H_2O)NCS] (**6**) through hydrogen bonding. For clarity Schiff base 4-MeOsalen hydrogens are omitted. Colour code for atoms: blue, N; red, O; grey C; purple, Mn. yellow S.

Table 5.6 Selected bond lengths [Å] and angles [°] for complex **6**

Mn-O1	1.8839(17)	Mn-N1	1.980(2)	Mn-O5	2.382(2)
Mn-O2	1.8742(17)	Mn-N2	1.959(2)	Mn-N3	2.225(2)
N3-C19	1.146(3)	C19- S1	1.630(3)		
O1-Mn-N1	92.58(9)	O2-Mn-N1	171.42(8)	O1-Mn-O2	92.37(7)
O1-Mn-N2	173.51(9)	O2-Mn-N2	92.27(9)	O1-Mn-O5	89.20(9)
O1-Mn-N3	93.22(9)	O2-Mn-N3	95.61(9)	O2-Mn-O5	89.04(9)
N1-Mn-N2	82.27(10)	N1-Mn-N3	91.10(9)	N2-Mn-N3	90.84(9)
N1-Mn-O5	84.02(9)	N2-Mn-O5	86.34(9)	N3-Mn-O5	174.65(8)
Mn-N3-C19	169.5(2)	N3-C19-S1	179.1(3)		

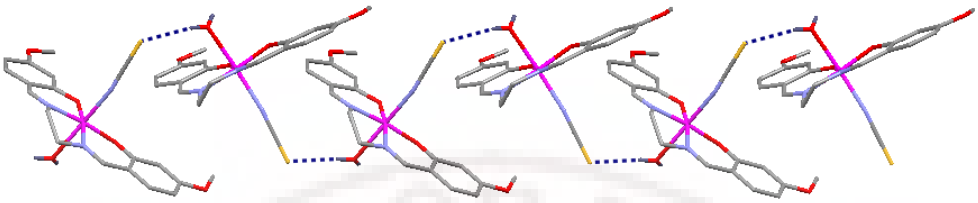

Figure 5.15 Perspective view of 1D-zig-zag polymeric chain in [Mn(4-MeOsalen)(H_2O)NCS] (**6**). For clarity Schiff base 4-MeOsalen hydrogens are omitted. Colour code for atoms: blue, N; red, O; grey C; purple, Mn. yellow S.

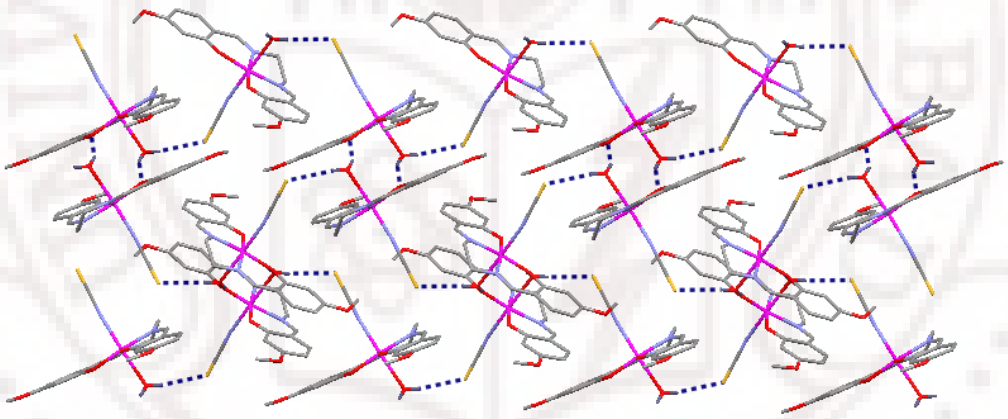

Figure 5.14 View of 2D-network in [Mn(4-MeOsalen)(H_2O)NCS] (**6**) through hydrogen bonds. For clarity Schiff base 4-MeOsalen hydrogens are omitted.

5.3.8. Spectral Studies

5.3.8a. FTIR Spectra

The IR spectrum of compound **1** exhibits sharp absorption at 2160 cm^{-1} which is assigned to the asymmetric stretching vibration of N-bonded cyanate group. Compound **2** exhibits sharp absorption at 2050 cm^{-1}, assigned to N-C stretching vibration of N-bonded terminal thiocyanate ion. Compound **3** exhibits sharp absorption at 2168 cm^{-1}, assigned to the asymmetric stretching vibration of N-bonded cyanate group. Compound **4** exhibits broad absorption band at 3379 cm^{-1} which is attributed to the coordinated stretching vibration (O-H) of water molecule and sharp absorption at 2160 cm^{-1}, assigned to the asymmetric stretching vibration of N-bonded terminal azide group. Compound **5** exhibits sharp absorption at 2031 cm^{-1}, assigned to the asymmetric stretching vibration of end-to end N-bonded azide group. Compound **6** exhibits broad absorption band at 3439 cm^{-1} which is attributed to the coordinated stretching vibration (O-H) of water molecule and sharp absorption at 2065 cm^{-1}, which is assigned to the asymmetric stretching vibration of N-bonded terminal thiocyanate group. All six compounds exhibit strong absorption at 1590-1630 cm^{-1}, which is assignable to the (-C=N) stretching vibration of Schiff-base. All these absorptions are with in the reported range.[16]

5.3.8b. Electronic Spectra

In all three complexes, the Mn^{III} (d^4) is a high-spin ion, and it has distorted octahedral geometry. For pure octahedral d^4 (^5D ground state term) system, only one electronic absorption ($^5T_{2g} \leftarrow {}^5E_g$) is possible, due to distorted octahedral geometry the

complexes **1-6** have four broad absorption bands. The solution spectra of the compounds **1-6** were measured in methanol (Figure 5.15). The low intensity absorption bands in the range 17.4, 270; 17.4, 123; 17.4, 263; 17.7, 212; 17.1, 185; 17.6, 203; for complex 1-6 ($\bar{\nu}_{max}$ /10^3cm^{-1}, ε_{max}/cm^{-1}M^{-1}) respectively, which are assigned to d-d transition. The high intensity absorption bands in the range 25.08, 8277; 29.11, 7935; 35.54, 20663 for complex **1,** 24.81, 5170; 29.24, 6934; 35.40, 19181; 42.03, 40140 for complex **2**, 24.21, 2456; 28.99, 3465; 35.40, 8976, 41.25, 20852 for complex **3,** 20.73, 1698; 26.00, 9201; 29.93, 16494; 33.89, 27953; 40.37, 45531 for complex **4**, 20.77, 6779; 26.29, 15459; 30.42, 23145; 33.76, 32570; 40.47, 50958 for complex **5**, and 20.68, 1529; 26.01, 9312; 30.21, 17164; 33.67, 26864; 40.49, 44757 for complex **6** ($\bar{\nu}_{max}$ /10^3cm^{-1}, ε_{max}/cm^{-1}M^{-1}) respectively, which are assigned to intraligand π-π* transitions in the complexes, the low intensity d-d transitions were masked in this range.

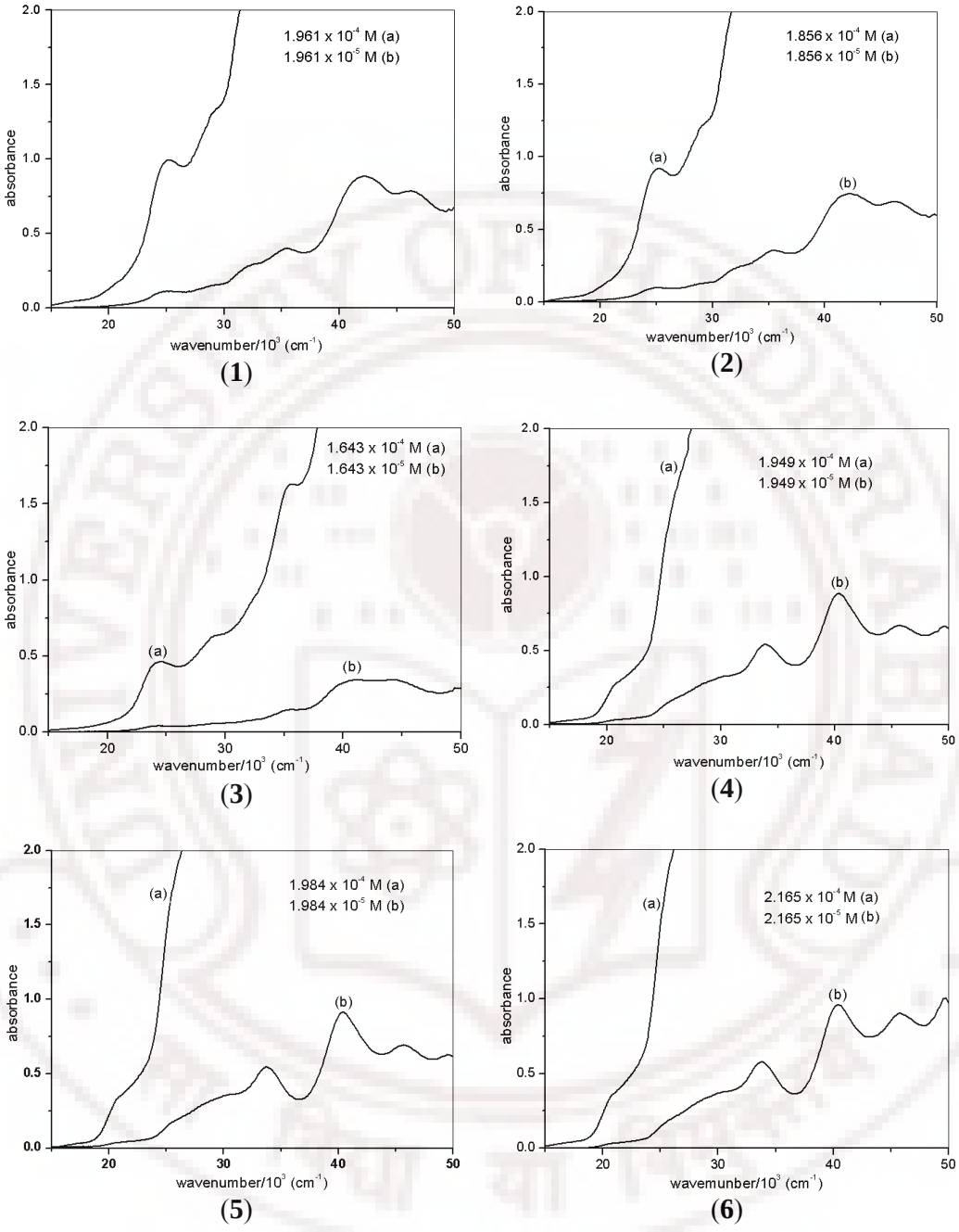

Figure 5.16 Electronic absorbance spectra of complexes **1-6** in methanol.

5.4. Conclusions

Compounds **1-3** are crystallographically characterized in the monoclinic system, space group $P2_1/n$, with 2 molecules present in the unit cell. The compounds **1-3** are phenoxo bridged dimers. The structure of compounds **1-3** are similar to those of dimeric out-of-plane Mn^{III} complexes reported previously.[5-7] The complex **1** and **2** have free methyl group on the Schiff base salmen, the distance between C9-C10 (1.39 Å) in compound **2** is shorter than compound **1** (1.43 Å). There are slight differences in the Mn-$(N,O)_{(eq,\ ax)}$ distances in the **1-3** compounds. The most important difference between the **1-3** compounds arises from the bridging bond lengths (Å) and angles (º): Mn–O, Mn···O, Mn–O···Mn are respectively, 1.90, 2.61, 97.94 in **1**; 1.91, 2.46, 99.6 in **2**; 1.91, 2.59, 100.3 in **3**. The Mn···Mn distance (Å) in the **1-3** dimers is respectively, 3.43 in **1**; 3.35 in **2**; 3.48 in **3**. The compound **4** and **6** are simple monomers, with inter molecular hydrogen bonds resulting 2-D net work. There are slight differences in the Mn-(N,O) distances in **4** and **6**: Mn-$O(eq)_{av}$, Mn-$N(eq)_{av}$, Mn-O,N(ax) are respectively, 1.89, 1.98, 2.33, 2.22 Å in **4**; 1.88, 1.97, 2.38, 2.23 Å in **6**. In all compounds the N-bonded pseudo-halide ion is coordinated in bent form and with coordinated angle 138, 150, 139, 152, 169°, respectively for **1-4** and **6**. The complex **5** is a 1D-polymeric chain. The important bond lengths (Å) and angles (º) of the 1D-polymeric chain in different compounds are compared in Table 5.9.

Table 5.9 Pertinent bond distances (Å) and angles (º) for the 1D *trans*-*μ*-(1,3)-azide bridged Mn(III)Schiff Base complexes.

	N-N	N-N-N	Mn-N	Mn-N-N	Mn···Mn (intrachain)	Ref.
5	1.165(5), 1.187(5)	179.6(4)	2.260(3), 2.297(3)	122.8(3), 124.5(3)	5.796	This work
a	1.185(4), 1.186(4)	179.8(3)	2.287(3), 2.327(3)	114.7(2), 118.5(2)	5.583	11
b	1.179(3), 1.205(3)	178.3(3)	2.300(3), 2.324(3)	116.5(2), 120.3(2)	5.592	
c	1.179(3), 1.179(3)	179.7(3)	2.280(2), 2.334(2)	114.6(2), 118.4(2)	5.557	9a
d	1.176(4), 1.179(4)	178.4(4)	2.299(3), 2.341(3)	119.0(3), 119.6(3)	5.634	10
e	1.165(5), 1.190(5)	178.7(4)	2.331(4), 2.348(4)	117.3(3), 137.8(3)	6.104	8a

[5][Mn(4-MeOsalen)N_3]$_n$, [a][Mn(5-Fsalen)N_3]$_n$, [b][Mn(5-OCH_3salen)N_3]$_n$, [c][Mn(salen)N_3]$_n$, [d][Mn(5-Brsalen)N_3]$_n$, [e][Mn(salpn)N_3]$_n$.

5.5. References

1. Nastase, S.; Tuna, F.; Maxim, C.; Muryn, C. A.; Avarvari, N.; Winpenny, R. E. P.; Andruh, M. *Crys. Growth. Des.* **2007**, *7*, 1825.
2. Sen, S.; Mitra, S.; Luneau, D.; Fallah M. S. El.; Ribas, J. *Polyhedron*, **2006**, *25*, 2737.
3. Chakraborty, J.; Brajagopal, S.; Pilet, G.; Mitra, S. *Struct. Chem.* **2006**, *17*, 585.
4. Zhang, K. -L.; Xu, Y.; Song, Y.; Zhang, Y.; Wang, Z.; You, X. -Z. *J. Mol. Struct.* **2001**, *570*, 137.
5. Miyasaka, H.; Saitoh, A.; Abe, S. *Coord. Chem. Rev.* **2007**, *251*, 2622.

6. Lu, Z.; Yuan, M.; Pan, F.; Gao, S.; Zhang, D.; Zhu, D. *Inorg. Chem.* **2006**, *45*, 3538 (and references therein). (b) Lecren, L.; Wernsdorfer, W.; Li, Y.-G.; Vindigi, A.; Miyasaka, H.; Clerac, R. *J. Am. Chem. Soc*. **2007**, *129*, 5045.

7. Miyasaka, H.; Clerac, R.; Ishii, T.; Chang, H.; Kitagawa, S.; Yamashita, M. *J. Chem. Soc., Dalton Trans*. **2002**, 1528.

8. (a) Reddy, K. R.; Rajasekharan, M. V.; Tuchagues, J.-P. *Inorg. Chem*. **1998**, *37*, 5978. (b) Sailaja, S.; Rajasekharan, M. V.; Hureau, C.; Riviere, E.; Cano, J.; Girerd J.-J. *Inorg. Chem*. **2003**, *42*, 180.

9. Li, H.; Zhong, Z. J.; Duan, C. Y.; Yu, X. Z.; Mak, T. C. W.; Wu, B. *Inorg. Chim. Acta* **1998**, *271*, 99.

10. (a) Panja, A.; Shaikh, N.; Vojtısek, P.; Gao, S.; Banerjee, P. *New J. Chem.* **2002**, *26*, 1025. (b) Kennedy, B. J.; Murray, K. S. *Inorg. Chem.* **1985**, *24*, 1552.

11. Ko, H. H.; Lim, J. H.; Kim, H. C.; Hong, C. S. *Inorg. Chem.* **2006**, *45*, 8847.

12. Yuan, M.; Zhao, F.; Zhang, W.; Wang, Z. -M. Gao, S. *Inorg. Chem.* **2006**, *45*, 11235.

13. SAINTPLUS, Bruker AXS Inc., Madison, Wisconsin, USA, 2003.

14. Sheldrick, G. M. SADABS, Program for Empirical Absorption Correction, University of Gottingen, Gottingen, Germany **1996**.

15. Sheldrick, G. M. SHELX-97, Programs for Crystal Structure Analysis, University of Gottingen, Gottingen, Germany **1997**.

16. Nakamoto, K. *Infrared and Raman Spectra of Inorganic and coordination Compounds*; 3 ed.; John Wiley & Sons, Inc.: New York, 1997, pp 270.

CHAPTER VI

Synthesis and Crystal Structure of Mn(III)/Fe(III) Chiral Schiff base complexes with pseudohalides

6. 1. Introduction

The pseudohalides ions, (N_3^-, NCS^- and NCO^-) are small linear ligands useful for building paramagnetic moeities into clusters, dimers, polymers. The azide ion exhibits different bridging modes, such as μ-(1,3)[1], μ-(1,1)[2], and rarely μ-(1,1,1).[3] The N_3^- ion coordinates the axial position in tetradentate Schiff base complexes of Mn(III) often form end-to-end μ-(1,3) bridge and have been investigated for their magnetic behavior.[4-7] Depending upon temperature and solvent NCS^- ion also exhibit different bridging modes.[8] Chiral molecule-based ferromagnets with helical structures[9] have also been reported. This chapter explores the formation and structural chemistry of complexes of the chiral Schiff base between salicylaldehyde and (1*R*, 2*R*)-diaminocyclohexane.

6. 2. Experimental Section

6.2.1. Synthesis

Salicyladehyde, (1R, 2R)-diaminocyclohexane and pseudohalides like NaN_3, KSCN and KOCN were of reagent grade. The Schiff bases were formed in situ in the presence of the appropriate metal salt. *Caution*: Azide compounds are potentially explosive and should be prepared only in small quantities and handled with care.

Preparation of Mn((*R,R*)-Salcy)N_3: In a beaker open to atmosphere (1R, 2R)-diaminocyclohexane (0.112 g, 1.00 mmol) was taken in 40 mL methanol, salicyaladehyde (0.244 g, 2.00 mmol) was a added and stirred for 10 minutes. To this solution, $Mn(CH_3COO)_2.4H_2O$ (0.245 g, 1.00 mmol) was added and stirring was continued for about 1 h. To the resulting solution, NaN_3 (0.130 g, 2.00 mmol) dissolved in 4 mL of water was added and the solution was allowed to stand for about 3 h to complete the aerial oxidation of Mn^{II}. Brown crystalline precipitate formed was filtered and dried. Yield: 0.396 g (0.949 mmol, 94.9 %). Anal. Calcd. for $MnC_{20}H_{20}N_5O_2$: C, 57.54; H, 4.83; N, 16.79. Found: C, 57.48; H, 4.77; N, 16.70. Characteristic IR absorptions (cm^{-1}): $\nu_a(N_3)$ 2050, $\nu_s(N_3)$ 1309, $\delta(N_3)$ 567, $\nu_{schiff\ base}$(C=N) 1610.

The precipitate was crystallized from different solvents, like acetonitrile, ethanol, methanol, tetrahydrofuran (THF) and propionitrile to get different kinds of crystals as listed below.

(1) $[Mn((R,R)\text{-Salcy})N_3]_n.CH_3CN$

(2) $[Mn((R,R)\text{-Salcy})N_3]_n$

(3) $[Mn((R,R)\text{-Salcy})(H_2O)N_3].C_4H_8O$

(4) $[Mn((R,R)\text{-Salcy})(CH_3OH)N_3]$

(5) $[Mn((R,R)\text{-Salcy})N_3]$

(a) Preparation of $[Mn((R,R)\text{-Salcy})N_3]_n.CH_3CN$ (1): The precipitate of Mn((*R,R*)-Salcy)N_3 was dissolved in acetonitrile and the clear saturated solution was allowed for crystallization at room temperature, good X-ray quality brown crystals of **1** were

obtained after one week. Anal. Calcd. for $MnC_{22}H_{23}N_6O_2$: C, 57.63; H, 5.06; N, 18.34. Found: C, 57.58; H, 4.99; N, 18.23. Characteristic IR absorptions (cm^{-1}): $\nu_a(N_3)$ 2037, $\nu_s(N_3)$ 1309, $\delta(N_3)$ 570, $\nu_{schiff\ base}$(C=N) 1610, ν_{ACN}(C ≡ N) 2249.

(b) Preparation of [Mn((*R,R*)-Salcy)N_3]$_n$ (2): The precipitate of Mn((*R,R*)-Salcy)N_3 was dissolved in distilled ethanol and warm on water bath, then the clear solution was kept at room temperature for crystallization. After 4-5 days, good X-ray quality needles type crystals formed were separated by simple filtration and dried. Anal. Calcd. for $Mn_2C_{40}H_{40}N_{10}O_4$: C, 57.54; H, 4.83; N, 16.79. Found: C, 57.49; H, 4.78; N, 16.72. Characteristic IR absorptions (cm^{-1}): $\nu_a(N_3)$ 2031, $\nu_s(N_3)$ 1309, $\delta(N_3)$ 567, $\nu_{schiff\ base}$(C=N) 1614.

(c) Preparation of [Mn((*R,R*)-Salcy)(H_2O)N_3].C_4H_8O (3): The precipitate of Mn((*R,R*)-Salcy)N_3 was dissolved in tetrahydrofuran and the clear solution kept at room temperature for crystallization. After one week dark brown good X-ray quality crystals formed were collected. Anal. Calcd. for $MnC_{24}H_{30}N_5O_4$: C, 56.79; H, 5.96; N, 13.81. Found: C, 56.73; H, 5.90; N, 13.77. Characteristic IR absorptions (cm^{-1}): $\nu_a(N_3)$ 2044, $\nu_s(N_3)$ 1313, $\delta(N_3)$ 567, $\nu_{schiff\ base}$(C=N) 1618.

(d) Preparation of [Mn((*R,R*)-Salcy)(CH_3OH)N_3] (4): The precipitate of Mn((*R,R*)-Salcy)N_3 was dissolved in methanol and the clear solution kept at room temperature for crystallization. After one week dark brown good X-ray quality crystals formed were collected. Anal. Calcd. for $MnC_{21}H_{24}N_5O_3$: C, 56.11; H, 5.39; N, 15.59. Found: C, 56.08; H, 5.34; N, 15.53. Characteristic IR absorptions (cm^{-1}): $\nu_a(N_3)$ 2042, $\nu_s(N_3)$ 1311, $\delta(N_3)$ 567, $\nu_{schiff\ base}$(C=N) 1616.

(e) Preparation of [Mn((*R,R*)-Salcy)N_3] (5): The precipitate of Mn((*R,R*)-Salcy)N_3 precipitate was dissolved in propionitrile and the clear solution kept at room temperature for crystallization. After one week dark brown good X-ray quality crystals formed were collected. Anal. Calcd. for $MnC_{20}H_{20}N_5O_2$: C, 57.54; H, 4.83; N, 16.79. Found: C, 57.49; H, 4.79; N, 16.71. Characteristic IR absorptions (cm^{-1}): $\nu_a(N_3)$ 2038, $\nu_s(N_3)$ 1307, $\delta(N_3)$ 567, $\nu_{schiff\ base}$(C=N) 1616.

(f) Preparation of [Mn((*R,R*)-Salcy)NCS] (6): In a beaker open to atmosphere (1R, 2R)-diaminocyclohexane (0.112 g, 1.00 mmol) was taken in 40 mL methanol, salicyaladehyde (0.244 g, 2.00 mmol) was a added and stirred for 10 minutes. To this solution, $Mn(CH_3COO)_2.4H_2O$ (0.245 g, 1.00 mmol) was added and stirring was continued for about 1 h. To the resulting solution, KSCN (0.194 g, 2.00 mmol) dissolved in 6-8 mL of water was added and the solution was allowed to stand for about 3 h to complete the aerial oxidation of Mn^{II}. The filtered solution was then kept in a refrigerator (5 ºC) for overnight yielding the dark-brown needles type crystals separated and dried. Yield: 0.416 g (0.938 mmol, 93.8 %). Anal. Calcd. for $MnC_{21}H_{20}N_3O_2S$: C, 58.19; H, 4.65; N, 9.70. Found: C, 58.12; H, 4.60; N, 9.62. Characteristic IR absorptions (cm^{-1}): ν(CN) 2044, ν(CS) 812, δ(NCS) 420, $\nu_{schiff\ base}$(C=N) 1612.

(g) Preparation of [Fe((*R,R*)-Salcy)NCS] (7): In a beaker open to atmosphere (1R, 2R)-diaminocyclohexane (0.112 g, 1.00 mmol) was taken in 40 mL methanol, salicyaladehyde (0.244 g, 2.00 mmol) was a added and stirred for 10 minutes. $Fe(ClO_4)_3.H_2O$ (0.355 g, 1.00 mmol) in 20 mL methanol was added and stirring continued for about 40 minutes. To the resulting solution, KNCS (0.194 g, 2.00

mmol) dissolved in 15 mL methanol was added and stirring was continued for about 30 minutes by the time brown precipitate formed was separated and dried. Yield: 0.429 g (0.988 mmol, 98.8 %). It was recrystallized from CH_3CN to obtain dark-brown X-ray quality crystals. Anal. Calcd. for $FeC_{21}H_{20}N_3O_2S$: C, 58.05; H, 4.64; N, 9.68. Found: C, 58.00; H, 4.57; N, 9.61. Characteristic IR absorptions (cm^{-1}): ν(CN) 2023, ν(CS) 812, δ(NCS) 412, $\nu_{schiff\ base}$(C=N) 1608.

(h) Preparation of [Mn((*R,R*)-Salcy)(CH_3OH)NCO] (8): In a beaker open to atmosphere (1R, 2R)-diaminocyclohexane (0.112 g, 1.00 mmol) was taken in 40 mL methanol, salicyaladehyde (0.244 g, 2.00 mmol) was a added and stirred for 10 minutes. To this solution, $Mn(CH_3COO)_2.4H_2O$ (0.245 g, 1.00 mmol) was added and stirring was continued for about 1 h. To the resulting solution, KOCN (0.162 g, 2.00 mmol) dissolved in 6-8 mL of water was added and the solution was allowed to stand for about 3 h to complete the aerial oxidation of Mn^{II}. The filtered solution was then kept in a refrigerator (5 ºC) for overnight yielding the dark-brown needles type crystals separated and dried. Yield: 0.376 g (0.837 mmol, 83.7 %). Anal. Calcd. for $MnC_{22}H_{24}N_3O_4$: C, 58.78; H, 5.39; N, 9.35. Found: C, 58.71; H, 5.32; N, 9.29. Characteristic IR absorptions (cm^{-1}): ν_a(NCO) 2189, ν_s(NCO) 1309, δ(NCO) 623, $\nu_{schiff\ base}$(C=N) 1614.

(i) Preparation of [Fe((*R,R*)-Salcy)NCO] (9): In a beaker open to atmosphere (1R, 2R)-diaminocyclohexane (0.112 g, 1.00 mmol) was taken in 40 mL methanol, salicyaladehyde (0.244 g, 2.00 mmol) was a added and stirred for 10 minutes. $Fe(ClO_4)_3.H_2O$ (0.355 g, 1.00 mmol) in 20 mL methanol was added and stirring continued for about 40 minutes. To the resulting solution, KOCN (0.162 g, 2.00

mmol) dissolved in 15 mL methanol was added and stirring was continued for about 30 minutes by the time brown precipitate formed was separated and dried. Yield: 0.353 g (0.856 mmol, 85.6 %). Anal. Calcd. for $FeC_{21}H_{20}N_3O_3$: C, 60.31; H, 4.82; N, 10.05. Found: C, 60.25; H, 4.75; N, 9.96. Characteristic IR absorptions (cm^{-1}): ν_a(NCO) 2202, ν_s(NCO) 1313, δ(NCO) 617, $\nu_{schiff\ base}$(C=N) 1612.

6.2.2. Physical measurements

IR spectra were obtained in KBr pellets using Shimadzu FT-IR 8000 spectrometer. Elemental analysis of the complexes was performed on a FLASH EA SERIES CHNS analyzer. Absorption spectrum for [Mn(Salcy)N_3] precipitate in acetonitrile was measured on a Shimadzu UV-3100 PC spectrometer and CD spectra was measured in acetonitrile solution phase with a JASCO J-810 spectropolarimeter.

6.2.3. X-ray Crystallography

X-ray data were collected for **1-9** on a Bruker SMART APEX CCD X-ray diffractometer, using graphite-monochromated Mo-Kα radiation (λ = 0.71073 Å). Data were reduced using SAINTPLUS,[9] and a multi-scan absorption correction using SADABS[10] was performed. The structures were solved using SHELXS-97 and full matrix least squares refinements against F^2 were carried out using SHELXL-97[11]. All ring hydrogen atoms were assigned on the basis of geometrical considerations and were allowed to ride upon the respective carbon atoms. All hydrogen atoms were assigned fixed U_{iso} values, equal to 1.2U_{eq} of the parent atom for ring and 1.5U_{eq} for methyl hydrogens. Crystallographic data are presented in Tables 6.1- 6.15.

Table 6.1 Crystallographic data and structure refinement for **1** and **2.**

	1	**2**
Formula	$C_{22}H_{23}MnN_6O_2$	$C_{40}H_{40}Mn_2N_{10}O_4$
Formula weight	458.40	834.70
Crystal system	monoclinic	monoclinic
a (Å)	7.3938(4)	11.7124(16)
b (Å)	12.2337(6)	13.4335(18)
c (Å)	11.4124(6)	13.2422(18)
α (º)	90	90
β (º)	92.737(1)	115.280(2)
γ (º)	90	90
V (Å^3)	1031.11(9)	1884.0(4)
Space group	$P2_1$	$P2_1$
Z	2	2
T (K)	100(2)	298(2)
ρ_{calcd} (g cm^{-3})	1.476	1.471
μ (mm^{-1})	0.673	0.727
θ range (º)	1.79 - 28.26	1.70 - 28.16
h/*k*/*l* indices	-9, 9/ -15, 15/	-15, 15/ -17, 17/
	-14, 14	-17, 17
Reflections collected	12023	21822
Unique reflection, R_{int}	4637, 0.0249	8722, 0.0231
GooF	1.045	1.011
*R*1 [$I > 2\sigma(I)$]	0.0304	0.0342
*wR*2[all data]	0.0736	0.0862
Weight. scheme (A, B)	0.0431, 0.00	0.0498, 0.00

6.3. Results and Discussion

6.3.1. Structure of $[Mn((R,R)\text{-Salcy})N_3]_n.CH_3CN$ (1)

The asymmetric unit of **1** contains one Mn^{III} ion, and the coordination of Mn^{III} is one tetradentate (*R,R*)-Salcy ligand coordinating in the equatorial mode and two azide ions in axial position (Figure 6.1). Each azide functions as a *trans*-μ-(1,3) bridge, resulting a one dimensional polymer. Each monomeric unit is related to its adjacent ones by a 2-fold screw axis, leading to a helical propagation along the crystallographic *b*-axis (Figure 6.2). In the equatorial plane the bond lengths of Mn1-$O_{(av)}$ and Mn1-$N_{(av)}$ are 1.89, 2.01 Å respectively, which are comparable to those observed in other $[Mn(SB)N_3]_n$.[4-7] The equatorial donor atoms (O_2N_2) are very nearly coplanar even though the manganese atom deviates significantly from this plane 0.035 Å (with rms diviation = 0.040 Å). The two halves of the Schiff base ligand, excluding the cyclohexane group, are also individually planar (rms deviation = 0.05 Å), with the Mn1 deviating by 0.17 and 0.58 Å from these planes. The two halves of the Schiff base excluding the cyclohexane group are inclined with respect to each other by 23º. Due to Jahn-Teller distortion the symmetrical elongated axial Mn1-N3 and Mn1-N5 lengths are 2.29 and 2.25 Å. The coordination of the azide bridge is almost symmetrical and the bond angles of Mn1-N3-N4 and Mn1-N5-N4 are 140 and 138º. As for N_3^- itself, N3-N4 (1.17 Å) and N4-N5 (1.18 Å) bond lengths are highly symmetrical and N3-N4-N5 bond angle is 176º.

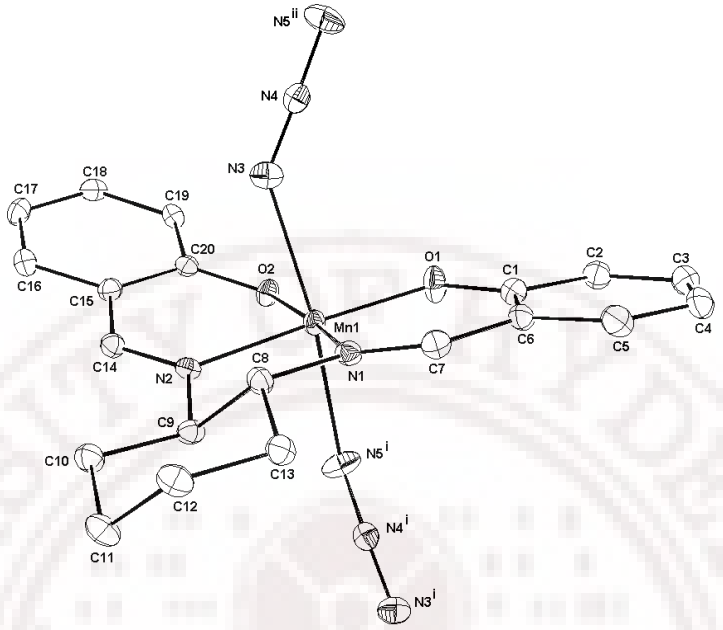

Figure 6.1 ORTEP view of one complex along the 1D chains of [Mn((*R,R*)-Salcy)N_3]$_n$.CH_3CN in **1**. Hydrogen atoms and solvent acetonitrile molecule are omitted for clarity. The thermal ellipsoids are represented at the 50% probability level. (i = -*x*, *y*+1/2, -*z*; ii = -*x*, *y*-1/2, -*z*).

Table 6.2. Selected bond lengths (Å) and bond angles (º) in **1**

Mn1-O1	1.8845(14)	O1-Mn1-O2	95.74(6)	O1-Mn1-N3	93.36(7)
Mn1-O2	1.8993(14)	O1-Mn1-N1	91.88(6)	O2-Mn1-N3	85.60(6)
Mn1-N1	2.0159(16)	O1-Mn1-N2	173.2(1)	O2-Mn1-N2	91.03(6)
Mn1-N2	1.9981(16)	O1-Mn1-N5#1	92.90(7)	O2-Mn1-N1	171.2(1)
Mn1-N3	2.2914(18)	O2-Mn1-N5#1	90.42(6)	N2-Mn1-N3	87.17(6)
Mn1-N5#1	2.2538(18)	N2-Mn1-N5#1	87.00(7)	N1-Mn1-N3	89.61(7)
N3-N4	1.174(3)	N1-Mn1-N5#1	93.55(7)	N4-N3-Mn1	140.1(2)
N4-N5	1.176(3)	N5#1-Mn1-N3	172.88(7)	N2-Mn1-N1	81.38(7)
C21-C22	1.456(3)	N4-N5-Mn1#2	138.1(2)	N3-N4-N5	176.2(2)
C22-N6	1.133(3)	#1 -*x*, *y*+1/2, -*z*; #2 -*x*, *y*-1/2, -*z*			

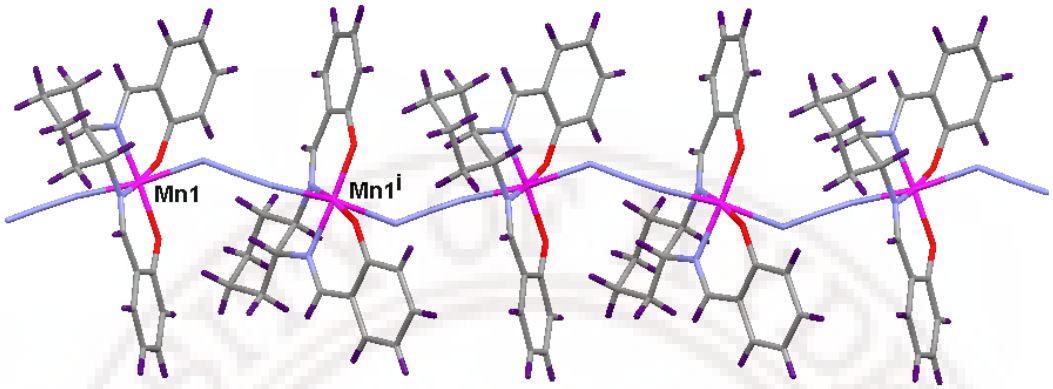

Figure 6.2 Perspective view of helical polymeric chain of complex **1** along the *b*-axis (i = -*x*, *y*+1/2, -*z*). Colour code for atoms: blue, N; red, O; grey C; violet H; purple, Mn.

The solvent acetonitrile molecule, which is present in the lattice, is building H-bonds between two polymeric chains. A strong H-bond is present between N3 and C21 with N3···H21, 2.45 Å; H21-C21, 0.96 Å and N3···C21, 3.40 Å bond lengths and N3···H21-C21 bond angle is 171º. Additionally a weak hydrogen-bond interaction is presente between methylene hydrogen (CH group from Schiff base), phenyl hydrogen (from Schiff base) and the N-atom from acetonitrile with N6···H14, 2.68 Å; N6···H16, 2.66 Å and H14···N6···H16, 52.1º. These H-bonds result in a 2D-network of the complex as shown in Figure 6.3. The shortest intrachain Mn···Mn bond distance is 6.16 Å, and interchain Mn···Mn distance is 11.4 Å. Selected bond distances (Å) and bond angles are shown in the Table 6.2. Finally the complex **1** has distorted octahedral geometry, and the N3-Mn-N5^{i} is the Jahn-Teller axis.

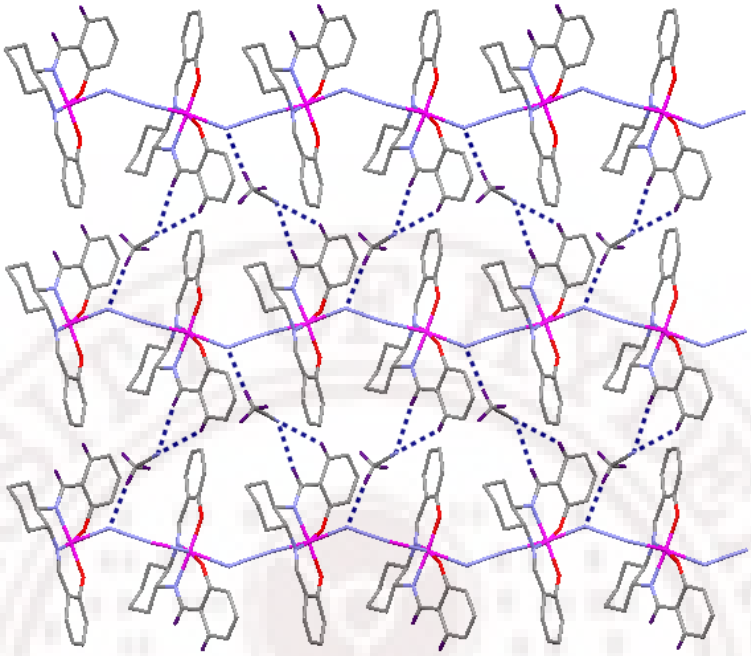

Figure 6.3 View of packing diagram of complex **1** through *bc*-plane. The 1D-polymeric chains of **1** connected through lattice solvent molecule acetonitrile with H-bonds and results 2D-network.

6.3.2. Structure of [Mn((*R,R*)-Salcy)N_3]$_n$ (2)

The asymmetric unit of **2** (Figure 6.4) contains two Mn^{III} ions, and the coordination of the Mn^{III} ions is with tetradentate (*R,R*)-Salcy ligand binding in the equatorial mode. The equatorial plane (N2O2) average distance of Mn1 is similar to that of the equatorial plane average distance of Mn2 (*ave* Mn1-salcy = 1.93 Å = Mn2-salcy). The two [Mn((*R,R*)-Salcy)]$^+$ units are connected through N_3^- ions. The axial *trans*-*μ*-(1,3)-azide ion coordinations of Mn1 and Mn2 are Mn1-N8, 2.24 Å; Mn1-N5, 2.44 Å; and Mn2-N3, 2.26 Å and Mn2-N10, 2.43 Å respectively, which are unsymmetrical and slightly different from complex **1**. The dimeric units are

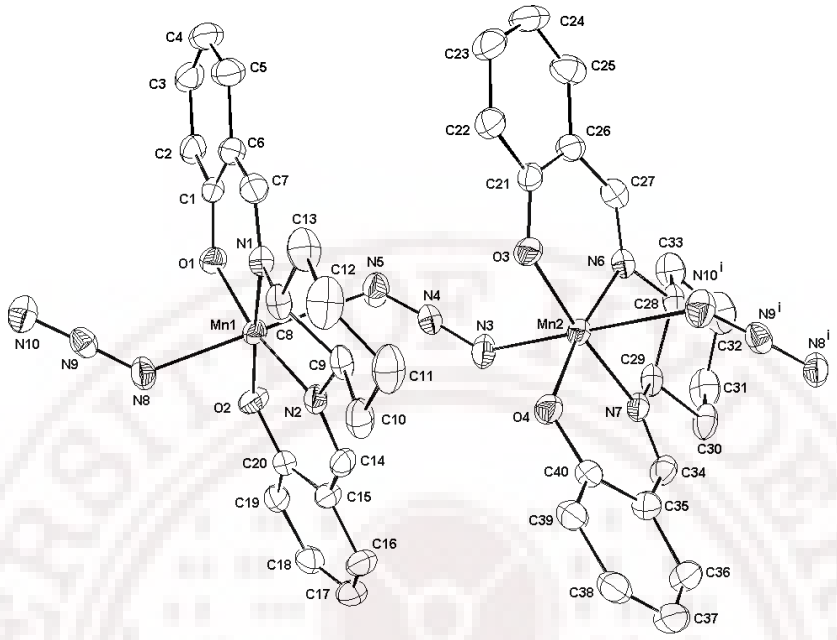

Figure 6.4 ORTEP view of one complex along the 1D chains of [Mn((*R,R*)-Salcy)N_3]$_n$ in **2**. Hydrogen atoms are omitted clarity. The thermal ellipsoids are represented at the 30% probability level. (i = *x*-1, *y*, *z*)

Table 6.3 Selected bond lengths (Å) and bond angles (º) in **2**

Mn1-O1	1.8730(16)	O2-Mn1-O1	93.33(8)	O3-Mn2-O4	93.88(8)
Mn1-O2	1.8727(17)	O2-Mn1-N1	174.9(8)	O3-Mn2-N7	174.5(7)
Mn1-N1	1.976(2)	O2-Mn1-N2	92.37(8)	O3-Mn2-N6	92.93(8)
Mn1-N2	1.9983(19)	O2-Mn1-N8	91.87(9)	O3-Mn2-N3	93.89(8)
Mn1-N8	2.239(2)	O1-Mn1-N1	91.68(8)	O3-Mn2-N8	91.10(8)
Mn1-N5	2.436(2)	O1-Mn1-N2	170.0(7)	O4-Mn2-N6	171.6(1)
Mn2-O3	1.8694(16)	O1-Mn1-N8	94.86(8)	O4-Mn2-N7	90.70(8)
Mn2-O4	1.8807(18)	N1-Mn1-N2	82.57(8)	O4-Mn2-N3	95.77(8)
Mn2-N6	1.9892	N1-Mn1-N8	88.39(9)	O4-Mn2-N8	90.24(8)
Mn2-N7	1.9869(19)	N2-Mn1-N8	93.13(8)	N6-Mn2-N3	88.74(8)
Mn2-N3	2.260(2)	N4-N3-Mn1	121.42	N7-Mn2-N3	88.75(8)
Mn2-N10#1	2.428(2)	O1-Mn1-N5	89.74(7)	O3-Mn2-N10#1	91.10(8)

N3-N4	1.176(3)	O2-Mn1-N5	92.34(9)	O4-Mn2-N10#1	90.24(8)
N4-N5	1.172(3)	N1-Mn1-N5	86.99(8)	N6-Mn2-N10#1	84.63(8)
N8-N9	1.178(3)	N2-Mn1-N5	81.85(8)	N7-Mn2-N10#1	85.75(8)
N9-N10	1.166(3)	N8-Mn1-N5	173.6(1)	N3-Mn2-N10#1	171.1(1)
N3-N4-N5	178.2(2)	Mn1-N5-N4	121.4(2)	Mn2-N3-N4	133.9(2)
N8-N9-N10	177.6(3)	Mn1-N8-N9	132.0(2)	N9-N10-Mn2#2	121.3(2)

#1 *x*-1, *y*, *z*. #2 *x*+1, *y*, *z*

translated along the crystallographic *a*-axis and leading to a polymeric zig-zag chain (Figure 6.5). The basic structure of this complex is similar to $[Mn(salen)CN]_{n.}$[12] The equatorial donor atoms (O_2N_2) are nearly coplanar (with rms deviation 0.066 Å for Mn1 and 0.016 Å for Mn2) even though the manganese atoms deviate significantly from these planes by 0.071 Å and 0.065 Å. The mean planes of the two halves of the Schiff base ligand, excluding the cyclohexane group, are also individually planar (rms diviation = 0.014 Å for Mn1 and 0.027 Å for Mn2), with the Mn1 deviating by 0.30, 0.11 Å, and with the Mn2 deviating by 0.028 and 0.52 Å from these planes. The mean planes of the two halves of the Schiff base ligands (excluding the cyclohexane groups) are inclined to each other by 24º for Mn1 and 29º for Mn2 in this crystal. The coordination of the azide bridges are not symmetrical; Mn1-N8-N9 (132º), Mn1-N5-N4 (121º), Mn2-N3-N4 (134º) and Mn2-N9-N8#2 (121º) when compare to complex **1**. As for N_3^- ions themselves, bond lengths N3-N4 (1.18 Å), N4-N5 (1.17 Å), N8-N9 (1.18 Å) and N9-N10 (1.17 Å) respectively, are symmetric and the N3-N4-N5 (N8-N9-N10) bond angle is 178º. The intrachain Mn1···Mn2 and Mn2···$Mn1^i$ distances are 5.89, 5.91 Å. The inter chain Mn1···$Mn2^i$ and Mn2···$Mn1^i$ distances are 7.78 and 8.93 Å correspondingly.

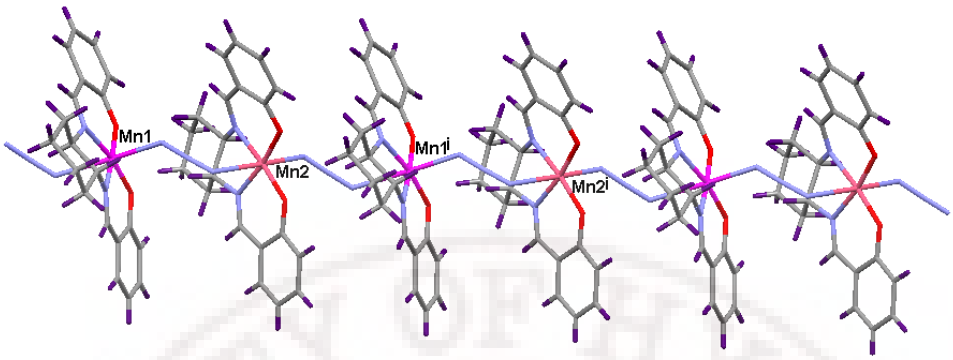

Figure 6.5 Perspective view of zig-zag polymeric chain of **2** along the *a*-axis (i = *x*-1, *y*, *z*). Colour code for atoms: blue, N; red, O; grey C; violet H; purple, Mn1; pale pink Mn2.

In summary the complex has distorted octahedral geometry, the Jahn-Teller elongation is going through N8-Mn1-N5 and N3-Mn2-N10 axis. Selected bond lengths and bond angles are shown in the Table 6.3. The view of the packing diagram of complex is shown in Figure 6.6.

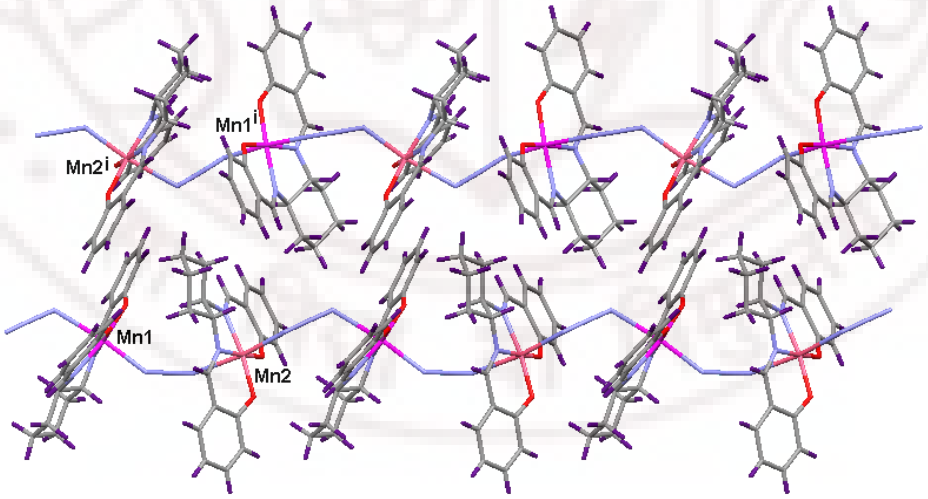

Figure 6.6 View of packing diagram of complex **2** through a*c*-plane (i = *x*-1, *y*, *z*).

Table 6.4. Crystallographic data and structure refinement for **3, 4** and **5.**

	3	**4**	**5**
Formula	$C_{24}H_{30}MnN_5O_4$	$C_{21}H_{24}MnN_5O_3$	$C_{20}H_{20}MnN_5O_2$
Formula weight	507.47	449.39	417.35
Crystal system	triclinic	triclinic	monoclinic
a (Å)	8.3680(6)	8.3373(6)	8.2408(14)
b (Å)	12.8014(10)	9.9021(7)	15.010(3)
c (Å)	12.8679(10)	12.1434(8)	15.698(3)
α (º)	63.0240(10)	96.7650(10)	90
β (º)	78.5210(10)	95.8970(10)	91.541(3)
γ (º)	72.0010(10)	95.8960(10)	90
V (Å^3)	1165.52(15)	983.56(12)	1941.0(6)
Space group	*P*1	*P*1	$P2_1$
Z	2	2	4
T (K)	100(2)	100(2)	293(2)
ρ_{calcd} (g cm^{-3})	1.446	1.517	1.428
μ (mm^{-1})	0.608	0.706	0.706
θ range (º)	1.78-28.34	1.70-28.10	1.30-28.32
h/*k*/*l* indices	-11, 11/ -17, 17/ -17, 16	-11, 10/-13,13/ -15,15	-10, 10/-20, 20/ -20,20
Reflections collected	10180	11399	22727
Unique reflection, R_{int}	8461, 0.0267	8621, 0.0259	9108, 0.0500
GooF	1.176	0.984	0.986
*R*1 [$I > 2\sigma(I)$]	0.0761	0.0463	0.0573
*wR*2[all data]	0.2325	0.0998	0.1180
Weight. scheme (*A*, *B*)	0.1473, 1.30	0.0409, 0.00	0.0467, 0.00

6.3.3. Structure of [Mn((*R,R*)-Salcy)(H_2O)N_3].C_4H_8O (3)

The asymmetric unit of **3 (**Figure 6.7) contains, structurally almost identical and crystallographically independent two monomeric Mn^{III} ions. The structure is entirely different from the previous structures **1** and **2**. The formation of polymer is prevented by the coordinated water molecule. The tetradentate (*R,R*)-Salcy ligand binds the Mn^{III} ions in the equatorial mode and the axial positions are occupied by an N-bonded terminal N_3^- ion and solvent molecule water. The equatorial plane (N2O2) average distance of Mn1 is similar to that of the equatorial plane average distance of Mn2 (*ave* Mn1-salcy = 1.93 Å = Mn2-salcy). The equatorial atoms (O_2N_2) are coplanar even though the manganese atom deviates significantly from this plane 0.073 Å for Mn1 and 0.090 Å for Mn2 (with rms deviation 0.017 Å for Mn1 and 0.039 Å for Mn2). The mean planes of the two halves of the Schiff base ligand, excluding the cyclohexane group, are also individually planar (rms diviation is 0.040 and 0.019 Å for Mn1 and 0.023, 0.079 Å for Mn2), with the Mn1 deviating by 0.40, 0.33 Å, and with the Mn2 deviating by 0.051 and 0.10 Å from these planes. The mean planes of the two halves of the Schiff base ligands (excluding the cyclohexane groups) are inclined to each other by 6º for Mn1 and 1º for Mn2 in this crystal. The N-bonded terminal N_3^- ion in complex **3** is less symmetrical than that in complexes **1** and **2**. The Mn-N(ax) lengths are longer than that in the complexes **1** and **2** for the azide ion act as a bridging ligand while a terminal ligand in **3**. The coordination of the azide bridges is unsymmetrical and the bond angles of Mn1-N3-N4 and Mn2-N8-N9 are 146 and 129º. As for N_3^- itself, N3-N4 (1.16 Å), N4-N5 (1.17 Å), N8-N9 (1.15 Å) and N9-N10 (1.17 Å) and N3-N4-N5 (N8-N9-N10) bond angle is 175º. The

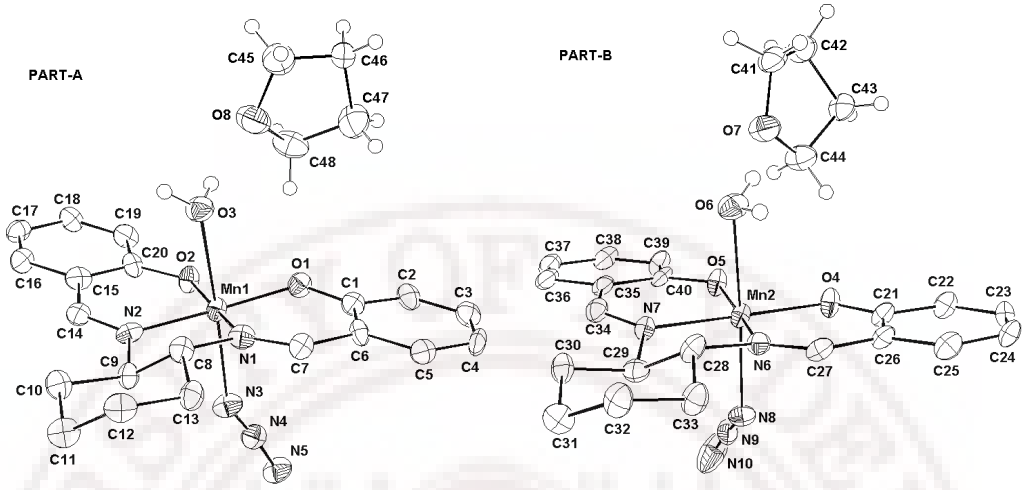

Figure 6.7 PART-A and PART-B are the ORTEP views of complex [Mn((*R,R*)-Salcy)(H_2O)N_3].C_4H_8O in **3**. Hydrogen atoms of the Schiff base ((*R,R*)-Salcy) are omitted for clarity. The thermal ellipsoids are represented at the 50% probability level.

Table 6.5 Selected bond lengths (Å) and bond angles (º) in **3**

Mn1-O1	1.886(5)	O1-Mn1-O2	91.32(2)	O5-Mn2-O4	93.3(2)
Mn1-O2	1.888(5)	O1-Mn1-N1	91.5(2)	O4-Mn2-N6	91.8(2)
Mn1-N1	1.974(6)	O1-Mn1-N2	174.2(2)	O4-Mn2-N7	173.5(3)
Mn1-N2	1.964(6)	O1-Mn1-N3	95.5(2)	O4-Mn2-N8	93.5(2)
Mn1-N3	2.196(6)	O1-Mn1-O3	88.8(2)	O4-Mn2-O6	89.8(2)
Mn1-O3	2.333(5)	O2-Mn1-N1	173.9(3)	O5-Mn2-N6	170.9(2)
N3-N4	1.157(8)	O2-Mn1-N2	93.3(2)	O5-Mn2-N7	92.3(2)
N4-N5	1.166(8)	O2-Mn1-N3	95.1(2)	O5-Mn2-N8	93.1(2)
Mn2-O4	1.878(5)	N2-Mn1-N1	83.6(3)	N6-Mn2-N7	82.2(2)
Mn2-O5	1.862(5)	N2-Mn1-N3	87.6(2)	N6-Mn2-N8	94.2(2)
Mn2-N6	2.009(6)	N1-Mn1-N3	90.1(2)	N7-Mn2-N8	89.4(2)
Mn2-N7	2.014(5)	N2-Mn1-O3	87.6(2)	N6-Mn2-O6	83.9(2)

Mn2-N8	2.210(5)	N3-Mn1-O3	172.5(2)	N8-Mn2-O6	176.3(2)
Mn2-O6	2.350(5)	O2-Mn1-O3	90.9(2)	O5-Mn2-O6	88.6(2)
N8-N9	1.154(8)	Mn1-N3-N4	146.1(5)	Mn2-N8-N9	129.2(5)
N9-N10	1.171(10)	N3-N4-N5	175.3(8)	N8-N9-N10	174.4(9)

monomeric units of complex **3** has strong hydrogen-bond contacts between O3(6) from coordinated water molecule and N5(10) from the terminal N_3^- ions with an O3(6)···N5(10) distances of 2.85 and 2.91 Å. Thus the monomeric units build one dimensional polymeric chains in the ladder fashion along the *a*-axis as shown in Figure 6.8. Selected bond distance and angles are shown in the Table 6.5.Two solvent tetrahydrofuran molecules are present in the lattice, which are also hydrogen bonded to the complex molecule as shown in Figure 6.8. The shortest intrachain and interchain Mn···Mn distances are 8.368 and 8.251 Å respectively. The hydrogen bonding parameters are presented in Table 6.6. Finally the complex has distorted octahedral geometry, the Jahn-Teller elongation is going through N3-Mn1-O3 and N8-Mn2-O6 axis.

Table 6.6 Hydrogen bonding parameters for **3**

D-H···A	D-H (Å)	H···A (Å)	D···A (Å)	D-H···A (º)
O3-H3A···N5#1	0.854	2.058	2.849	153.69
O6-H6A···N10#2	0.854	2.103	2.908	157.02
O3-H3B···O8	0.861	1.959	2.793	162.70
O6-H6B···O7	0.855	1.902	2.707	162.70

#1 *x*+1, *y*, *z*; #2 *x*-1, *y*, *z*.

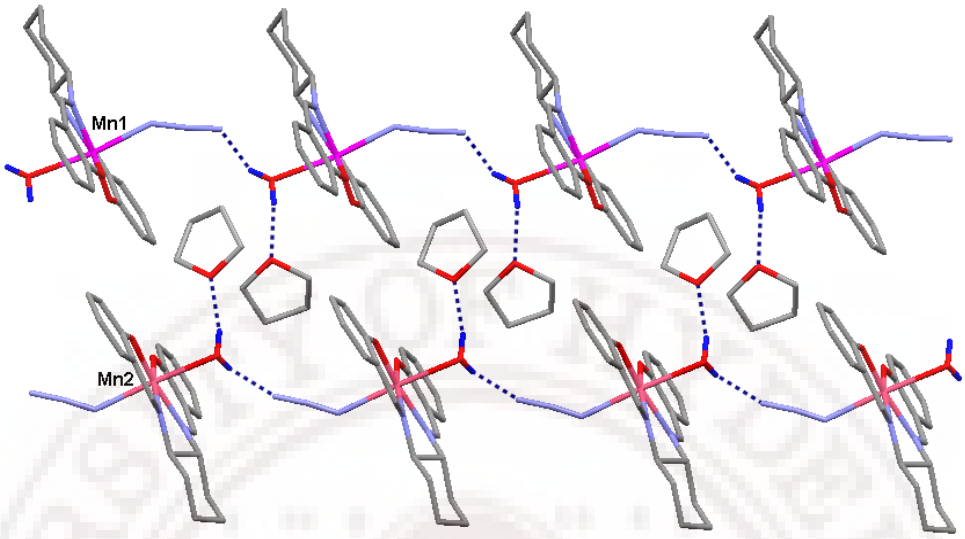

Figure 6.8 View of a ladder type One-dimensional hydrogen bonded chains in complex **3** along the *a*-axis. The coordinated water molecule hydrogens are building the polymeric chain through N-bonded terminal azide and solvent tetrahydrofuran. For clarity Schiff base (*R,R*)-Salcy and solvent tetrahydrofuran molecules hydrogens were omitted. Colour code for atoms: blue, N; red, O; grey C; dark blue H; purple, Mn1. pale pink Mn2.

6.3.4. Structure of [Mn((*R,R*)-Salcy)(CH_3OH)N_3] (4)

The asymmetric unit of **4** contains two structurally almost identical and crystallographically independent monomeric Mn^{III} ions as shown in Figure 6.9. The basic structure of this complex is similar to complex **3**. In this case the coordination around the Mn^{III} atom is one tetradentate (*R,R*)-Salcy ligand in the equatorial mode, with the axial position occupied by one N-bonded terminal N_3^- ion and solvent molecule, methanol. The equatorial plane (N2O2) average distance of Mn1 is similar to that of the equatorial plane average distance of Mn2 (*ave* Mn1-salcy = 1.93 Å =

Mn2-salcy). In the unit cell, the equatorial atoms (O_2N_2) of Mn1 and Mn2 are coplanar even though the manganese atom deviates significantly from this plane 0.11 Å for Mn1 and Mn2 (with rms deviation 0.060 Å for Mn1 and 0.026 Å for Mn2). The mean planes of the two halves of the Schiff base ligand, excluding the cyclohexane group, are also individually planar (rms diviation = 0.015 and 0.055 Å for Mn1 and 0.015, 0.017 Å for Mn2), with the Mn1 deviating by 0.049, 0.082 Å, and with the Mn2 deviating by 0.33 and 0.31 Å from these planes. The mean planes of the two halves of the Schiff base ligands (excluding the cyclohexane groups) are inclined to each other by 9º for Mn1 and 11º for Mn2. The Mn-N(ax) coordination bond distances in complex **4** are similar to those in complex **3**. The axial Mn-N_{azide} distances are same (2.20 Å) for Mn1 and Mn2 in **4** while Mn-$O_{methanol}$ distances are different **(**Mn1-O3 2.45 Å; Mn2-O6 2.39 Å). The N-bonded terminal N_3^- ion in complex **4** is less symmetrical than that *trans*-μ-(1,3)-azide ion complexes **1** and **2** and like complex **3**. The coordination of the azide bridges is unsymmetrical and the bond angles of Mn1-N3-N4 and Mn2-N8-N9 are 124 and 131º. As for N_3^- itself, N3-N4 (1.19 Å), N4-N5 (1.17 Å), N8-N9 (1.17 Å) and N9-N10 (1.16 Å) and N3-N4-N5(N8-N9-N10) bond angles is 178º (176)º. The Mn-N(ax) lengths of this complex are very near to complex **3** and shorter than that of the complexes **1** and **2** for the azide ion act as a terminal ligand in **4** while a *trans*-μ-(1,3)-azide bridging ligand in **1** and **2**. The monomeric units of complex **4** have strong hydrogen-bond contacts between O3(6) atom from coordinated methanol molecule and N5(10) atom from the terminal N_3^- ions with an O3(6)···N5(10) distances of 2.852 and 2.794 Å. Thus the monomeric units build one dimensional polymeric chains along the *a*-axis

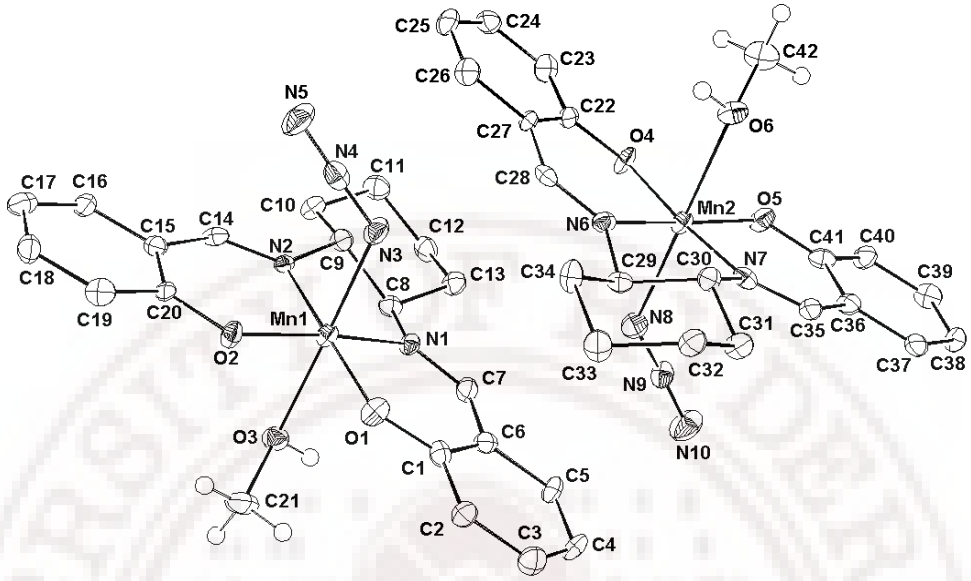

Figure 6.9 ORTEP view of complex [Mn((*R,R*)-Salcy)(CH_3OH)N_3] in **4**. Hydrogen atoms of the Schiff base (*R,R*)-Salcy are omitted for clarity. The thermal ellipsoids are represented at the 50% probability level.

Table 6.7 Selected bond lengths (Å) and bond angles (º) in **4**

Mn1-O1	1.869(3)	O1-Mn1-O2	92.74(16)	O5-Mn2-O4	93.11(15)
Mn1-O2	1.879(3)	O1-Mn1-N1	92.23(16)	O4-Mn2-N6	91.82(15)
Mn1-N1	1.995(4)	O1-Mn1-N2	173.9(2)	O4-Mn2-N7	170.4(2)
Mn1-N2	1.991(4)	O1-Mn1-N3	96.16(15)	O4-Mn2-N8	96.45(16)
Mn1-N3	2.199(4)	O1-Mn1-O3	88.49(14)	O4-Mn2-O6	89.29(13)
Mn1-O3	2.452(3)	O2-Mn1-N1	168.2(2)	O5-Mn2-N6	172.6(2)
N3-N4	1.194(5)	O2-Mn1-N2	91.93(15)	O5-Mn2-N7	91.58(16)
N4-N5	1.168(5)	O2-Mn1-N3	93.15(15)	O5-Mn2-N8	96.12(16)
Mn2-O4	1.872(3)	N2-Mn1-N1	82.46(17)	N6-Mn2-N7	82.75(18)
Mn2-O5	1.895(4)	N2-Mn1-N3	87.50(16)	N6-Mn2-N8	88.79(16)
Mn2-N6	1.972(4)	N1-Mn1-N3	96.90(15)	N7-Mn2-N8	91.43(16)
Mn2-N7	1.998(4)	N2-Mn1-O3	87.63(14)	N6-Mn2-O6	84.58(14)

Mn2-N8	2.201(4)	N3-Mn1-O3	174.6(2)	N8-Mn2-O6	171.4(2)
Mn2-O6	2.387(3)	O2-Mn1-O3	89.39(13)	O5-Mn2-O6	89.98(14)
N8-N9	1.168(5)	Mn1-N3- N4	124.0(3)	Mn2-N8-N9	131.2(4)
N9-N10	1.156(5)	N3-N4-N5	178.6(5)	N8-N9-N10	175.6(6)

and the weak hydrogen-bond interactions between carbon and nitrogen atoms lead to a two dimensional supramolecular network in the crystal structure of complex **4**. The hydrogen bonding parameters are shown in the Table 6.8. The shortest intra chain and inter chain Mn···Mn distances are 8.337 and 6.776 Å respectively.

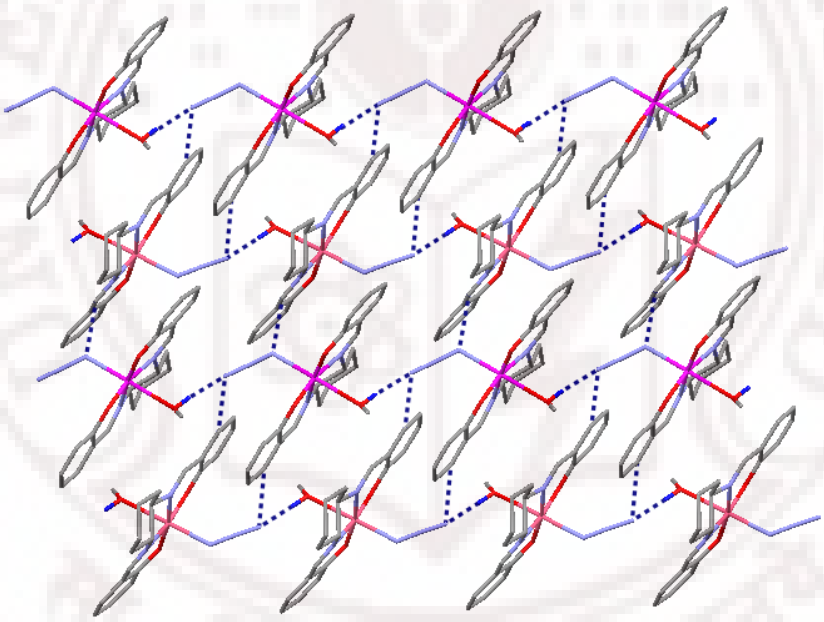

Figure 6.10 View of the 2D-dimensional hydrogen bonded chains in complex **4**. Colour code for atoms: blue, N; red, O; grey C; dark blue H; purple, Mn1 and pale pink Mn2.

Table 6.8 Hydrogen bonding parameters for **4**

D-H···A	D-H (Å)	H···A (Å)	D···A (Å)	D-H···A (º)
O3-H3A···N5#1	0.800	2.058	2.852	171.59
O6-H6A···N10#2	0.853	1.943	2.794	175.56
N5-H37···C37#3	2.520	0.930	3.301	141.8
N3-H28···C28#4	2.572	0.929	3.360	142.9
N10-H16···C16#5	2.520	0.930	3.260	136.8

#1 *x*-1, *y*, *z*; #2 *x*+1, *y*, *z*; #3 *x*+1, *y*, *z*+1; #4 *x*, *y*, *z*; #5 *x*-1, *y*, *z*-1

6.3.5. Structure of [Mn((*R*,*R*)-Salcy)N_3]$_2$ (5)

The complex **5** is structurally characterized as a phenoxo-bridged dimer shown in Figure 6.11. The basic structure of this complex is similar to other phenoxo-bridged dimers reportrd.[13-15] Each unit of the phenoxo-bridged dimer is made up of a tetradentate schiff base ligand (*R,R*)-Salcy chelating the Mn^{III} ion in equatorial mode and an N-bonded terminal azide ion occupying the axial position. In this phenoxo-bridged dimer, the two halves are not centrosymmetrically related like other dimers reported. Due to chirality of the complex, an inversion centre of the dimeric core is not present. The Mn-O(N)$_{ave}$ equatorial bond distancesin complex **5** 1.87 (1.98) Å are similar to those in complexes **1-4**. The Mn-N_{azide} coordination bond distance is 2.08 Å, very shorter than the above complexes **1-4**. The equatorial plane (N2O2) average distance of Mn1 is similar to that of the equatorial plane average distance of Mn2 (*ave* Mn1-salcy = 1.93 Å = Mn2-salcy). In the unit cell, the equatorial atoms (O_2N_2) of Mn1 and Mn2 are coplanar even though the manganese atom deviates significantly from this plane 0.27 Å for Mn1 and Mn2 (with rms deviation 0.090 Å

for Mn1 and 0.097 Å for Mn2). The mean planes of the two halves of the Schiff base ligand, excluding the cyclohexane group, are also individually planar (rms diviation = 0.016 and 0.056 Å for Mn1 and 0.037, 0.058 Å for Mn2), with the Mn1 deviating by 0.025, 0.056 Å, and with the Mn2 deviating by 0.50 and 0.35 Å from this planes. The mean planes of the two halves of the Schiff base ligands (excluding the cyclohexane groups) are inclined to each other by 16º for Mn1 and 11º for Mn2. The intradimer Mn···Mn bond distance is 3.70 Å. The important bond distances (Å) and bond angle (º) of the dimeric core: Mn-O, Mn···O, Mn-O···Mn are 1.87, 3.20 and

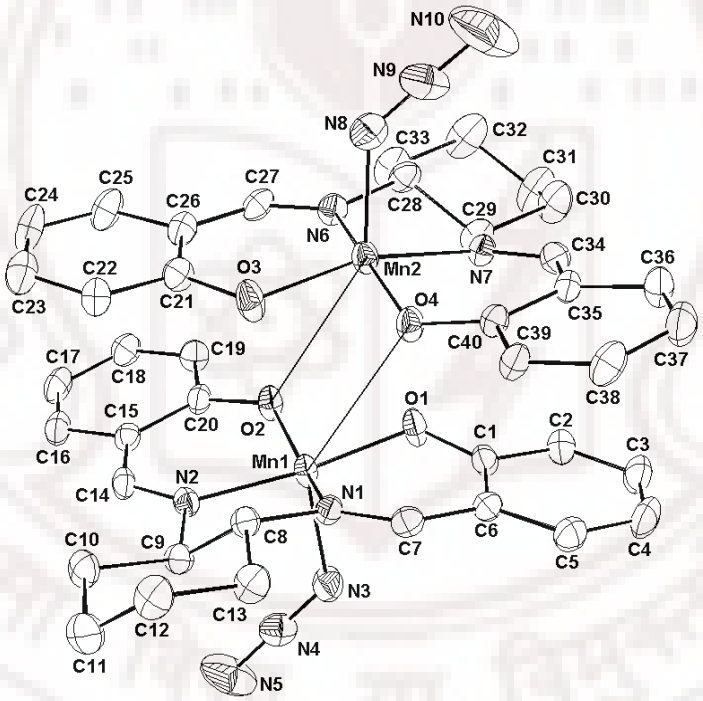

Figure 6.11 ORTEP view of complex $[Mn((R,R)\text{-Salcy})N_3]_2$ in **5**. Hydrogen atoms are omitted for clarity. The thermal ellipsoids are represented at the 30% probability level.

Table 6.9 Selected bond lengths (Å) and bond angles (º) in **5**

Mn1-O1	1.870(3)	O2- Mn1-O1	92.62(10)	O3- Mn2-O4	94.23(10)
Mn1-O2	1.872(3)	O1- Mn1-N1	91.77(14)	O3- Mn2-N4	168.59(15)
Mn1-N1	1.983(3)	O1- Mn1-N2	158.46(14)	O3- Mn2-N5	91.16(14)
Mn1-N2	1.979(4)	O1- Mn1-N3	102.55(16)	O3- Mn2-N6	95.54(17)
Mn1-N3	2.088(4)	O2- Mn1-N1	168.36(14)	O4- Mn2-N4	157.58(15)
N3-N4	1.163(5)	O2- Mn1-N2	91.03(14)	O4- Mn2-N5	91.15(16)
N4-N5	1.151(7)	O2- Mn1-N3	96.92(16)	O4- Mn2-N6	105.27(17)
Mn2-O4	1.872(3)	N3- Mn1-N1	93.56(14)	N6-Mn2-N7	81.95(16)
Mn2-O5	1.875(3)	N3- Mn1-N2	98.50(16)	N6-Mn2-N8	96.54(16)
Mn2-N6	1.985(3)	N2-Mn1-N1	82.38(15)	N7-Mn2-N8	94.29(17)
Mn2-N7	1.992(4)	N4-N3- Mn1	125.9(4)	N9-N8-Mn2	126.3(5)
Mn2-N8	2.079(4)	N3-N4- N5	177.5(6)	N8-N9-N10	176.3(8)
N8-N9	1.107(6)	N9-N10	1.167(8)		

89.9º respectively, which are with in the range of phenoxo bridged dimer compounds. The coordination of the azide bridges is symmetrical and the bond angle of Mn1-N3-N4 (Mn2-N8-N9) is 126º. As for N_3^- itself, N3-N4 (1.16 Å), N4-N5 (1.15 Å), N8-N9 (1.11 Å) and N9-N10 (1.17 Å) respectively, bond lengths are not symmetrical; moreover bond length of N8-N9 is very smaller to those in complexes **1-4**. The azide ions are symmetrical and their bond angle N3-N4-N5, 178º and N8-N9-N10, 176º. Selected bond lengths and bond angles are mentioned in the Table 6.9. Finally the molecule has distorted octahedral geometry and the Jahn-Teller elongation going through N3-Mn···O axis. There is no specific inter dimer interaction between the molecules and packing diagram of the complex as shown in Figure 6.12.

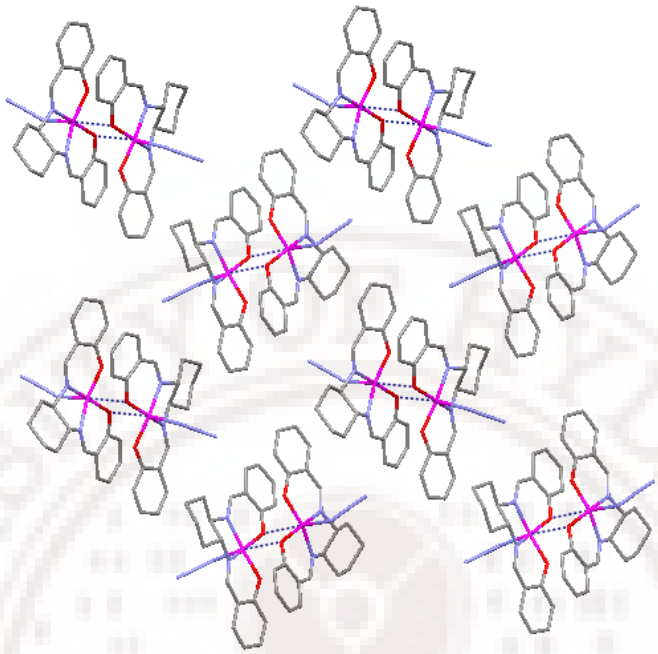

Figure 6.12 The packing view of $[Mn((R,R)\text{-Salcy})N_3]_2$ in **6** through *ab*-plane. Colour code for atoms: blue, N; red, O; grey C; purple, Mn.

6.3.6. Structure of $[Mn((R,R)\text{-Salcy})NCS]_2$ (6)

The complex **6** is structurally characterized as a phenoxo-bridged dimer shown in Figure 6.13. The basic structure of this complex is similar to other phenoxo-bridged dimers reportrd.[13-15] Each unit of the phenoxo-bridged dimer is made up of a tetradentate schiff base ligand (*R,R*)-Salcy chelating the Mn^{III} ion in equatorial mode and an N-bonded terminal thiocyanate ion occupying the axial position. In this phenoxo-bridged dimer, the two halves are not centrosymmetrically related like other dimers reported. Due to chirality of the complex, an inversion centre of the dimeric core is not present. The Mn-$O(N)_{ave}$ equatorial bond distancesin complex **6** 1.87 (1.99) Å are similar to those in complexes **1-5**. The Mn-$N_{thiocyanate}$ coordination bond distance is 2.11 Å. The equatorial plane (N2O2) average distance of Mn1 is similar to

Table 6.10 Crystallographic data and structure refinement for **6** and 7**.**

	6	**7**
Formula	$C_{21}H_{20}MnN_3O_2S$	$C_{21}H_{20}FeN_3O_2S$
Formula weight	433.41	434.31
Crystal system	monoclinic	monoclinic
a (Å)	13.631(5)	13.6267(7)
b (Å)	10.373(4)	10.3030(5)
c (Å)	13.915(6)	13.8462(7)
α (º)	90	90
β (º)	97.028(6)	96.237(1)
γ (º)	90	90
V (Å^3)	1952.1(1)	1932.4(2)
Space group	$P2_1$	$P2_1$
Z	4	4
T (K)	298(2)	100(2)
ρ_{calcd} (g cm^{-3})	1.474	1.493
μ (mm^{-1})	0.805	0.911
θ range (º)	1.47 - 28.44	1.48 - 28.13
h/*k*/*l* indices	-17, 18/ -13, 13/	-18, 18/ -13, 13/
	-18, 18	-18, 18
Reflections collected	22452	22564
Unique reflection, R_{int}	8998, 0.0323	8896, 0.0361
GooF	1.073	1.019
*R*1 [$I > 2\sigma(I)$]	0.0544	0.0416
*wR*2[all data]	0.1197	0.0938
Weight. scheme (A, B)	0.0595, 0.00	0.0483, 0.00

that of the equatorial plane average distance of Mn2 (*ave* Mn1-salcy = 1.93 Å = Mn2-salcy). In the unit cell, the equatorial atoms (O_2N_2) of Mn1 and Mn2 are coplanar even though the manganese atom deviates significantly from this plane 0.30 Å for Mn1 and Mn2 (with rms deviation 0.090 Å for Mn1 and 0.093 Å for Mn2). The mean planes of the two halves of the Schiff base ligand, excluding the cyclohexane group, are also individually planar (rms diviation = 0.035 and 0.012 Å for Mn1 and 0.046, 0.056 Å for Mn2), with the Mn1 deviating by 0.48, 0.098 Å, and with the Mn2 deviating by 0.30 and 0.26 Å from this planes. The mean planes of the two halves of the Schiff base ligands (excluding the cyclohexane groups) are inclined to each other by 10º for Mn1 and 4º for Mn2. The intradimer Mn···Mn bond distance is 4.12 Å. The important bond distances and bond angle of the dimeric core Mn-O, 1.87 Å, Mn···O 3.68 Å, and Mn-O···Mn 89.7º respectively, which are with in the

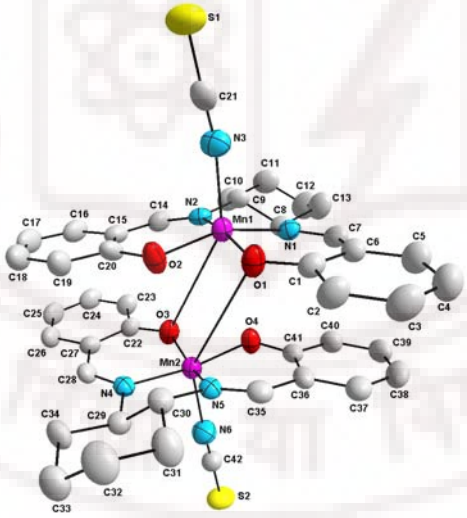

Figure 6.13 ORTEP view of complex [Mn((*R,R*)-Salcy)NCS]$_2$ in **6**. Hydrogen atoms are omitted for clarity. The thermal ellipsoids are represented at the 30% probability level.

Table 6.10 Selected bond lengths (Å) and bond angles (º) in **6**

Mn1-O1	1.873(3)	O2- Mn1-O1	92.62(10)	O3- Mn2-O4	94.23(10)
Mn1-O2	1.870(3)	O1- Mn1-N1	90.68(12)	O3- Mn2-N4	91.81(13)
Mn1-N1	2.004(3)	O1- Mn1-N2	166.11(13)	O3- Mn2-N5	155.97(14)
Mn1-N2	1.978(3)	O1- Mn1-N3	98.57(15)	O3- Mn2-N6	103.22(15)
Mn1-N3	2.106(4)	O2- Mn1-N1	155.95(13)	O4- Mn2-N4	166.89(13)
N3-C21	1.164(5)	O2- Mn1-N2	91.60(12)	O4- Mn2-N5	91.28(12)
C21-S1	1.609(5)	O2- Mn1-N3	105.56(15)	O4- Mn2-N6	101.98(14)
Mn2-O4	1.867(3)	N3- Mn1-N1	98.06(14)	N6- Mn2-N4	90.61(13)
Mn2-O5	1.864(2)	N3- Mn1-N2	82.08(12)	N5- Mn2-N4	82.79(13)
Mn2-N4	1.976(3)	N2-Mn1-N3	94.19(15)	N5-Mn2-N6	100.2(1)
Mn2-N5	1.984(3)	Mn1-N3-C21	170.6(4)	Mn2-N6-C42	164.7(4)
Mn2-N6	2.117(4)	N3-C21- S1	178.6(4)	N6-C42- S2	178.8(4)
N6-C42	1.147(5)	C42-S2	1.633(5)		

range of out-of-plane phenaxo-bridged dimers.[13-15] The phenoxo bridged distance (Mn···O) of this complex is almost equal to the highest Mn···O distance (3.76 Å) of complex in $[Mn(naphtmen)NCS]_2$.[15] The coordination angle of NCS^- ion with Mn^{III} atom, Mn1-N3-C21 (Mn2-N6-C42) is 171º (165º). These angles are far away from the thiocyante ion which is coordinated in bend form. The NCS^- ion is well known bridging ligand, but in this case NCS^- ion is an N-bonded terminal thiocyanate ion and there is no specific interactions with S atom. Selected bond lengths and bond angles are mentioned in the Table 6.10. There are no specific interactions between the dimeric molecules and the packing diagram of the complex as shown in Figure 6.14.

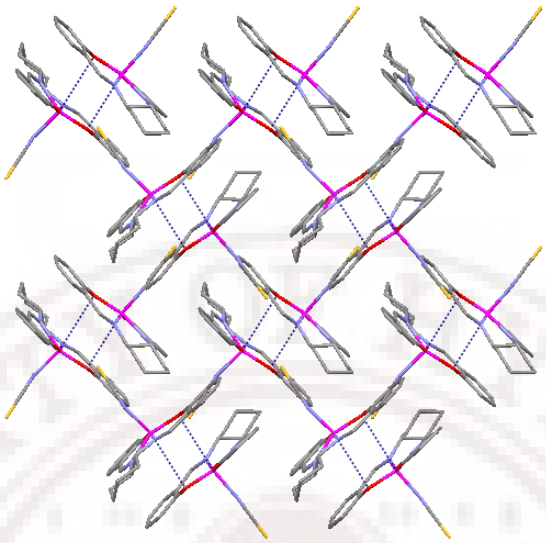

Figure 6.14 The packing view of [Mn((*R,R*)-Salcy)NCS]$_2$ in **6** through *ab*-plane. Colour code for atoms: blue, N; red, O; grey C; yellow S; purple, Mn.

6.3.7. Structure of [Fe((*R,R*)-Salcy)NCS] (7)

The asymmetric unit of complex **7** contains two structurally identical and crystallographically independent five coordinated molecules shown in Figure 6.15. The complex has square pyramidal geometry. In each molecule the coordination around the Fe^{III} is one tetradentate schiff base ligand (*R,R*)-Salcy in the equatorial mode with bond distances Fe-O(N)$_{ave}$ 1.88(2.09) Å, and the axial position is occupied by an N-bonded terminal thiocyanate ion with bond distance 2.00 Å. The equatorial plane (N2O2) average distance of Fe1 is similar to that of the equatorial plane average distance of Fe2 (*ave* Fe1-salcy = 1.98 Å = Fe2-salcy), as well as this distance is 0.05 Å more than Mn((*R,R*)-Salcy)X complexes, where X is N_3^-/NCS^-/NCO^- ion. In the unit cell, the equatorial atoms (O_2N_2) of Fe1 and Fe2 are nearly coplanar even though the iron atoms deviated significantly from this plane

0.50 Å from the plan (with rms deviation 0.014 Å for Fe1 and 0.015 Å for Fe2). The mean planes of the two halves of the Schiff base ligands (excluding the cyclohexane groups) are inclined to each other by 7º for Fe1 and 13º for Fe2. The coordination angle of NCS^- ion with Fe^{III} atom, Fe1-N3- C21 (Fe2-N6-C42) is 162º (169º). The thiocyanate ion is coordinated in bent form. In this complex the equatorial Fe-O distances are same as complex **6**, but the Fe-N equatorial distances are longer than the axial Fe-N bond distance (Table 6.11).

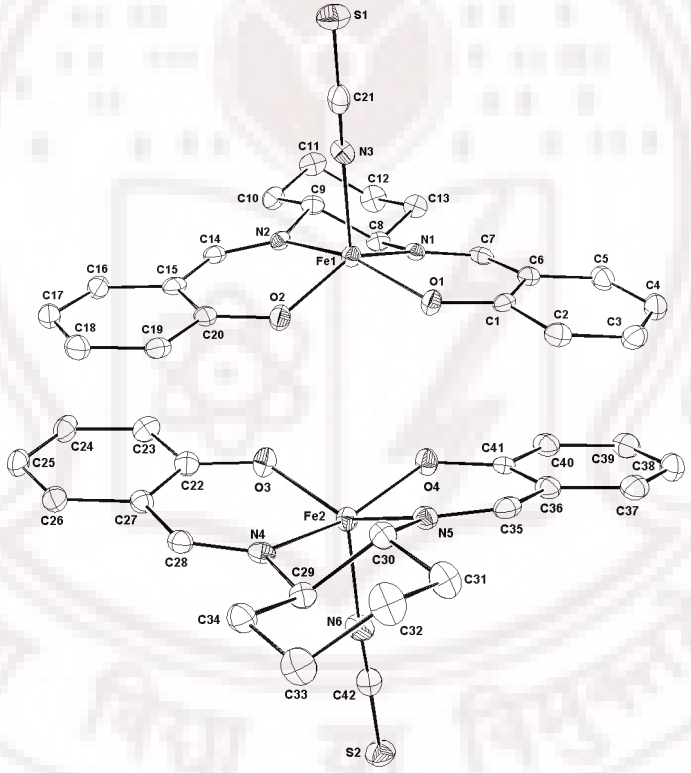

Figure 6.15 ORTEP view of complex [Fe((*R,R*)-Salcy)NCS] in **7**. Hydrogen atoms are omitted for clarity. The thermal ellipsoids are represented at the 50% probability level.

The NCS^- ion is well known bridging ligand, but in this case NCS^- ion is an N-bonded terminal thiocyanate ion and there is no specific interactions with S atom. Selected bond lengths and bond angles are mentioned in the Table 6.11.

Table 6.11 Selected bond lengths (Å) and bond angles (º) in **7**

Fe1-O1	1.883(2)	O2-Fe1-O1	92.62(10)	O3-Fe2-O4	94.23(10)
Fe1-O2	1.874(2)	O1-Fe1-N1	87.64(9)	O3-Fe2-N4	87.52(9)
Fe1-N1	2.091(2)	O1-Fe1-N2	157.30(9)	O3-Fe2-N5	140.96(9)
Fe1-N2	2.077(2)	O1-Fe1-N3	107.03(10)	O3-Fe2-N6	113.02(10)
Fe1-N3	2.004(3)	O2-Fe1-N1	141.90(9)	O4-Fe2-N4	158.58(9)
N3-C21	1.130(4)	O2-Fe1-N2	88.18(9)	O4-Fe2-N5	87.72(9)
C21-S1	1.626(4)	O2-Fe1-N3	109.60(10)	O4-Fe2-N6	102.29(11)
Fe2-O4	1.875(2)	N3-Fe1-N1	106.67(10)	N6-Fe2-N4	96.59(11)
Fe2-O5	1.892(2)	N3-Fe1-N2	93.99(9)	N6-Fe2-N5	104.54(10)
Fe2-N4	2.089(2)	N1-Fe1-N2	77.98(9)	N4-Fe2-N5	77.76(9)
Fe2-N5	2.095(2)	Fe1-N3-C21	161.9(3)	Fe2-N6-C42	169.1(3)
Fe2-N6	1.978(3)	N3-C21- S1	178.3(3)	N6-C42- S2	179.3(3)
N6-C42	1.169(4)	C42-S2	1.604(3)		

The intrachain and interchain Fe···Fe distances are 4.571 and 7.084 Å respectively. There are no specific intermolecular interactions with S atom of the NCS^- ion. The packing diagram of the complex **7** is shown in Figure 6.16.

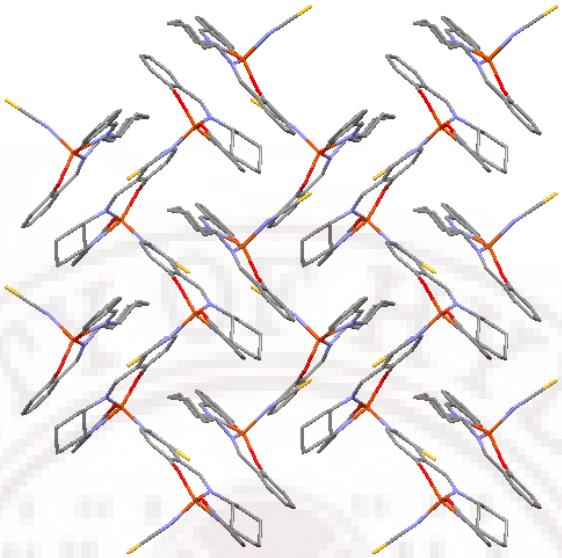

Figure 6.16 The packing view of [Fe((*R,R*)-Salcy)NCS] in **7** through *ab*-plane. Colour code for atoms: blue, N; red, O; grey C; yellow S; brick orange, Fe.

Table 6.12. Crystallographic data and structure refinement for **8** and **9.**

	8	**9**
Formula	$C_{22}H_{24}MnN_3O_4$	$C_{21}H_{20}FeN_3O_3$
Formula weight	449.38	418.25
Crystal system	triclinic	monoclinic
a (Å)	8.4810(7)	12.811(3)
b (Å)	9.8847(8)	10.171(2)
c (Å)	12.096(1)	14.728(3)
α (º)	96.976(1)	90
β (º)	97.500(1)	95.757(3)
γ (º)	95.674(1)	90
V (Å^3)	991.1(1)	1909.4(6)
Space group	*P*1	$P2_1$
Z	2	4
T (K)	100(2)	298(2)
ρ_{calcd} (g cm^{-3})	1.506	1.455
μ (mm^{-1})	0.702	0.817
θ range (º)	1.71 - 26.05	1.39 - 25.93
h/*k*/*l* indices	-10, 10/12, 12/	-15, 15/ -12, 12/
	-14, 14	-18, 18
Reflections collected	10375	19684
Unique reflection, R_{int}	7609, 0.0185	7339, 0.0843
GooF	1.040	1.023
*R*1 [$I > 2\sigma(I)$]	0.0335	0.0792
*wR*2[all data]	0.0764	0.1285
Weight. scheme (A, B)	0.0364, 0.00	0.0489, 0.55

6.3.8. Structure of [Mn((*R,R*)-Salcy)(CH_3OH)NCO] (8)

The asymmetric unit of **8** contains two structurally almost identical and crystallographically independent mononeric Mn^{III} ions as shown in Figure 6.17. The basic structure is similar to the complex **3** and **4**. In this case the coordination around the Mn^{III} atom is one tetradentate (*R,R*)-Salcy ligand in the equatorial mode, with the axial position occupied by an N-bonded terminal NCO^- ion and solvent molecule, methanol. The equatorial plane (N2O2) average distance of Mn1 is similar to that of the equatorial plane average distance of Mn2 (*ave* Mn1-salcy = 1.94 Å = Mn2-salcy). In the unit cell, the equatorial atoms (O_2N_2) of Mn1 and Mn2 are very nearly coplanar even though the manganese atoms deviated significantly from this plane 0.16 Å for Mn1 and Mn2 (with rms deviation 0.078 Å for Mn1 and 0.0062 Å for Mn2). The mean planes of the two halves of the Schiff base ligand, excluding the cyclohexane group, are also individually planar (rms diviation = 0.019 and 0.072 Å for Mn1 and 0.022, 0.035 Å for Mn2), with the Mn1 deviating by 0.054, 0.25 Å, and with the Mn2 deviating by 0.39 and 0.52 Å from these planes. The mean planes of the two halves of the Schiff base ligands (excluding the cyclohexane groups) are inclined to each other by 5.50º for Mn1 and 7.80º for Mn2. The Mn-$N_{cyanate}$ distances are same (2.16 Å) for Mn1 and Mn2 in **8** while Mn-$O_{methanol}$ distances are different (Mn1-O3 2.52 Å; Mn2-O6 2.45 Å). Selected bond lengths and bond angles are listed in the Table 6.13. The monomeric units of complex **8** have strong hydrogen-bonding contacts between O4(8) atom from coordinated methanol molecule and O3(7) from the terminal NCO^- ions with an O4(8)···O3(7) distances of 2.82 and 2.78 Å, thus the monomeric units are building one dimensional polymeric chains in ladder fashion

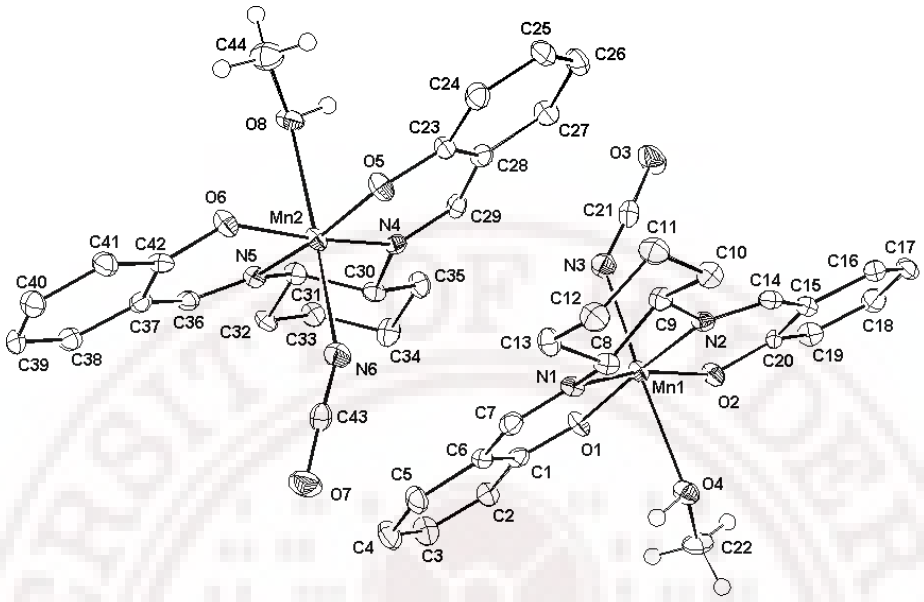

Figure 6.17 ORTEP view of complex [Mn((*R,R*)-Salcy)(CH_3OH)NCO] in **8**. Hydrogen atoms of the Schiff base (*R,R*)-Salcy are omitted for clarity. The thermal ellipsoids are represented at the 50% probability level.

Table 6.13 Selected bond lengths (Å) and bond angles (º) in **8**

Mn1-O1	1.872(3)	O1-Mn1-O2	92.10(11)	O5-Mn2-O6	93.3(1)
Mn1-O2	1.885(3)	O1-Mn1-N1	92.24(12)	O5-Mn2-N4	91.85(12)
Mn1-N1	1.998(3)	O1-Mn1-N2	173.29(13)	O5-Mn2-N5	169.18(12)
Mn1-N2	1.987(3)	O1-Mn1-N3	97.77(12)	O5-Mn2-N6	98.51(12)
Mn1-N3	2.167(3)	O2-Mn1-N1	165.06(12)	O6-Mn2-N4	169.48(12)
Mn1-O4	2.518(3)	O2-Mn1-N2	91.83(12)	O6-Mn2-N5	91.27(12)
N3-C21	1.176(5)	O2-Mn1-N3	94.11(12)	O6-Mn2-N6	95.64(12)
C21-O3	1.213(4)	N1-Mn1-N2	82.62(13)	N4-Mn2-N6	92.67(12)
Mn2-O5	1.875(3)	N1-Mn1-N3	99.46(12)	N5-Mn2-N6	90.80(12)
Mn2-O6	1.897(3)	N2-Mn1-N3	94.19(15)	N4-Mn2-N5	82.16(13)
Mn2-N4	1.978(3)	N1-Mn1-O4	78.71(10)	N4-Mn2-O8	82.58(10)

Mn2-N5	2.012(3)	N2-Mn1-O4	87.53(10)	N5-Mn2-O8	81.32(10)
Mn2-N6	2.154(3)	Mn1-N3-C21	138.3(3)	Mn2-N6-C43	155.7(3)
Mn2-O8	2.450(3)	N3-C21-O3	177.3(4)	N6-C43-O7	177.7(4)
N6-C43	1.161(5)	N3-Mn1-O4	174.8(1)	N6-Mn2-O8	171.3(1)
C43-O7	1.214(4)				

along the *a*-axis and the weak hydrogen-bond interactions between carbon (from Schiff base) and oxygen/nitrogen atoms of NCO^- ion lead to a two dimensional supramolecular network in the crystal structure of complex **8**. The hydrogen bonding parameters are shown in the Table 6.14. As for NCO^- itself, symmetrical the coordination of the cyanate ion is not symmetrical and the bond angles of Mn1-N3-C21 and Mn2-N6-C43 are 138 and 154º. The shortest intrachain and interchain Mn···Mn distance are 8.48 and 6.78 Å. Packing diagram of the complex 8 as shown in Figure 6.18.

Table 6.14 Hydrogen bonding parameters for **8**

D-H···A	D-H (Å)	H···A (Å)	D···A (Å)	D-H···A (º)
O3-H3A···O3#1	0.856	1.970	2.816	169.47
O8-H6A···O7#2	0.923	1.854	2.775	176.59
O3-H38···C38#3	2.568	0.930	3.319	138.1
N3-H29···C29#4	2.622	0.931	3.424	144.7
O7-H16···C16#5	2.639	0.929	3.308	129.4

#1 *x*-1, , *z*; #2 *x*+1, *y*, *z*; #3 *x*+1, *y*, *z*+1; #4 *x*, *y*, *z*; #5 *x*-1, *y*, *z*-1

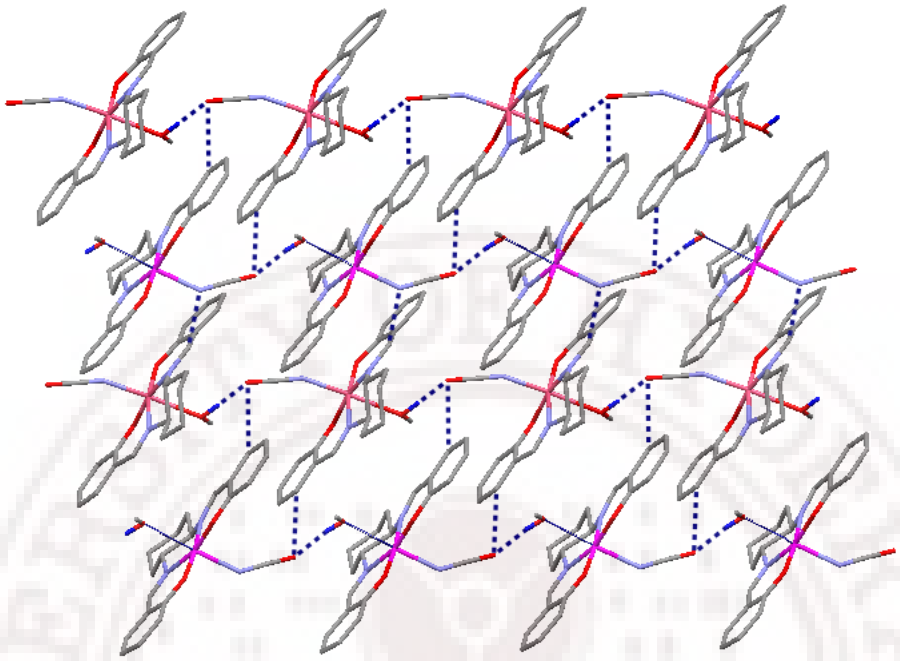

Figure 6.18 View of the 2D-dimensional hydrogen bonded chains in complex **8**. Hydrogen atoms of the Schiff base (*R,R*)-Salcy are omitted for clarity. blue, N; red, O; grey C; dark blue H; purple, Mn1 and pale pink Mn2.

6.3.9 Structure of [Fe((*R,R*)-Salcy)NCO] (9)

The asymmetric unit of complex **9** contains two structurally identical and crystallographically independent five coordinated molecules shown in Figure 6.19. The complex has square pyramidal geometry. In each molecule the coordination around the Fe^{III} is one tetradentate schiff base ligand (*R,R*)-Salcy in the equatorial mode with bond distances Fe-$O(N)_{ave}$ 1.87(2.09) Å, and the axial position is occupied by an N-bonded terminal cyanate ion with bond distance 1.92 Å. The equatorial plane average distance of Fe1 is similar to that of the equatorial plane average distance of Fe2 (*ave* Fe1-salcy = 1.98 Å = Fe2-salcy), as well as this distance

is 0.05 Å is similar to that of complex **7**. In the unit cell, the equatorial atoms (O_2N_2) of Fe1 and Fe2 are nearly coplanar even though the iron atoms deviated significantly from the plane 0.52 Å (with rms deviation 0.013 Å for Fe1 and 0.016 Å for Fe2).

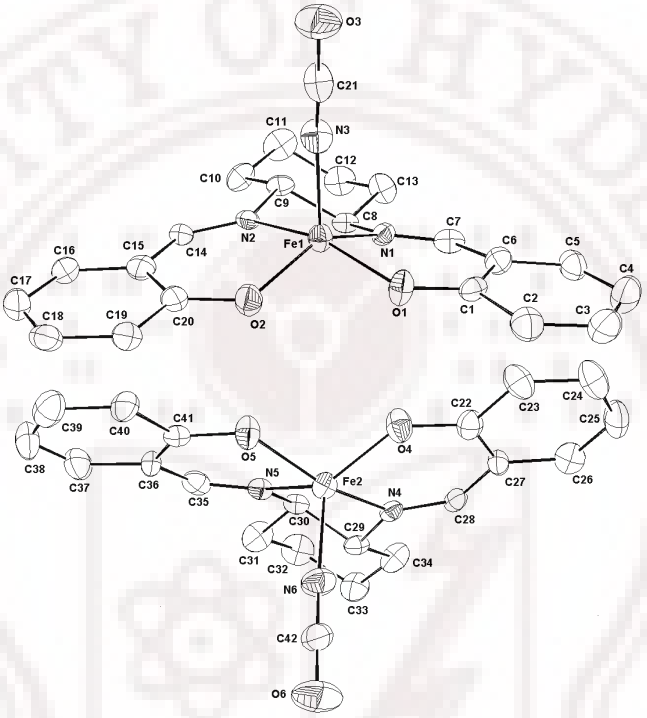

Figure 6.19 ORTEP view of complex [Fe((*R,R*)-Salcy)NCO] in **9**. Hydrogen atoms of the Schiff base (*R,R*)-Salcy are omitted for clarity. The thermal ellipsoids are represented at the 50% probability level.

The mean planes of the two halves of the Schiff base ligands (excluding the cyclohexane groups) are inclined to each other by 9º for Fe1 and 14º for Fe2. The coordination angle of NCO^- ion with Fe^{III} atom, Fe1-N3- C21 (Fe2-N6-C42) is 160º (168º). In this complex the equatorial Fe-O distances are same as complex **6** and **7**,

but the Fe-N equatorial distances are longer than the axial Fe-N bond distance (Table 6.15). The NCO^- ion is well known bridging ligand, but in this case NCO^- ion is an N-bonded terminal cyanate ion and there is no specific interactions with O atom. Selected bond lengths and bond angles are mentioned in the Table 6.15. The intrachain and interchain Fe···Fe distances are 4.75 and 7.06 Å respectively. There are no specific intermolecular interactions with O atom of the NCO^- ion. The packing diagram of the complex **9** is shown in Figure 6.20.

Table 6.15 Selected bond lengths (Å) and bond angles (º) in **9**

Fe1-O1	1.882(5)	O2-Fe1-O1	92.0(3)	O4-Fe2-O5	94.3(3)
Fe1-O2	1.866(6)	O1-Fe1-N1	87.2(2)	O4-Fe2-N4	87.5(2)
Fe1-N1	2.085(6)	O1-Fe1-N2	155.9(2)	O4-Fe2-N5	138.8(3)
Fe1-N2	2.086(6)	O1-Fe1-N3	107.6(3)	O4-Fe2-N6	114.3(3)
Fe1-N3	1.920(10)	O2-Fe1-N1	140.7(3)	O5-Fe2-N4	156.8(3)
N3-C21	1.156(12)	O2-Fe1-N2	88.4(3)	O5-Fe2-N5	86.2(3)
C21-O3	1.193(12)	O2-Fe1-N3	111.8(3)	O5-Fe2-N6	103.2(3)
Fe2-O4	1.881(6)	N3-Fe1-N1	105.8(3)	N6-Fe2-N4	97.1(3)
Fe2-O5	1.900(7)	N3-Fe1-N2	94.5(3)	N6-Fe2-N5	105.5(3)
Fe2-N4	2.082(6)	N1-Fe1-N2	77.5(2)	N4-Fe2-N5	77.5(3)
Fe2-N5	2.109(6)	Fe1-N3-C21	160.1(8)	Fe2-N6-C42	168.5(8)
Fe2-N6	1.922(9)	N3-C21-O3	176.5(12)	N6-C42-O6	178.2(12)
N6-C42	1.145(12)	C42-O6	1.196(11)		

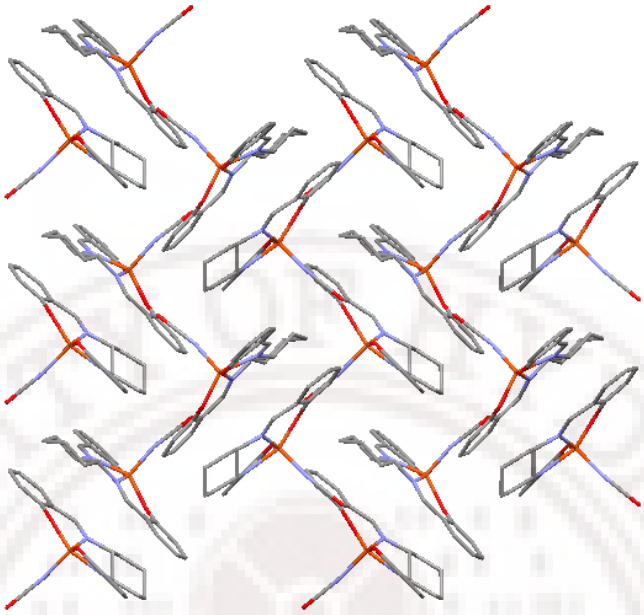

Figure 6.20 The packing view of [Fe((*R,R*)-Salcy)NCO] in **9** through *bc*-plane. Hydrogen atoms of the Schiff base (*R,R*)-Salcy are omitted for clarity. Colour code for atoms: blue, N; red, O; grey C; brick orange, Fe.

6.3.10 Infrared spectral properties

The IR spectra of the compounds **1-5** exhibit strong absorption at the range 2030-2050 cm^{-1}, which is attributed to the asymmetric stretching vibration of N-bonded azide absorption. The asymmetric stretching vibration of N-bonded terminal azide ion higher (**3**, **4** and **5**) than the bridging azide(**1** and **2**). The compounds **6** and **7** exhibits strong absorption at the range 2020-2045 cm^{-1}, which is attributed to N-C stretching vibration of N-bonded thiocyanate ion. The compounds **8**-**9** exhibit strong absorption at the range 2160-2210 cm^{-1}, which is attributed to the asymmetric stretching vibration of N-bonded cyanate group. The IR spectra of all compounds exhibit strong absorption at 1600-1620 cm^{-1}, which is assignable to the (-C=N)

stretching vibration of Schiff-base and the IR spectra of all compounds are with in the range reported.[16]

6.3.11 Electronic and circular dichroism spectra of Mn((*R,R*)-Salcy)N_3

The electronic absorption spectra and CD spectra for complex Mn((*R,R*)-Salcy)N_3 (Figure 6.21) measured with different concentration in acetonitrile. The low intensity absorption band (λ/nm, ε_{max}/$cm^{-1}M^{-1}$) in the range 587, 221; which is assigned to d-d transition.

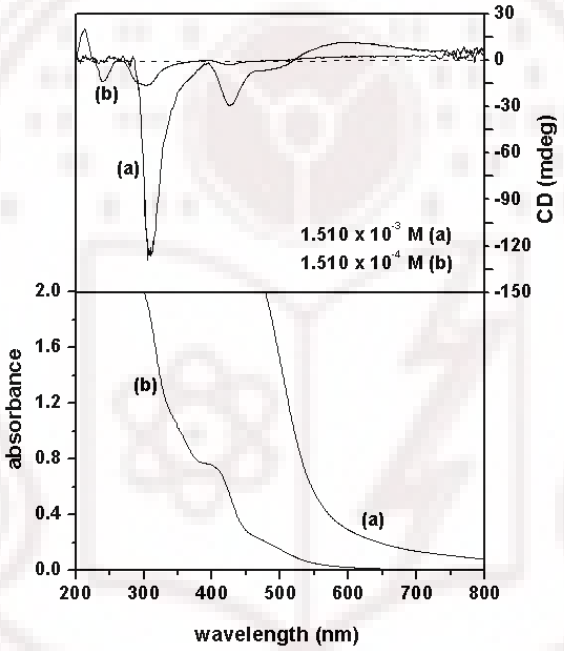

Figure 6.21. The solution circular dichroism spectra (top) and electronic absorbance spectra (bottom) of complex Mn((*R,R*)-Salcy)N_3 with different concentrations.

The absorption bands in the range 515, 753; 450, 1903; 392, 5087; and 325, 9042 (λ/nm, ε_{max}/$cm^{-1}M^{-1}$) respectively, which are assigned to intraligand π-π* transitions

in the complex. The corresponding circular dicroism spectra shows positive Cotton effect at low intensity and negative Cotton effect at high intensity.

6.4 Conclusion

All the complexes **1-9** were crystallized in the chiral space group ($P2_1$ or $P1$). The complex Mn((*R,R*)-Salcy)N_3, crystallized with different solvents in different conditions to obtain compounds **1-5**. Even though the both complexes **1** and **2** have $P2_1$ space group the complex **1** is showing 'helical 1D- polymeric' chain, the complex **2** is in 'zig-zag' fashion. The complex **3**, **4** and **8** are simple monomers, and they are build ledder type 1D- polymeric chains through axial ligands. Compound **5** and **6** are phenoxo bridged dimers, due to chirality of the complex centosymmetry is not present in these dimers. Finally the compounds **7** and **9** are five coordinated mononuclear having square pyramidal geometry. The tetradentate chiral Schiff base (1*R*,2*R*)-salcy coordinates the Fe(III) in equatorial mode and the axial position is occupied with a N-bonded pseudohalide ion (NCS^-, NCO^-).

6.5. References

1. (a) Ribas, J.; Monfort, M.; Ghosh, B. K.; Cortes, R.; Solans, X.; Font-Bardia, M. *Inorg. Chem.* **1996**, *35*, 864. (b) Tuczek, F.; Bensch, W. *Inorg. Chem.* **1995**, *34*, 1482. (c) Escuer, A.; Vicente, R.; Goher, M. A. S.; Mautner, F. A. *Inorg. Chem.* **1995**, *34*, 5707. (d) Stults, B. R.; Marianelli, R. S.; Day, V. W. *Inorg.* Chem. **1975**, *14*, 722.

2. (a) Ribas, J.; Monfort, M.; Diaz, C.; Bastos, C.; Solans, X. *Inorg. Chem.* **1994**, *33*, 484. (b) Mautner, A. F.; Goher, M. A. S. *Polyhedron* **1996**, *15*, 1133. (c) Cortes, R.; Pizarro, J. L.; Lezama, L.; Arriortua, M. I.; Rojo, T. *Inorg. Chem.* **1994**, *33*, 2697. (d) De Munno, D.; Poerio,T.; Viau, G.; Julve, M.; Lloret, F. *Angew. Chem.*, *Int. Ed. Engl.* **1997**, *36*, 1459.

3. Wemple, M. W.; Adams, D. M.; Hagen, K. S.; Folting, K.; Hendrickson, D. N.; Christou, G. *J. Chem. Soc., Chem. Commun.* **1995**, 1591.

4. (a) Reddy, K. R.; Rajasekharan, M. V.; Tuchagues, J.-P. *Inorg. Chem*. **1998**, *37*, 5978. (b) Li, H.; Zhong, Z. J.; Duan, C. Y.; Yu, X. Z.; Mak, T. C. W.; Wu, B. *Inorg. Chim. Acta* **1998**, *271*, 99.

5. (a) Panja, A.; Shaikh, N.; Vojtısek, P.; Gao, S.; Banerjee, P. *New J. Chem.* **2002**, *26*, 1025. (b) Kennedy, B. J.; Murray, K. S. *Inorg. Chem.* **1985**, *24*, 1552.

6. Ko, H. H.; Lim, J. H.; Kim, H. C.; Hong, C. S. *Inorg. Chem.* **2006**, *45*, 8847.

7. Yuan, M.; Zhao, F.; Zhang, W.; Wang, Z. -M. Gao, S. *Inorg. Chem.* **2006**, *45*, 11235.

8. Sailaja, S.; Rajasekharan, M. V.; Hureau, C.; Riviere, E.; Cano, J.; Girerd J.-J. *Inorg. Chem*. **2003**, *42*, 180.

9. *SAINTPLUS*, Bruker AXS Inc., Madison, Wisconsin, USA 2003.

10. Sheldrick, G. M. *SADABS, Program for empirical absorption correction*, University of Gottingen, Gottingen, Germany **1996**.

11. Sheldrick, G. M. *SHELX-97*, *Programs for crystal structure analysis*, University of Gottingen, Gottingen, Germany **1997**.

12. Matsumoto, N.; Sunatsuki, Y.; Miyasaka, H.; Hashimoto, Y.; Luneau, D.; Tuchagues, J. -P. *Angew. Chem. Int. Ed*. **1999**, *38*, 171.

13. Miyasaka, H.; Saitoh, A.; Abe, S. *Coord. Chem. Rev.* **2007**, *251*, 2622.

14. (a) Lu, Z.; Yuan, M.; Pan, F.; Gao, S.; Zhang, D.; Zhu, D. *Inorg. Chem.* **2006**, *45*, 3538. (b) Lecren, L.; Wernsdorfer, W.; Li, Y.-G.; Vindigi, A.; Miyasaka, H.; Clerac, R. *J. Am. Chem. Soc*. **2007**, *129*, 5045. (c) Saha, S.; Mal, D.; Koner, S.; Bhattacherjee, A.; Gutlich, P.; Mondel, S.; Mukherjee, M.; Okamoto, K.-I. *Polyhedron*, **2004**, *23*, 1811. (d) Miyasaka, H.; Clerac, R.; Wernsdorfer, W.; Lecren, L.; Bonhomme, C.; Sugiura, K.; Tamashita, M. *Angew. Chem. Int. Ed.* **2004**, *43*, 2801.

15. Miyasaka, H.; Clerac, R.; Ishii, T.; Chang, H.; Kitagawa, S.; Yamashita, M. *J. Chem. Soc., Dalton Trans*. **2002**, 1528.

16. Nakamoto, K. *Infrared and Raman Spectra of Inorganic and coordination Compounds*; 3 ed.; John Wiley & Sons, Inc.: New York, 1997, pp 270.